COMPUTER MODELLING OF PYROTECHNIC COMBUSTION.

THESIS

Submitted in fulfilment of the requirements
for the degree of

Doctor of Philosophy
of Rhodes University

by

STEVEN JOHN TAYLOR
December 1994.

For my parents and all their support.

And for Debbie, for waiting.

In memory of Luke (1965 - 1992)

Killed pursuing our dream of flight

Only the good die young and you were one of the best.

ABSTRACT.

One of the most important industrial uses of pyrotechnic compositions is as delay fuses in electric detonators. Many factors influence the rate of burning of such fuses. These include (a) the primary choice of chemical components, followed by (b) the physical properties of these components, particularly the particle-size and distribution of the fuel, (c) the composition of the system chosen and (d) the presence of additives and/or impurities.

A full experimental study of the influences of even a few of these factors, while attempting to hold other potential variables constant, would be extremely time consuming and hence attention has been focused on the possibilities of modelling pyrotechnic combustion. Various approaches to the modelling of pyrotechnic combustion are discussed. These include:-

(i) one-dimensional finite-difference models;

(ii) two-dimensional finite-element models;

(iii) particle-packing considerations;

(iv) Monte Carlo models.

Predicted behaviour is compared with extensive experimental information for the widely-used antimony/potassium permanganate pyrotechnic system, and the tungsten /potassium dichromate pyrotechnic system.

The one-dimensional finite-difference model was investigated to give a simple means of investigating the effects of some parameters on the combustion of a pyrotechnic.

The two-dimensional finite-difference model used similar inputs, but at the expense of considerably more computer power, gave more extensive information such as the shape of the burning front and the temperature gradients throughout the column and within the casing material.

Both these models gave improved results when allowance was made for autocatalytic kinetics in place of the usual assumption of an "order-of-reaction", $\mathbf{n \leq 1}$.

The particle-packing model investigated the qualitative relationship between the maximum burning rate of a pyrotechnic system and the maximum number of contact points (per 1.00 g composition) calculated for that system. Qualitative agreement was found for those systems which are presumed to burn mainly via solid-solid reactions.

The Monte Carlo model investigated the effect of the random packing of fuel and oxidant particles on the variability of the burning rate of a pyrotechnic composition.

ACKNOWLEDGEMENTS.

With the writing of every thesis there are many people who contribute both directly and indirectly to the production of that thesis. I would like to express my thanks to the following who have contributed to this work.

Professor Mike Brown, for his infinite patience, outstanding support and supervision. I hope one day to be able to emulate your professional approach to research.

Dr. Mike Taylor and Dr. Anil Rugunanan of AECI, whose efforts allowed me access to the TOPAZ codes and both have provided technical support over these three years.

Ian Dore and Justin Jonas for their advice on computer matters and Bruce Brown for his insight into the FEM mathematics.

AECI, FRD and Rhodes University for providing funding for the project and for myself.

My support group at Rhodes, all my colleagues for their help both with the project and personally, in particular, Ruth^2, Cathy, Ross, Dean, Mel, Justin and Henk. Thanks for keeping me on track over the past few years.

To my parents for all their support, showing me that the impossible is attainable, it only takes a little faith in oneself.

Lastly, to Debbie, for waiting for three long years, listening to my ups and downs, and easing me through the rough patches. Thanks.

TABLE OF CONTENTS.

LIST OF FIGURES.

Section 3.

Section 4.

Section 5.

Section 6.

Section 7.

Section 8.

Section 9.

Section 10.

Section 11.

LIST OF TABLES.

Section 5.

Section 6.

Section 7.

Section 8.

Section 11

LIST OF SYMBOLS AND UNITS

A	Pre-exponential factor (s^{-1})
B_i	Biot number
D	Thermal diffusivity ($m^2\ s^{-1}$)
E_a or E	Activation energy (kJ mol^{-1})
F_0	Fourier number
G	Power function
N_R	Number of contact points
Q	Heat output (kJ g^{-1})
R	Universal gas constant (8.314 J K^{-1} mol^{-1})
T	Temperature ($^{\circ}C$ or K)
U	Excess temperature (K)
c	Specific heat capacity (J K^{-1} g^{-1})
h	convection heat transfer coefficient
k	rate coefficient
n	Order of reaction
q	Heat of reaction (kJ mol^{-1})
t	Time (s)
v	Linear burning rate (mm s^{-1})
α	Fractional reaction
σ	Stephan-Boltzmann constant
ϕ/ß	Heating rate (K min^{-1})
ϵ	Surface emissivity

λ Thermal conductivity (W m^{-1} K^{-1})

ρ Density (g cm^{-3})

Subscript:

calc Calculated value

exp Experimental value

ign Ignition value

obs Observed value

max Maximum value

min Minimum value

ref Reference value

TA Thermal analysis value

th Thermal relaxation value

TP Temperature profile value

r Rise value

d Decay value

I Ignition

0 Initial

a Ambient

f Final

s Surface

1. AIMS OF THIS RESEARCH.

Since 1980 the Department of Chemistry at Rhodes University has been involved in studies of the combustion of pyrotechnic systems of both commercial importance and fundamental interest. To avoid unnecessary complication, attention has been directed mainly at binary fuel/oxidant combinations. Where appropriate, studies have been extended to some ternary systems to try to determine the influence of one fuel (or one oxidant) on the behaviour of another.

The main experimental technique used has been the measurement of temperature-time profiles during combustion. These profiles have been used to extract kinetic and thermochemical information about the combustion reactions, following the methods of analysis developed by T.A. Boddington and P.G. Laye, in the School of Chemistry at the University of Leeds. A fair amount of such information has thus been gathered and attempts have been made (see detailed references in later chapters) to draw some general conclusions regarding factors which determine important combustion parameters, such as burning rates and combustion temperatures.

McLain [1] has pointed out that the number of potential binary fuel/oxidant combinations is of the order of 4020 and this increases to about 250 000 when ternary combinations are considered. It is thus of considerable importance to be able to "design" a pyrotechnic composition with properties suitable for some specific application from the information which is available, with the minimum of additional experimentation.

Such an aim is neither new, nor probably ever completely achievable, but access permitted to a finite-element code, TOPAZ, (see below for details) prompted an examination of various ways of modelling pyrotechnic combustion and relating such models to experimental data available.

2. RESEARCH STRATEGY.

The main aims have been stated in section 1. The main facility available for use was the two-dimensional finite-element code TOPAZ (which is described in detail in section 8). In addition, it was decided to examine the information obtainable from simpler one-dimensional finite-difference models. These studies are described in section 7 and provide a useful comparison with the TOPAZ results (section 8).

Different approaches were used to examine some aspects of pyrotechnic combustion which are not easily modelled by either the finite-difference or finite-element models. These are the packing of and hence the contact between fuel/oxidant particles and the influence of this contact on combustion. The approaches used were Monte Carlo types of calculation based on probabilities (Section 11) and geometrical models of the packing of spheres (Section 10).

Because so many variables can influence pyrotechnic combustion, attention was also given to the statistical design of computations involving simultaneous variation of several variables (Section 6).

Because of the computational nature of this research, the structure of this thesis differs in some aspects from a conventional thesis based on laboratory experiments. After a survey of previous work on modelling of pyrotechnic combustion (Section 3), the background material relevant to each of the particular computational approaches used is reviewed, before presentation and discussion of the results obtained using that approach.

Finally there is a general discussion of the overall results and conclusions are drawn.

3. INTRODUCTION.

3.1 Computer modelling. [2]

The words *simulation* and *modelling* are often used interchangeably but often mean different things to different people. *Modelling* is generally used in a much broader context than *simulation*. A simulation tries to imitate the dynamic behaviour of a system and to predict subsequent events. Modelling has a much broader meaning, and a system can be modelled by looking at all the dynamic phenomenon without specifying where those phenomenon came from or what they will evolve into. Modelling tries to reproduce the more prominent features of a system, and as such is not an exact representation of the system. A simulation is the implementation of a model using certain defined physical characteristics, initial conditions and boundary conditions.

A simulation does not directly solve the set of partial differential equations which make up the mathematical model of the system. Rather a set of discrete algebraic equations, known as the computational model, which are derived from the original partial differential equations, are solved. With improving numerical methods and computing power simulation will become more accurate.

There are basically three types of physical model :-

i) *Detailed model*: which uses as many basic physical assumptions, or first principles, as possible in detailing the problem. This tends to limit the complexity of the model. Detailed models are generally used in cases where there are a set of well-defined ranges of validity. The more general, and hence more flexible, a detailed model is, the more expensive (computationally) the model becomes.

ii) *Phenomenological models*: these models (along with the empirical models, see next point) are used when the scales of the physical processes are too dissimilar to be resolved in one calculation. The modelling is done by deriving a series of averaged models of the small scale processes, and these are present in the governing equations. These governing equations are often too complex to solve easily, or cannot be given numerical values,

and so simpler approximate forms are used. These approximate forms are often derived from experimental results, or more fundamental theories or simulations and are often calibrated from experiment. The model usually starts from a simple (and hence approximate) theory about the system to be modelled, and so does not require detailed information about the processes going on in the model, only the apparent effect of these processes.

iii) *Empirical* models: these are either direct fits of data to mathematical formulae, or are data used directly in tabular form. The data are almost always derived from experiments. The data often include errors, usually in measurement or equipment calibration errors, and so should only be used in a model for interpolation and not extrapolation. Chemical rate constants are examples of empirical models.

Numerical simulations are a way to bridge the gap between theoretical analysis and laboratory experiment. They hence have both advantages and disadvantages from both areas of research. The simulation can be treated in many ways like a laboratory experiment. They contain similar types of errors, and they both incorporate complicated interactions. Bugs in the computer program of the simulation can be analogous to experimental errors such as leaks in a closed experimental system. Calibration errors in an experiment are similar to the invalid input of parameters, constants or sub-models in a detailed simulation.

Simulations give the researcher a tool which enables them to look at the effect of altering a specific parameter (or physical effect) on the overall system. This is often not possible in experimental work.

3.2 **Background aspects of heat transfer.** [3]

Conduction is the transfer of thermal energy through a solid or a fuel as a result of a temperature gradient. The transfer of thermal energy occurs at the molecular and atomic levels without net mass transfer. The rate equation describing heat transfer by conduction is Fourier's law. For an isotropic medium Fourier's law is :

$$\left(\frac{dq}{dt}\right) = \lambda\left(\frac{\delta T}{\delta n}\right)$$

where ***dq/dt*** is the rate of heat flow per unit area in the ***n*** direction and λ is the thermal conductivity (which may be a function of the temperature ***T***). The temperature gradient ***δT/δn*** is negative in the direction of positive heat flow. For a two-dimensional object, the components of the heat flow in Cartesian coordinates are :-

$$\left(\frac{\delta q}{\delta t}\right)_x = \lambda\left(\frac{\delta T}{\delta x}\right) \quad \textit{and} \quad \left(\frac{\delta q}{\delta t}\right)_y = \lambda\left(\frac{\delta T}{\delta y}\right)$$

For a two-dimensional isotropic problem, with temperature-dependent thermal conductivity, the law of conservation of energy combined with Fourier's law yields the thermal energy equation:-

$$-\left\{\left(\frac{\delta q_x}{\delta x}\right) + \left(\frac{\delta q_y}{\delta y}\right)\right\} + \frac{dQ}{dt} = \rho c\frac{dT}{dt} \qquad (3.1)$$

where **dQ/dt** is the internal heat generation rate per unit volume, **ρ** is the density, **c** is the specific heat capacity, and **t** is time.

Equation **3.1** must be solved for an initial set of conditions, (i.e. specifying the temperature throughout the solid at an initial time), and the appropriate boundary conditions. The boundary conditions can have several forms and may be linear or non-linear (i.e. dependent on temperature). Typical boundary conditions used in a finite element model are :-

i) Prescribed temperature, where the surface temperature of a boundary is specified to be constant or is related to some function of a boundary coordinate and/or the time. This is an example of a Dirichlet boundary condition, which is used by TOPAZ (see Chapter **8**).

ii) Prescribed heat flow, where the rate of heat flow across a boundary is specified to be constant or a function of the boundary coordinate and/or time. Can be expressed as :-

$$-k\frac{\partial T}{\partial n} = q_s$$

where n is normal to the boundary and q_s is the rate of surface heat flow per area. This is an example of a Neumann boundary condition, which is also used in TOPAZ (chapter 8).

iii) No heat flow, (adiabatic boundary) a special case of the prescribed heat flow, heat flow across the boundary is zero.

iv) Convective heat exchange, where the rate of heat flow across a boundary is proportional to the difference between the surface temperature, T_s, of the solid and the temperature, T_e, of the surroundings. The rate is given by :-

$$-k\frac{\partial T}{\partial n} = h(T_s - T_e)$$

where h is a convection heat transfer coefficient. The convection coefficient can be either linear or non-linear (i.e. dependent on temperature), and can be dependent on time.

v) Radiation heat exchange, where heat flow across a boundary is specified in terms of the emitted energy from the surface and the incident radiant thermal energy, emitted and reflected from other solids. The boundary condition is :-

$$-k\frac{\partial T}{\partial n} = \sigma\epsilon(T_s)^4 - \alpha q_i$$

where σ is the Stephan-Boltzmann constant, ϵ is the surface emissivity, and T_s is the surface temperature. The coefficient α is the surface absorptivity and q_i is the incident radiation thermal energy. Radiation contributions are often neglected in treatments of pyrotechnic combustion.

vi) Other boundary conditions include the boundary conditions between two contacting solids not in perfect contact. Many examples can be found in the literature [2,4].

3.3 Background aspects of chemical kinetics.

During combustion heat is generated through chemical reaction. Reaction is often assumed to follow a simple "order-of-reaction" model :

$$\frac{d\alpha}{dt} = k(1 - \alpha)^n \qquad (3.2)$$

where α is the extent of reaction, **k** is a rate coefficient and **n** is the apparent order of reaction. Since the reactions involved in pyrotechnic combustion are heterogeneous reactions, the interpretation of kinetic parameters such as "order of reaction" has to be modified appropriately [5].

Rate equations of the form of equation (3.2) above all give rise to α, time curves which are deceleratory in shape with maximum rate at time $t = 0$. More realistic kinetic models for pyrotechnic combustion would probably be those which give rise to a sigmoidal α,time curve. Such rate equations include :

$$\frac{d\alpha}{dt} = k\alpha(1 - \alpha) \qquad (3.3)$$

or more generally :

$$\frac{d\alpha}{dt} = k\alpha^p(1 - \alpha)^q \qquad (3.4)$$

which are based on autocatalysis of reaction by the product formed. Equation (3.3) is also known, in solid-state kinetics, as the Prout-Tompkins equation [6]. Also from solid-state kinetics, are the Johnson-Mehl-Avrami-Erofe'ev-Kolmogorov models :

$$\alpha = 1 - exp\left[-(kt)^n\right] \qquad (3.5)$$

for which the differential form is [5] :

$$\frac{d\alpha}{dt} = kn(1 - \alpha)\,[-\ln(1 - \alpha)]^{\frac{n-1}{n}} \qquad (3.6)$$

with **n** normally between 1.5 and 4.0. Neither of equations (3.4) or (3.6) can apply from $\alpha = 0$, so a "starting" term is required [5]. In the simplest form this would involve setting α initially to some small non-zero value.

A further, empirical kinetic function containing three exponents has been suggested by Sestak and Berggren, [6]

$$\frac{d\alpha}{dt} = \alpha^p(1 - \alpha)^q\,[-\ln(1 - \alpha)]^r$$

but was not considered further.

The rate coefficients, **k**, are generally assumed to show Arrhenius temperature dependence :

$$k = A\,e^{\frac{-E_a}{RT}} \qquad (3.7)$$

where **A** is the Arrhenius pre-exponential factor and E_a is the *apparent* activation energy.

There have been discussions of the applicability of the Arrhenius equation to reactions involving solids. Gray and Harper [8] list various functions which have been used in place of the Arrhenius equation. These are :-

Exponential approximation :	$\exp\Theta \bullet \exp(-E/RT_0)$
Quadratic approximation :	$(1 + 0.72\Theta + \Theta^2)\exp(-E/RT_0)$
Linear approximation :	$(1 + \beta\Theta)\exp(-E/RT_0)$

where Θ is the dimensionless temperature excess, $(T - T_0)\,E/RT_0^2$, and T_0 is the ambient or initial temperature.

As a test of the potential usefulness of these alternative expressions, various values

of E and T_0 were used. The quadratic approximation resembles the Arrhenius exponential term most closely over the range 300 - 500 K, see Figure 3.1, when E = 20 kJ mol^{-1} and T_0 = 298 K, than with E = 100 kJ mol^{-1} (Figure 3.2) or E = 10 kJ mol^{-1} (Figure 3.3). The exponential approximation always overestimates the Arrhenius term and the linear approximation always underestimates the Arrhenius term. So, in the absence of more promising alternatives, all temperature dependences in this study were assumed to be of the simplest Arrhenius form.

Kinetic analysis of temperature profiles (chapter 4) generally gives low values for the activation energy (<40 kJ mol^{-1}) and such low values are explained [5] in terms of diffusion mechanisms. Kinetic analysis of thermal analysis curves [10] generally gives much higher activation energies. Activation energies determined from thermal analysis are presumed to be more representative of the chemical processes occurring. As discussed by Boddington and Laye [10], the values obtained from temperature profiles predict unreasonably high rates of reaction at lower temperatures. They thus suggested a more complex temperature dependence of the rate constant for pyrotechnic reactions:

$$\frac{1}{k_{TP}} = \frac{1}{k_{TA}} + \frac{1}{BT^m}$$

where $\mathbf{k_{TP}}$ and $\mathbf{k_{TA}}$ are the rate coefficients predicted at temperature **T** from the temperature profile results and the thermal analyses, respectively, **B** is a diffusion coefficient and **m** is a constant. This behaviour is illustrated in Figure 3.4 for results obtained on the 20% Fe/BaO_2 composition [9].

3.4 Previous work on modelling/simulation of pyrotechnic combustion.

Hardt and Phung [11] reported results of studies of exothermic intermetallic reactions, i.e. reactions of mixtures of particles of different metals, where the heat of alloy formation could lead to thermally propagating waves similar to combustion in a pyrotechnic fuel/oxidant mixture. They developed a numerical model relating the reaction rates to the thermochemical properties of the intermetallic mixtures studied. On the basis

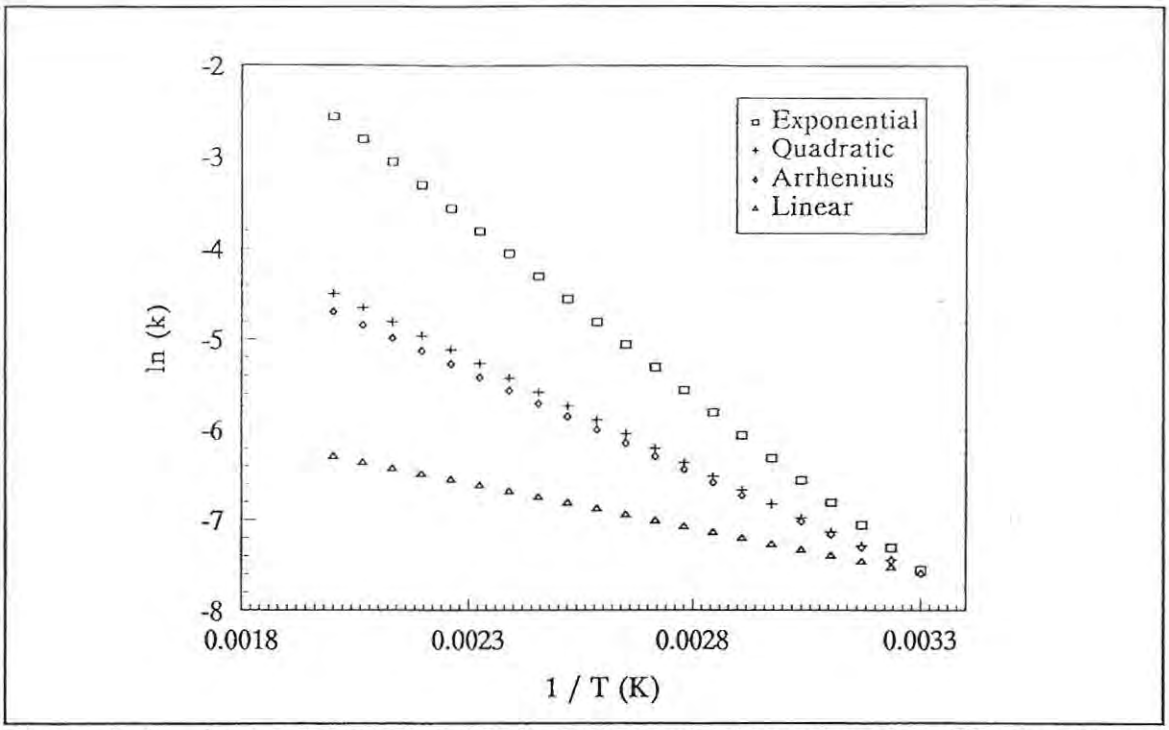

Figure 3.1: Approximation to the Arrhenius equation using E = 20 kJ mol^{-1} and T_0 = 298 K, over the temperature range 300 - 500 K.

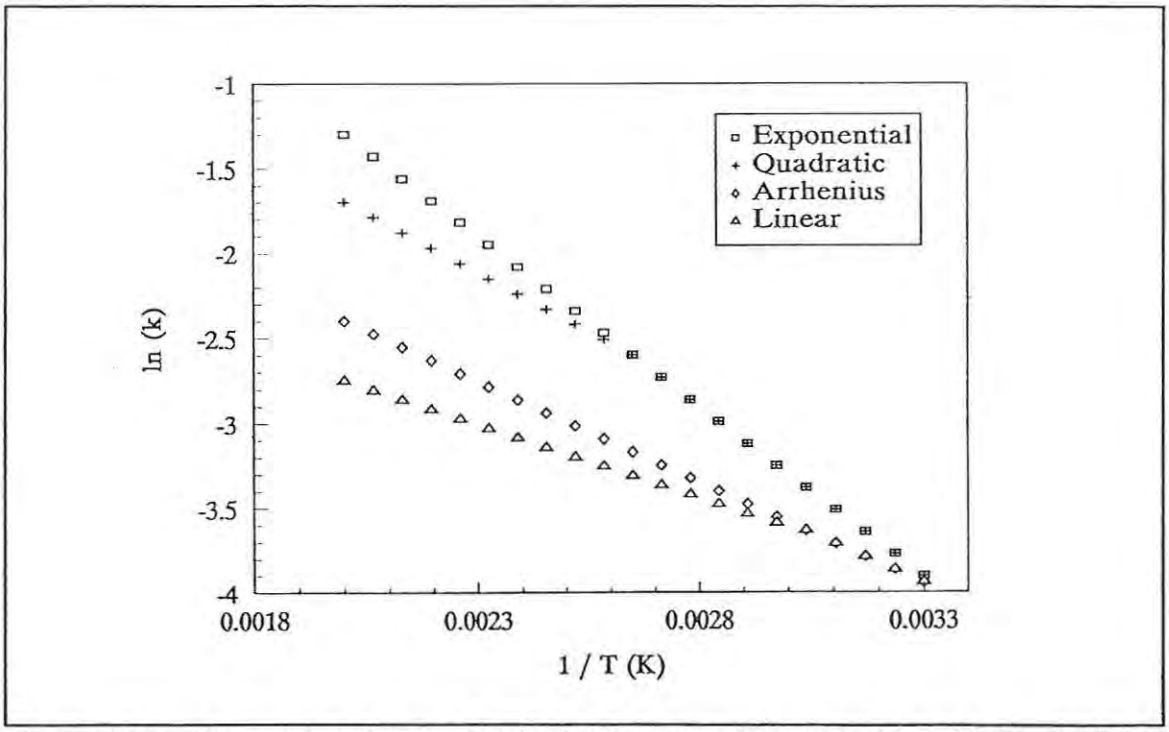

Figure 3.2: Approximation to the Arrhenius equation using E = 10 kJ mol^{-1} and T_0 = 298 K, over the temperature range 300 - 500 K.

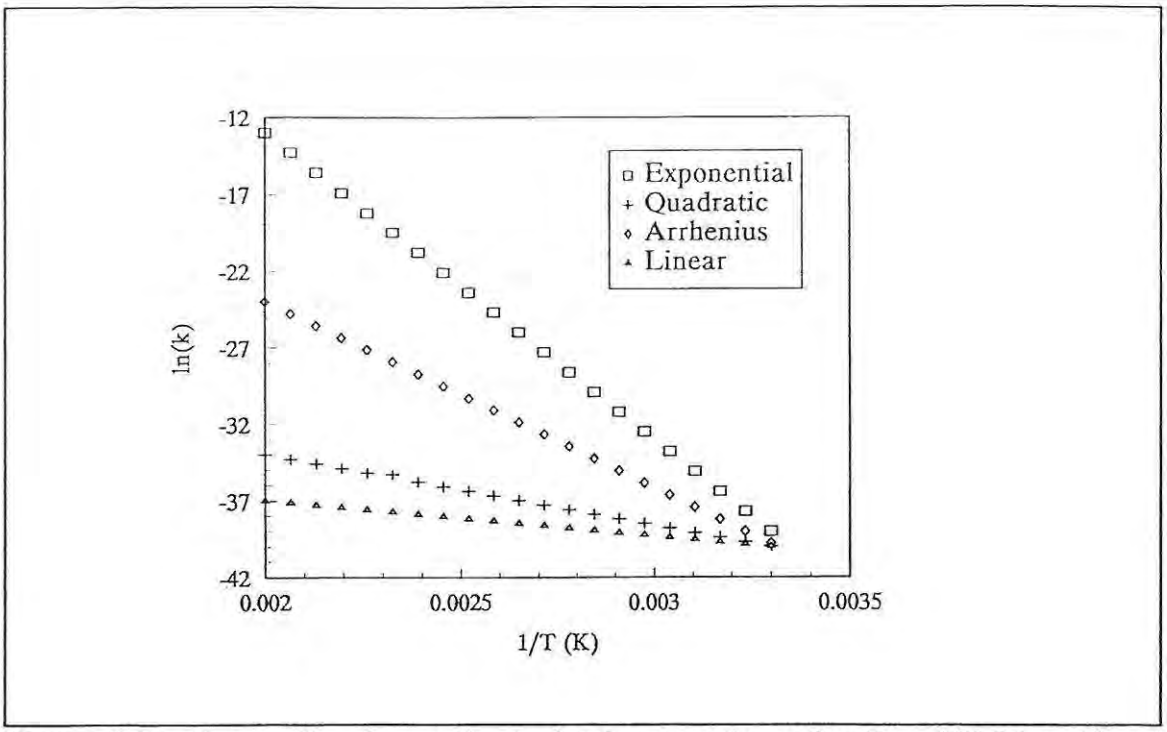

Figure 3.3: Approximation to the Arrhenius equation using E = 100 kJ mol^{-1} and T_0 = 298 K, over the temperature range 300 - 500 K.

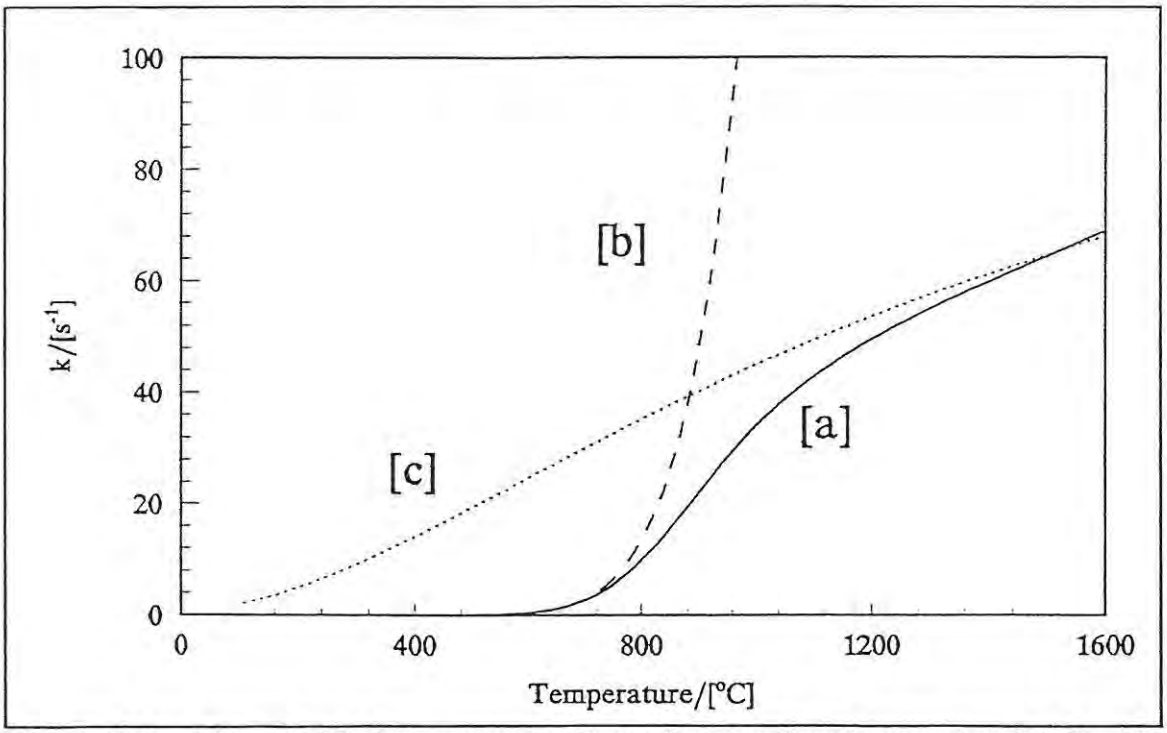

Figure 3.4: The modified temperature dependencies: Leeds equation [a], k_{TA} [b] and k_{TP} [c] plotted against temperature for the 20% Fe/BaO_2 composition [9].

that reaction would be limited by diffusion, they represented mixing of reactants **A** and **B** by formation of a series of uniform **A/B** layers to give small diffusion cells which consist of half a particle of each kind. The initial thickness of the diffusion cell ($\mathbf{a_0}$ + $\mathbf{b_0}$) is determined by the stoichiometric fractions, $\mathbf{N_a}$ and $\mathbf{N_b}$, the atomic masses, **A** and **B**, and the densities ρ_a and ρ_b.

$$b_0 = a_0 \frac{N_b}{N_a} \frac{B}{A} \frac{\rho_a}{\rho_b}$$

The product layer grows at the expense of the layers $\mathbf{a_0}$ and $\mathbf{b_0}$. Its thickness, **s**, increases by an amount **ds** in time **dt** where :-

$$ds = -da - db = \frac{D}{s}\left(1 + \frac{b_0}{a_0}\right)dt = \frac{Dw}{s}dt$$

where $\mathbf{w} = (1 + \mathbf{b_0/a_0})$ and D is diffusion coefficient expressed in the form :-

$$D = D_0 \exp\left(-\frac{E}{RT}\right)$$

where D_0 is a constant (frequency factor), E the activation energy, and R the gas constant.

The unreacted fraction

$$F = (1 - \alpha) = 1 - \frac{s}{wa_o}$$

where α is the fractional extent of reaction,

$$\frac{dF}{dt} = -\frac{d\alpha}{dt} = -\frac{1}{wa_0}\frac{ds}{dt} = -\frac{D}{wa_0^2\alpha}$$

$$i.e. \quad \frac{d\alpha}{dt} = \frac{k}{\alpha} \qquad where \quad k = \frac{D}{wa_0^2}$$

At $t = 0$, D is small (low T) but finite, and α is zero, so $d\alpha/dt$ is infinite. To avoid this, α is set to some small value representing surface layers acting as diffusion barriers.

The Hardt and Phung model thus uses a form of the 1-D diffusion model (D1) [5] as its rate equation. Arising from their model, Hardt and Phung [12] developed several approximate expressions for calculation of the linear burning rates, v, based on the relationships, (equations 3.7 - 3.9) :

$$v = \left(\frac{\lambda}{wa_0c}\right)\left(\frac{T_{ad} - T_{amb}}{T_{ign} - T_{amb}}\right) \qquad (3.7)$$

where $w = 1 + (b_0/a_0)$;

T_{ad}, T_{amb} and T_{ign} are the adiabatic reaction temperature, the starting temperature (surroundings) and the initiation (ignition) temperature, respectively,

and c is the heat capacity.

$$v = \left(\frac{RQD_0\rho}{\lambda E}\right)^{0.148} \frac{0.307\,\lambda Q}{w^{0.705}a_0\rho c^2(0.045E - T_0)} \qquad (3.8)$$

where $0.045\,E$ results from the division of $0.09\,E$ by R, and has the dimension of temperature;

a_0 is the initial thickness of the metal,

R, Q, ρ, λ and c are the gas constant, heat of reaction, density and thermal conductivity, respectively,

and D_0, E and T_0 are the diffusion pre-exponential factor, activation energy for diffusion and the starting temperature, respectively.

This expression simplifies to :-

$$v = \frac{0.80\lambda Q}{wa_0 \rho c^2 (0.035E - T_0)} \qquad (3.9)$$

Propagation rates calculated from the above expressions were compared with experimental values and were found to be within acceptable ranges.

Booth [13] developed a more complicated, semi-empirical treatment based upon the assumption that the kinetics of reaction at each point are a function of physical factors, P, the extent of reaction, α, and the temperature.

$$\frac{d\alpha}{dt} = f(P, \alpha, T)$$

Booth derived the following expression (assuming stoichiometric proportions of reactants and complete reaction) :

$$\frac{d\alpha}{dT} = \frac{\lambda f(P, \alpha, T)}{\rho v^2 \left[Q(1 - \alpha) - c(T_{max} - T)\right]}$$

As $T \rightarrow T_{max}$, $\alpha \rightarrow 1$ and $f(P,\alpha,T) \rightarrow 0$, where Q is the heat of reaction.

From this expression, Booth argued that if all other factors except the thermal conductivity, λ, were kept fixed, then v would be proportional to $\lambda^{1/2}$. Similarly, for variation of density only, $v \propto \rho^{-1/2}$.

If all factors except the parameter(s) P, related to physical factors, are fixed and it is assumed that

$$f(P, \alpha, T) = f_1(P) f_2(\alpha, T)$$

then $v \propto [f_1(P)]^{1/2}$ and the variation of v with physical parameters, such as particle diameter, can be used to obtain information about the form of the function $f_1(P)$.

Norgrove *et al.* [14] studied the one-dimensional unsteady propagation of a flame-front down a detonator delay element filled with a porous 30% $Sb/KMnO_4$ pyrotechnic composition. Their studies were based on experiments carried out by Beck [15] on the

effect of puncturing of detonator tubes on the burning rate of the delay element.

The model was based on single-step first-order reaction kinetics and examined the effect of the gases produced by the burning of the pyrotechnic on the overall rate of burning. Several assumptions were made :-

i) flow was one-dimensional and all variables were dependent on **x**, the distance down the element, and the time, **t**;

ii) the temperature of the gas and the reacting solid were equal;

iii) gas flow was according to Darcy's law, and the solid did not move;

iv) below an "ignition" temperature no reaction occurred, and above this temperature, the temperature dependence of the reaction rate followed an Arrhenius-type equation; and

v) transfer of heat by radiation between fuel particles was neglected.

The one-dimensional model was an element of uniform width and length L, with $x=0$ at the fuse end, and $x=L$ at the charge end. $T(x,t)$ is the absolute temperature and $n(x,t)$ the mass per unit volume of porous solid (the effective solid density). As the reaction proceeds, the value of **n** changes from its initial value, n_0, (solid reactant), to a final value, n_∞, (solid product), so the value of **n** can be used as a measure of the extent of reaction. $p(x,t)$, $\rho(x,t)$, $\eta(x,t)$ and $u(x,t)$ are the gas pressure, gas density, solid fraction and volume flux of gas per unit cross-sectional area of porous solid, respectively. The energy equation can then be written as :-

$$\frac{\partial}{\partial t}\{(nc_s + (1-\eta)\rho c_g)(T - T_0)\} + \frac{\partial}{\partial x}\{\rho u c_g (T - T_0)\} - K\frac{\partial^2 T}{\partial x^2} = -q\frac{\partial n}{\partial t} \qquad (3.10)$$

where c_s and c_g are the specific heat capacities of the solid and the gas, respectively.

K is the effective thermal conductivity of the solid,

T_0 is the initial temperature of the solid,

q is the effective heat of reaction, observed if the solid is burnt at T_0.

The solid fraction η varies as the reaction proceeds, and is governed by the relationship :-

$$\eta = \eta_0 \frac{n}{n_0} \tag{3.11}$$

The equation of mass continuity is :-

$$\frac{\partial}{\partial t}(n + (1 - \eta)\rho) + \frac{\partial}{\partial x}(\rho u) = 0 \tag{3.12}$$

since mass can only be transported by gas motion. The reaction rate is assumed to depend only on n and T as follows :-

$$\frac{\partial n}{\partial t} = -f(n)r(T) \tag{3.13}$$

where

$$r(T) = r_0 exp\left(-\frac{E}{RT}\right) \quad when\ T \geq T^* \quad (ignition\ temperature) \tag{3.14}$$

(i.e. Arrhenius behaviour) and

$$r(T) = 0 \qquad when\ T < T^*$$

$$f(n) = n_0\left(\frac{n - n_\infty}{n_0 - n_\infty}\right)^l \tag{3.15}$$

where l is the order of reaction. In equation **(3.14)**, r_0 is a pre-exponential factor, E is the activation energy and R is the gas constant.

Gas flow through the porous solid is assumed to follow Darcy's law :-

$$u = -k\frac{\partial p}{\partial x} \qquad (3.16)$$

where k is the gas permeability constant. Finally they assumed that the gas obeys the perfect gas law :-

$$p = \frac{R\rho T}{M} \qquad (3.17)$$

where M is the molar mass of the gas.

The explicit method of solving the set of equations **3.10** to **3.17**, with the terms $\partial\rho/\partial t$ neglected, was developed with a fair degree of success. The requirement that the pressure must be prescribed at one end and the gas mass flux at the other, severely limited the model's application. Results showed that the major effect of gas production on the burning rate was though its influence on the combustion temperature, T_{max}. Hot gas moving ahead of the combustion front, increases the value of T_{max}. The fraction of evolved gas which moves ahead of the combustion front can vary with the conditions under which the burning mixture is confined and may vary as burning proceeds. The model was used to model the confinement conditions investigated by Beck [15]. The implicit solution used had the disadvantage of not working for orders of reaction l, less than 1. Beck used an order of reaction of 2/3 in his study of the $Sb/KMnO_4$ system.

Loyd and Andersson *et al.* [16] used a program THAFEM (Thermal and Heat Analysis by Finite Element Methods), a special-purpose medium-sized program for heat transfer analysis, to analyze slow burning gasless pyrotechnic compositions. The effect of parameters such as the initial temperature, the heat flux to the casing and surroundings, the heat of combustion and the thermal properties of the composition on the burning rate of the pyrotechnic were investigated. Simulations were done using the delay composition present in an illuminating compound as an example. Combination of both experimental results and simulations lead to a reduction in the total number of tests which needed to be carried out on the compound.

Widlund [17] made use of THAFEM to model the burning and the influences of

thermal perturbations on the combustion of a pyrotechnic. The model was a column of pyrotechnic composition surrounded by a metal (effectively inert) casing. Three examples were studied: a steel case and initial temperature of 20°C; an aluminum case and initial temperature 20°C; and a steel case with initial temperature of -40°C. Results obtained from the simulations were in good agreement with those obtained by experiment.

Beck and Brown [18] have made use of the two-dimensional finite element program TOPAZ, to simulate the heating of a pyrotechnic composition in a differential thermal analysis (DTA) instrument, by modelling the reaction within a DTA sample pan. This allowed for the investigation of the progress of the reaction and the temperature distribution in the sample, sample container and the instrument sensors.

Boddington and Laye *et al.* [19] used a numerical model to study the propagation of a combustion wave through a gasless pyrotechnic mixture. Their model was based on a pseudo one-dimensional approach which allowed for heat loss using a simple Newtonian heat transfer term. The model was used to reproduce trends in the burning rate, which were found experimentally, and for the prediction of conditions which would result in combustion failure. Calculations were performed using 121 moving mesh points, packed tightly around the area of maximum temperature gradient. This approach saved computer time without decreasing the precision.

Simulations carried out using the input parameters for three different pyrotechnic compositions gave reasonable reproduction of experimental results. Like all such studies, the availability of good kinetic data for the system being investigated is crucial. The model could be used to indicate conditions which might lead to combustion failure. The model [20] was extended to predict whether combustion transfer would occur between two pyrotechnics. The maximum thickness of a metal septum place between two pyrotechnic mixtures which would allow for combustion to be transferred could be predicted.

4. MEASUREMENT AND ANALYSIS OF TEMPERATURE PROFILES.

4.1 Experimental measurement.

The procedures used in the measurement of temperature-time profiles during pyrotechnic combustion have been described in detail [10,21-24]. The pyrotechnic composition is packed into a stainless-steel channel (shown in Figure 4.1). A noble metal thermocouple is imbedded in the composition during packing. This channel (1 mm thick and 30 mm long) packed with a 6 mm wide column of pyrotechnic mixture was modelled as a finite-element mesh, using the program MAZE, as shown in Figure 8.4.

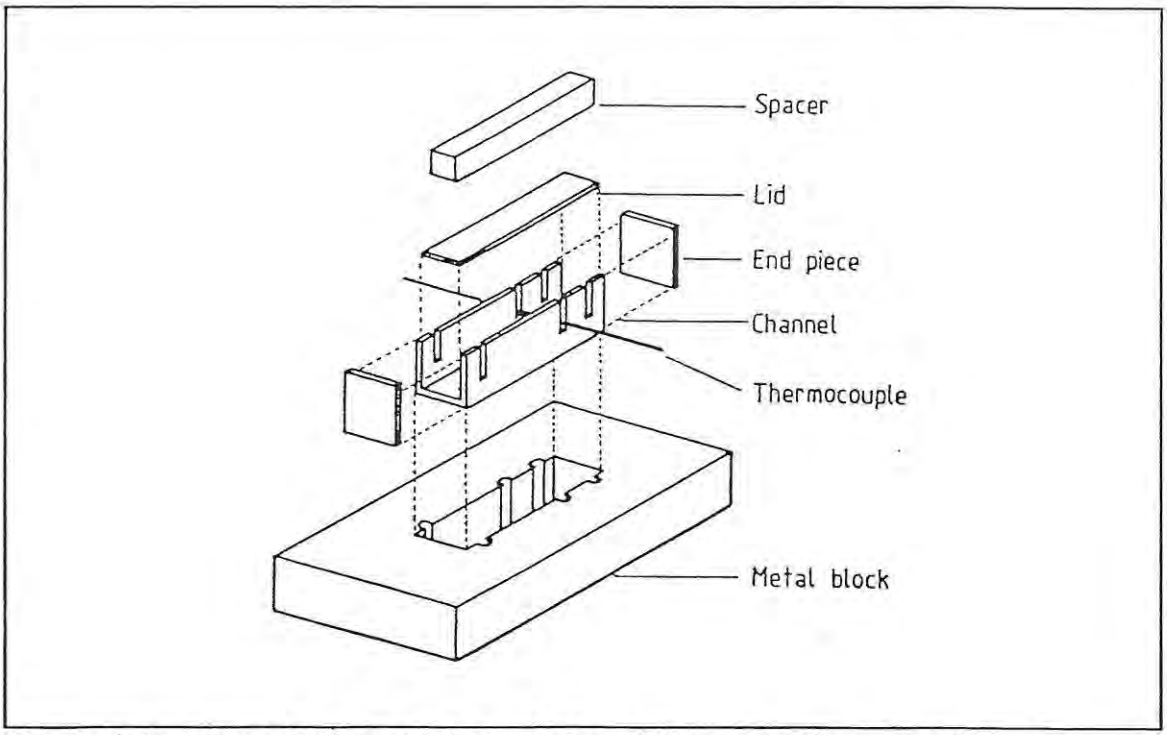

Figure 4.1: The stainless steel channel used in combustion experiments.

4.2 Extraction of kinetic and thermochemical information from profiles.

Several formulations of a model to describe the generation and conduction of heat in one-dimension along a column of a burning gasless pyrotechnic mixture have been proposed. These usually have many features in common while differing in some details, in the assumptions made and the symbols used. The usual starting point is the local heat balance equation (4.1) :-

$$\frac{\lambda}{v^2} T_{tt} - \rho c T_t + \rho w - h\left(T - T_a\right) = 0 \qquad (4.1)$$

where

$T_{tt} = d^2T/dt^2$ and $T_t = dT/dt$

v velocity of propagation of the combustion wave = dx/dt

λ thermal conductivity

c specific heat capacity

ρ density

w rate of evolution of heat per unit mass of reaction mixture

h lateral heat transfer coefficient.

Boddington *et al.* [10] substituted $U = T - T_a$, divided equation (4.1) by **ρc** and substituted $D = \lambda/\rho c$ (thermal diffusivity). This gives :-

$$Dv^{-2}U_{tt} - U_t + \frac{w}{c} - \frac{U}{t_{th}} = 0 \qquad (4.2)$$

where t_{th} (= ρc/h) is the thermal relaxation time of the system due to lateral conduction alone. In many treatments this term is neglected.

Substitution of **G** (the rate of temperature rise) for **w/c**, gives :-

$$t^*U_{tt} - U_t + G - Ut_{th}^{-1} = 0$$

where $t^* = Dv^{-2}$ is the rise time. The rise time, t^*, and thermal relaxation times, t_{th}, are

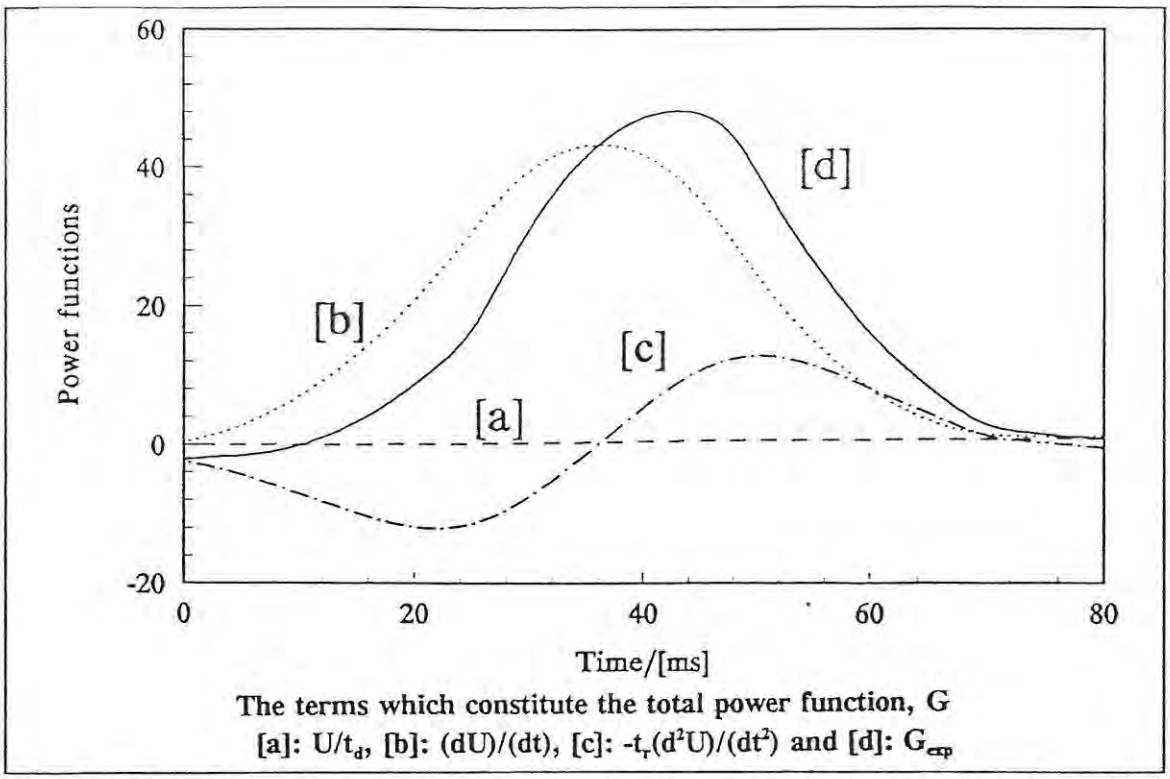

Figure 4.2: Thermal power components for a mixture containing 30% tungsten/potassium dichromate mixture burned in a 6 x 6 mm steel channel [10].

important parameters of temperature profiles and may be estimated from plots of ln U against time over the rise and decay regions, respectively. The relative contributions of the terms in equation (4.2) are illustrated [10] in Figure 4.2.

Since

$$t^* = \frac{\lambda}{\rho c v^2} = \frac{D}{v^2}$$

measurements of t^* can be used to predict the burning rate on the assumption of known λ, ρ and c, or values of t^* may be used, together with experimentally determined burning rates, to determine effective values of λ or D.

5. ESTABLISHMENT OF A "REFERENCE SYSTEM".

The "reference system" for modelling was chosen as the antimony (Sb) - potassium permanganate ($KMnO_4$) system, on account of the detailed experimental information available [15,25,26], see Tables 5.1 - 5.4.*

Table 5.1
Burning rates for Sb (< 8 μm)/$KMnO_4$ compositions in the open stainless-steel channel.

% Sb	Burning rate / mm s^{-1}	T_{max} / K
30	7.8 ± 0.1	1423
35	8.2 ± 0.1	
40	8.4 ± 0.1	
45	9.7 ± 0.1	
50	9.9 ± 0.2	1573

Table 5.2
Burning rate for Sb/$KMnO_4$ compositions containing 35% Sb of different particle size.

Sample No.	Particle-size range / μm	Burning rate / mm s^{-1}	T_{max} / K
1 "plant"	0 - 53	2.5 ± 0.1	1573
2	25 - 32	1.7 ± 0.1	1573
3	10 - 25	4.3 ± 0.1	1573
4	0 - 10	8.4 ± 0.1	1573
5	0 - 8	8.2 ± 0.1	1573

* Note that input to TOPAZ requires values in non-SI units and tables include such values for convenience.

Table 5.3
Enthalpies of reaction from bomb calorimetry.

% Sb	Heat Output / kJ g^{-1}	Heat Output / kcal g^{-1}
30	-1.22	-0.291
40	-1.23	-0.294
50	-1.15	-0.275
60	-1.97	-0.471
70	-0.68	-0.163

Table 5.4
Thermal properties of Sb/$KMnO_4$ compositions.

	measured		calculated		measured	
Sb/mass %	λ / W $m^{-1}K^{-1}$	λ / cal $s^{-1}cm^{-1}K^{-1}$	c^* / J K^{-1} g^{-1}	c / cal $K^{-1}g^{-1}$	ρ / g cm^{-3}	$D = \lambda/\rho c$ / 10^{-7} m^2s^{-1}
0†	0.22	5.3	0.753	0.180	1.69	1.7
30	0.28	6.7	0.589	0.141	2.22	2.1
40			0.535	0.128		
45			0.507	0.121		
50	0.32	7.6	0.480	0.114	2.57	2.6
100†	0.40	9.6	0.207	0.049	4.05	4.8

* by conversion from Table 5.3.
† References [10,25,26]

The composition was fixed at 30% Sb, again on account of the most reliable experimental results. The composition affects some of the other parameters; e.g. density, heat capacity, thermal conductivity and heat of reaction (see below).

In examining the experimental results [10,25,26] for the reference system, Tables 5.1 - 5.4, it is important to note that :

(i) the effect on the burning rate of changing the particle size of the fuel (Table 5.2) is large, giving burning rates ranging from 1.7 mm s^{-1} (coarse) to 8.4 mm s^{-1} (fine) (35% Sb). T_{max} values were approximately constant at 1300 °C, i.e. 1573 K.

(ii) The effect on the burning rate of changing the composition (with fixed particle size [0 - 8 μm = fine]) (Table 5.1) is much less than in (i). Burning rates increase from 7.8 mm s^{-1} at 30% Sb to 9.9 mm s^{-1} at 50% Sb. T_{max} increased slightly from 1200 to 1300 °C (1473 - 1573 K) with composition.

The experimental temperature profile for the 30% Sb/$KMnO_4$ composition [10,25,26] used as a reference in simulations (Figure 5.1) can be represented approximately by a sigmoid function of the type :

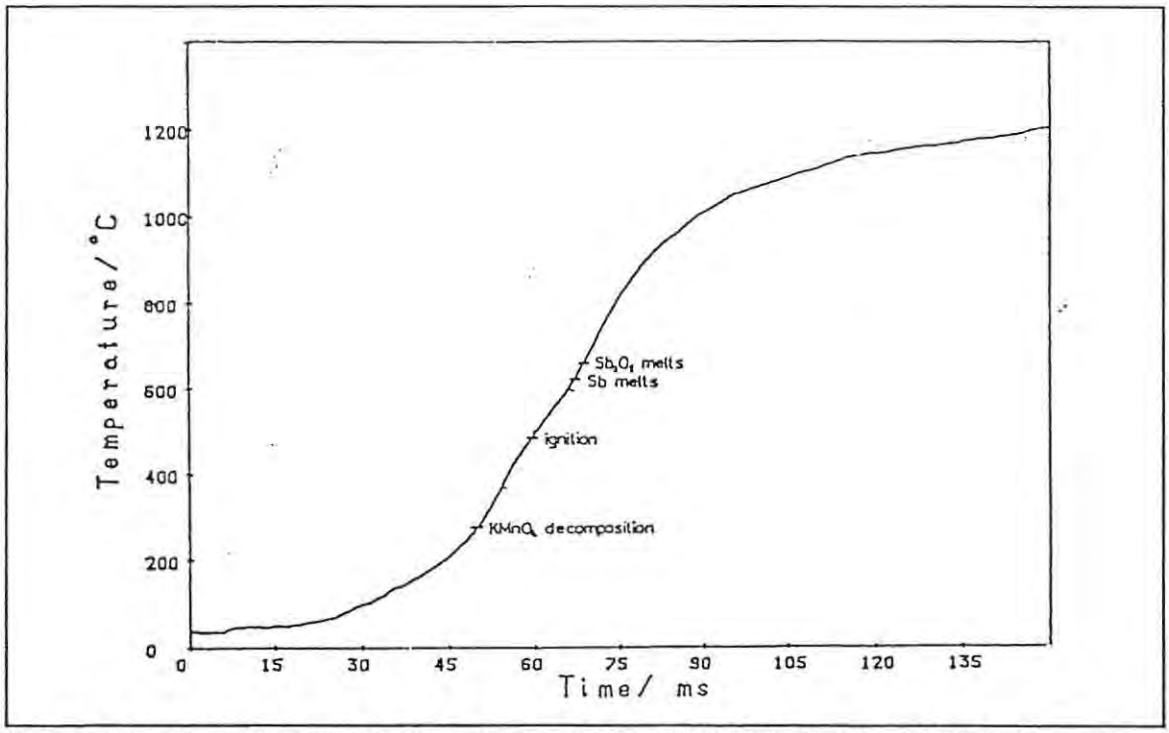

Figure 5.1: Experimental temperature profile of 30% Sb (< 8μm)/$KMnO_4$ system. NB. The onset temperatures of various changes, as determined from thermal analysis, are indicated.

$$\frac{U}{U_{max}} = 1 - exp\left[-(kt)^n\right] \qquad (5.1)$$

with constants $k = 4.2$ and $n = 12$.

This approximation allows the experimental profile to be generated as required for comparison with simulations (see Figure 5.2). The function in equation 5.1 is of the same form as the Avrami-Erofeev equation [5] used in solid state kinetics.

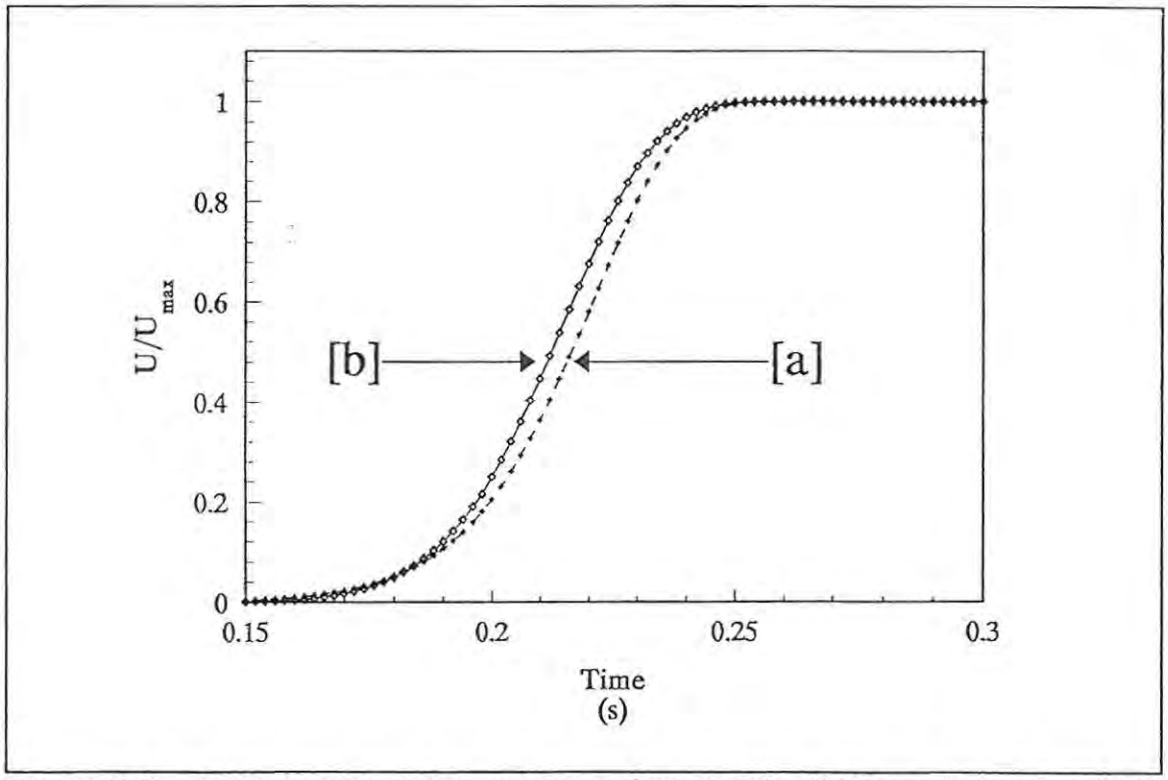

Figure 5.2: [a] Experimental temperature-time profile; [b] Plot of equation (5.1) n = 12 and k = 4.2.

6. ASPECTS OF STATISTICAL DESIGN OF CALCULATIONS FOR SIMULTANEOUS VARIATION OF SEVERAL VARIABLES.

6.1 Introduction.

Important parameters of pyrotechnic compositions, such as the burning rates and combustion temperatures, are influenced by many variables, as indicated in the previous section. Some attention was thus given to ways of reducing the numbers of possible combinations to manageable levels.

6.2 Central composite experimental design

Palasota and Deming [27] have given examples of the use of central composite designs to study the responses of chemical systems to simultaneous variation of two parameters, x_1 and x_2. For each of the i set of x_1 and x_2 values there is a single response, y_{1i}, assumed to be described by a second-order polynomial of the form :

$$y_{1i} = \beta_0 + \beta_1 x_{1i} + \beta_2 x_{2i} + \beta_{11}(x_{1i})^2 + \beta_{22}(x_{2i}1)^2 + \beta_{12} x_{1i} x_{2i} + r_{1i}$$

where β_0 is the intercept term; β_1 and β_2 are slopes with respect to each of the two factors; β_{11} and β_{22} are curvature terms; and β_{12} is the interaction term. The interaction term is a measure of how much the slope, with respect to one factor, changes as the other factor increases or decreases.

On the assumption that the polynomial above adequately describes the behaviour of the two-factor system, it is necessary to choose an experimental design which will provide sufficient data to estimate the ß coefficients. A central composite design [27] consists of a two-level full factorial design superimposed on a star design, as shown in Figure **6.1**. The centres of the two designs coincide. This design allows for the estimation of the ß coefficients in a codes factor space, where the coded values in the design matrix represent the following values that the two factors, x_1 and x_2, take for this particular design in a specified region of factor space :

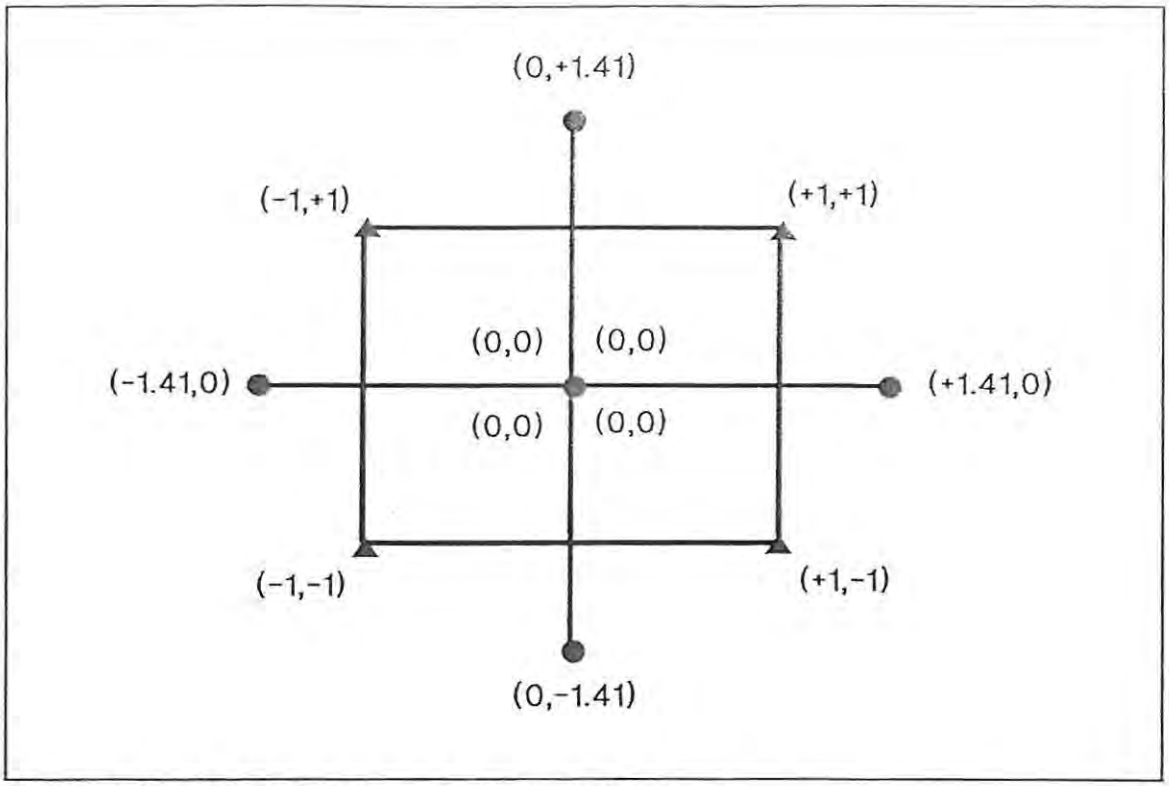

Figure 6.1: A two-factor central composite design.

the lowest value	$-\alpha$
the low value	-1
the middle value	0
the high value	+1
the highest value	$+\alpha$

where $\alpha = 2^{k/4}$ and k is the number of factors. For a two factor system $k = 2$ and $\alpha = 2^{½} = 1.41$. So a coded composite design for a system with two factors will take the form shown in Table 6.1.

Although the central composite design specifies only nine combinations of factors, three additional replicates, using the central point (0,0) factors, are usually done to determine the reproducibility of the experimental measurements.

This approach was used to investigate the effect of varying two parameters on the combustion of the pyrotechnic, in section 8.3.3.

Table 6.1
Coded central composite design for a system with two factors.

Design Point	Factor, x_1	Factor, x_2
1	+1	+1
2	+1	-1
3	-1	+1
4	-1	-1
5	0	0
6	+1.41	0
7	-1.41	0
8	0	+1.41
9	0	-1.41

7 ONE-DIMENSIONAL FINITE-DIFFERENCE SIMULATIONS.

7.1 Background.

7.1.1 Introduction

Use of finite difference methods to simulate one-dimensional heat transfer along a bar of uniform material is a standard application [28]. Some discussions of such problems allow for the presence of heat sinks or heat sources. Occurrence of phase transitions (such as melting), or an endothermic chemical reaction could act as a heat sink, while the presence of an electrical heating element, or the occurrence of an exothermic chemical reaction could act as a heat source.

Attention has also been focused on simulation of flames [29] which is a more complicated process involving mass transfer and heat transfer, together with chemical reaction. Norgrove *et al.* [14] have simulated one-dimensional combustion of a porous column of pyrotechnic composition, with allowance for the diffusion of gases (see section 3.3).

7.1.2 The one-dimensional conduction model

The one-dimensional column, see Figure 7.1, is divided into $n+2$ elements separated by nodes. The elements have a uniform width of Δx and unit cross-sectional area. The two end elements 0 and $n+1$, are "fictitious" elements which are used to allow for heating or cooling processes at either or both ends. The specific heat capacity of the material is c and hence the heat capacity per unit volume is ρc where ρ is the density. The thermal conductivity of the material in the element is λ. It is assumed that values of λ, ρ and c are independent of temperature.

Given a set of initial conditions, the problem then is to calculate the way in which the temperature of node i varies with time. This temperature will be represented by $T_{i,j}$ where j is the number of time intervals, Δt, which have elapsed.

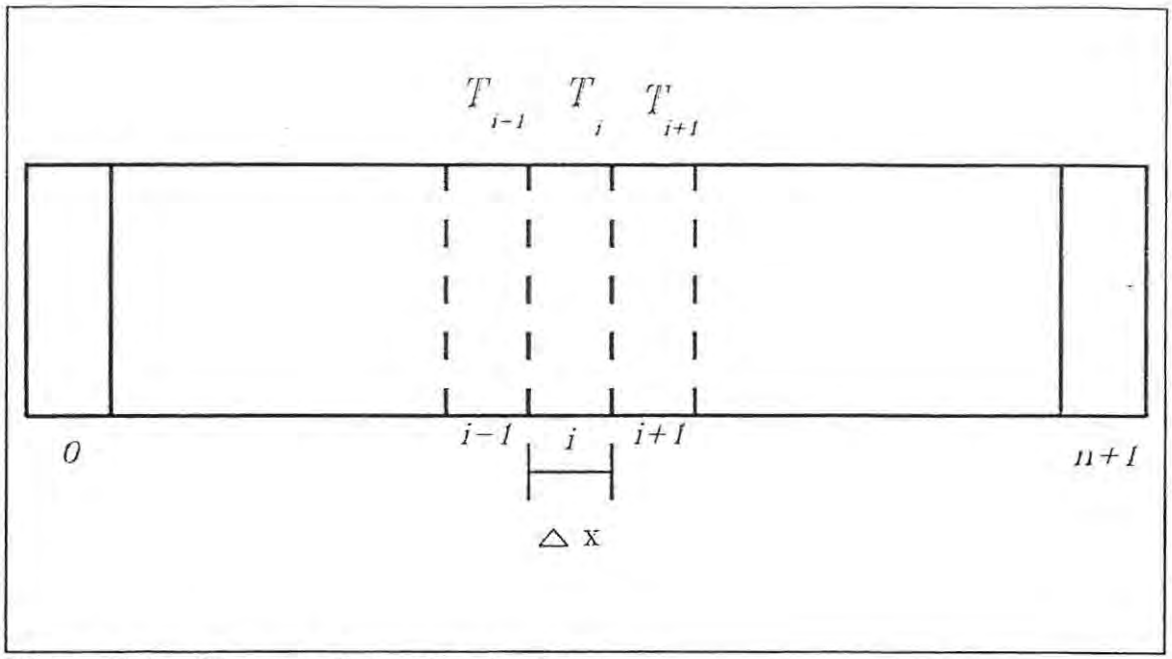

Figure 7.1: The one-dimensional column.

The various types of idealized boundary conditions [30] for the problem are :-

(1) prescribed surface temperatures (Dirichlet condition).

(2) prescribed heat input (Neumann condition), with one limit being a perfectly insulated surface (no heat transfer).

(3) convection cooling to ambient temperature, T_a (Robbins condition)

$$\frac{\partial T}{dx} = -\frac{h}{\lambda}\left(T - T_a\right)$$

(4) radiative cooling

$$\frac{\partial T}{\partial x} = -\frac{FE\sigma}{\lambda}\left(T^4 - T_a^4\right)$$

(F= geometrical factor, E= emissivity and σ= Stefan-Boltzmann constant)

7.1.3 Methods of solution

Finite difference problems may be solved [28] by explicit methods, implicit methods, or mixed explicit/implicit methods.

In *explicit* methods the temperatures at nodes, T_i', at time $t + \Delta t$, are predicted from the known temperatures, T_{i-1}, T_i and T_{i+1} at time t.

In *implicit* methods, values of T_i' are obtained by solving sets of simultaneous equations involving values of T'_{i-1} and T'_{i+1} as well as the value of T_i.

The *explicit* solution in one-dimension [31] is :

For internal nodes ($i \neq 0$ or $n+1$)

$$T_{i,j+1} = T_{i,j} + F_o \left[T_{i-1,j} - 2T_{i,j} + T_{i+1,j}\right]$$

which may be written as :

$$T_{i,j+1} = F_o\left[T_{i-1,j} + T_{i+1,j} + T_{i,j}\left(\frac{1}{F_o} - 2\right)\right]$$

where F_o is the Fourier number,

$$F_o = \left(\frac{\lambda}{\rho c}\right)\left(\frac{\Delta t}{(\Delta x)^2}\right) = D\left(\frac{\Delta t}{(\Delta x)^2}\right)$$

and where $D = \lambda/\rho c$ is the thermal diffusivity. (Low values of F_o imply that a long time is required to heat or cool the body).

For the two boundary nodes ($i = 1$ and $i = n$)

(a) assuming convective cooling

$$T_{i,j+1} = 2F_o\left[Bi \cdot T_a + T_{2,j} + T_{1,j}\left(\frac{1}{2F_o} - 1 - Bi\right)\right]$$

$$T_{n,j+1} = 2F_o\left[Bi \cdot T_a + T_{n+1,j} + T_{n,j}\left(\frac{1}{2F_o} - 1 - Bi\right)\right]$$

where Bi is the Biot number ($Bi = (h/\lambda)\Delta x$) and h is the surface heat transfer coefficient. (Bi thus indicates the ratio of surface conductance to internal conduction).

(b) Assuming that the left-hand end is held constant at T_I, then

$$T_{1,j} = T_I = constant$$

The right-hand end will cool as in (a).

The *explicit* method only provides stable solutions for values of $F_o \leq 0.5$ [32]. Since $F_o = D(\Delta t/(\Delta x)^2)$, this condition restricts the choices of Δt and Δx, i.e. once the internodal spacing has been chosen, the maximum time interval which can be used in simulations of the system with thermal diffusivity, D, is determined. Norgrove *et al.* [14] also point out that for a narrow reaction zone ("thin flame") there is a restriction on the mesh spacing that $\Delta x < D/v$ where v is the burning rate.

The mixed *explicit/implicit* solution incorporates an adjustable weighting parameter, g. The finite difference equation for evaluating $T_{i,j+1}$ then becomes [33] :

$$-F_o \cdot g \cdot T_{i-1,j+1} + (1 + 2F_o \cdot g)T_{i,j+1} - F_o \cdot g \cdot T_{i+1,j+1}$$
$$= F_o(1 - g)T_{i-1,j} + [1 - 2F_o(1 - g)T_{i,j}] + F_o(1 - g)T_{i+1,j}$$

Putting $g = 0$ gives the *explicit* form and $g = 1$ gives the *implicit* form.

The choice of the value of g may be governed by the complexity of the equations to be solved. Croft and Lilley [33] mention that for problems involving variable conductivity or heat generation terms, g should be close to 1. The choice of $g = 0.5$ gives the least truncation error for the always stable system [33], and the choice of $F_o = 1$ gives the simplest formulation of the Crank - Nicholson method [34], i.e. at the interior points :

$$-T_{i-1,j+1} + 4T_{i,j+1} - T_{i+1,j+1} = T_{i-1,j} + T_{i+1,j}$$

For convective cooling at each end

$$\frac{\partial T}{\partial x} = \frac{h}{\lambda}(T - T_a) \quad on\ LH\ end \quad and \quad = -\frac{h}{\lambda}(T - T_a) \quad on\ RH\ end$$

The equations for the ends are :

Left-hand end:

$$-(4 + 2Bi)T_{1,j+1} + 2T_{2,j+1} = -2T_{2,j} + 2Bi(T_{1,j} - 2T_a)$$

Right-hand end:

$$2T_{n-1,j+1} - (4 + 2Bi)T_{n,j+1} = -2T_{n-1,j} + 2Bi(T_{n,j} - 2T_a)$$

Solution of the set of simultaneous equations is done by Gauss elimination in a tridiagonal matrix [35].

7.1.4 **Allowance for chemical reaction**

In a small time interval, Δt, a uniform amount of reaction, $\Delta\alpha$, is assumed to occur throughout the element, where α is the extent of reaction. Generally reaction is assumed to be of order, n, and to follow Arrhenius temperature dependence, (see sections **3.3**) so that, in the simplest approximation (see below for extensions):

$$\therefore \Delta\alpha = A\ exp\left(\frac{-E}{RT}\right)(1 - \alpha)^n\ \Delta t$$

where **T** is the average temperature over the time interval, but is often taken as the temperature at the **start** of the interval; **A** is the pre-exponential factor; and **E** is the activation energy.

Carslaw and Jaeger [36] discuss the possible origins of heat production in solids and mention that as an alternative to Arrhenius-type behaviour, the rate of heat production may be linear, or some other exponential function of **T**.

The energy change accompanying an amount of reaction, $\Delta\alpha$, is

$$\Delta q = \Delta\alpha\ Q$$

where Q is the heat output for complete reaction. The temperature change due to reaction, ΔT_r, is then :-

$$\Delta T_r = \frac{\Delta q}{mc} = \frac{\Delta \alpha \, Q}{mc}$$

where c is the specific heat capacity and m is the mass. So, for a first-order reaction,

$$\Delta T_r = \frac{QA}{mc} \, exp\left(\frac{-E}{RT}\right)(1 - \alpha) \, \Delta t$$

Because of the small values of $\Delta\alpha$ calculated at low temperatures, it is sometimes convenient to introduce an "ignition temperature", T_{ign}. For reaction to occur, the temperature of the element at the start of the time interval, Δt, must then be equal to or greater than the ignition temperature, T_{ign}. If $\alpha \geq 1$ then $\Delta T_r = 0$, because the reaction is complete.

In their simulation of combustion transfer in pyrotechnic systems, Boddington and Laye [19,20] expressed $\Delta\alpha$ more accurately, through use of a second-order Taylor expansion, as :

$$\Delta \alpha = \frac{\left(\phi_i \Delta t + \phi_u \Delta U \Delta t + 0.5 \Delta t \phi_{UU} \Delta U^2\right)}{\left(1 - \phi_\alpha \Delta t - \phi_{U\alpha} \Delta U \Delta t\right)} = \frac{N}{D}$$

The numerator, N (for first-order reaction)

$$N = \Delta t\left(\phi_i + \phi_U \Delta U + 0.5 \phi_{UU} \Delta U^2\right)$$

where

$$\phi_i = f(U)g(\alpha) = Ae^{\frac{-B}{T}}(1 - \alpha)$$

$$\phi_U = f'(U)g(\alpha) = \frac{AB}{T^2} e^{\frac{-B}{T}}(1 - \alpha)$$

$$\phi_{UU} = f''(U)g(\alpha) = \frac{AB}{T^3} e^{\frac{-B}{T}}\left(\frac{B}{T} - 2\right)(1 - \alpha)$$

and where $B = E/R$.

So

$$N = (1 - \alpha)Ae^{\frac{-B}{T}}\Delta t\left[1 + \frac{B}{T^2}\Delta U + 0.5\Delta U^2\left(\frac{B}{T^3}\right)\left(\frac{B}{T} - 2\right)\right]$$

$$= k(1 - \alpha)\Delta t\left[1 + \frac{B}{T^2}\Delta U + 0.5\Delta U^2\left(\frac{B}{T^3}\right)\left(\frac{B}{T} - 2\right)\right]$$

The Denominator, D (for first-order reaction)

$$D = 1 - \phi_\alpha \Delta t - \phi_{U\alpha}\Delta U\Delta t$$

where

$$\phi_\alpha = f(U)g'(\alpha) = 0 \quad for \quad n = 1$$
$$\phi_{U\alpha} = f'(U)g'(\alpha) = 0 \quad for \quad n = 1$$
$$\therefore D = 1$$
$$\Delta\alpha = N$$
$$\Delta U = \frac{Q}{mc}\Delta\alpha$$

7.1.5 **Conversion to dimensionless quantities**

There is a divergence of opinion [37] on the use of dimensionless quantities in finite difference equations. Such conversions add to the generality of the solutions [38], but may hide the intrusion of errors which can best be monitored by comparison of simulations with experimental results. Smith [39] illustrates the transformation to non-dimensional form by making the substitutions :-

$$x = \frac{X}{L} \quad and \quad u = \frac{T}{T_{ref}}$$

where L is the conduction length and T_{ref} is some selected reference temperature. Non-dimensional time is obtained by taking $\frac{t}{t_{ref}}$, where $t_{ref} = \frac{L^2}{D} = \frac{\rho c L^2}{\lambda}$.

Boddington *et al.* [19,20] used a non-dimensional form of their model equation (see section 4.2) :-

$$\rho c \frac{dT}{dt} = \lambda \frac{d^2T}{dx^2} - h(T - T_a) + w \qquad (7.1)$$

which was obtained by writing

$$\tau = \frac{t}{t_0} \qquad X = \frac{x}{L} \qquad \text{and} \qquad U = \frac{(T - T_a)}{(T_0 - T_a)}$$

where $\frac{1}{t_0} = A_0 \exp\left(\frac{-E_0}{RT}\right)$ and $L = (D_0 t_0)^{1/2}$

where A_o, E_0 and D_0 are arbitrary reference values of **A**, **E** and **D**.

The dimensionless rate of reaction :-

$$\frac{d\alpha}{d\tau} = f(U) \cdot g(\alpha)$$

$g(\alpha) = 1 - \alpha$ was assumed (i.e. first order reaction).

So equation (7.1) becomes :-

$$\frac{dU}{d\tau} = \frac{D}{D_0} \frac{d^2U}{dX^2} - ZU + \frac{U_{ad}}{T_0 - T_a}(1 - \alpha) \frac{A \exp\left(\frac{-E}{RT}\right)}{A_0 \exp\left(\frac{-E_0}{RT_0}\right)}$$

where $Z = \frac{Rt_0}{(\lambda c)}$ and $U_{ad} = \frac{Q}{c}$.

7.2 Results for finite-difference simulation of combustion in a 1-D column of pyrotechnic composition.

7.2.1 Assumptions.

In applying this model to the simulation of combustion in a column of pyrotechnic composition, it is assumed that :-

(i) the temperature sensors measure the temperature without interfering with the system;

(ii) energy is transported in the column by conduction only;

(iii) values of the heat capacity, density and thermal conductivity are uniform throughout the column and are independent of the temperature;

and (iv) there is no lateral heat loss through the walls of the container.

The validity of these assumptions is discussed later.

7.2.2 Initial and boundary conditions.

Initially all nodes, other than the left-hand end, are set to ambient temperature. The right-hand end is cooled by convection (controlled by the value set for the Biot number) relative to ambient temperature. The ignition process is simulated by setting the left-hand end node to an initial temperature T_1 (usually $\geq$ the ignition temperature, T_{ign}). This temperature can either be maintained, or the end can be allowed to cool after some selected time interval.

7.2.3 Program for first-order kinetics.

Program I (see Appendix I) was devised, using the explicit method and first-order

Table 7.1
Input data for the "reference system" (Chapter 5).

Name	Symbol	Value	Units
Density	dens	2.2×10^6	$g\ m^{-3}$
Specific heat capacity	spht	0.60	$J\ K^{-1}\ g^{-1}$
Thermal conductivity	cond	0.30	$J\ s^{-1}\ m^{-1}\ K^{-1}$
Heat of reaction	q	820	$J\ g^{-1}$
Activation energy	e!	35000	$J\ mol^{-1}$
Pre-exponential factor	a	100	s^{-1}
Reaction order		1	
The length of column used	el	0.002	m
Fourier number	fo	0.40	
Biot number	biot	0.0010	
The internodal spacing	delx	0.0001	m

kinetics, to produce temperature-time profiles at selected nodes. Burning rates were calculated from corresponding points on profiles using the internodal distance and the elapsed time. The input data used initially are given in Table **7.1**. Density, Specific heat capacity and thermal conductivity are taken (and rounded) from Table **5.4**. Heat of reaction, activation energy and the pre-exponential factor were taken from previous work done by Beck [15]. The initial simulations were based closely on this work.

7.2.4 Results for simulations using first-order kinetics and alternative kinetic expressions.

The profiles at node (8) and (14) obtained using the data in Table **7.1** are shown in Figure **7.2** relative to the experimental profile. The calculated burning rate is 3.1 mm s^{-1} and the maximum temperature was 1500 K, both of which are of the right order. It

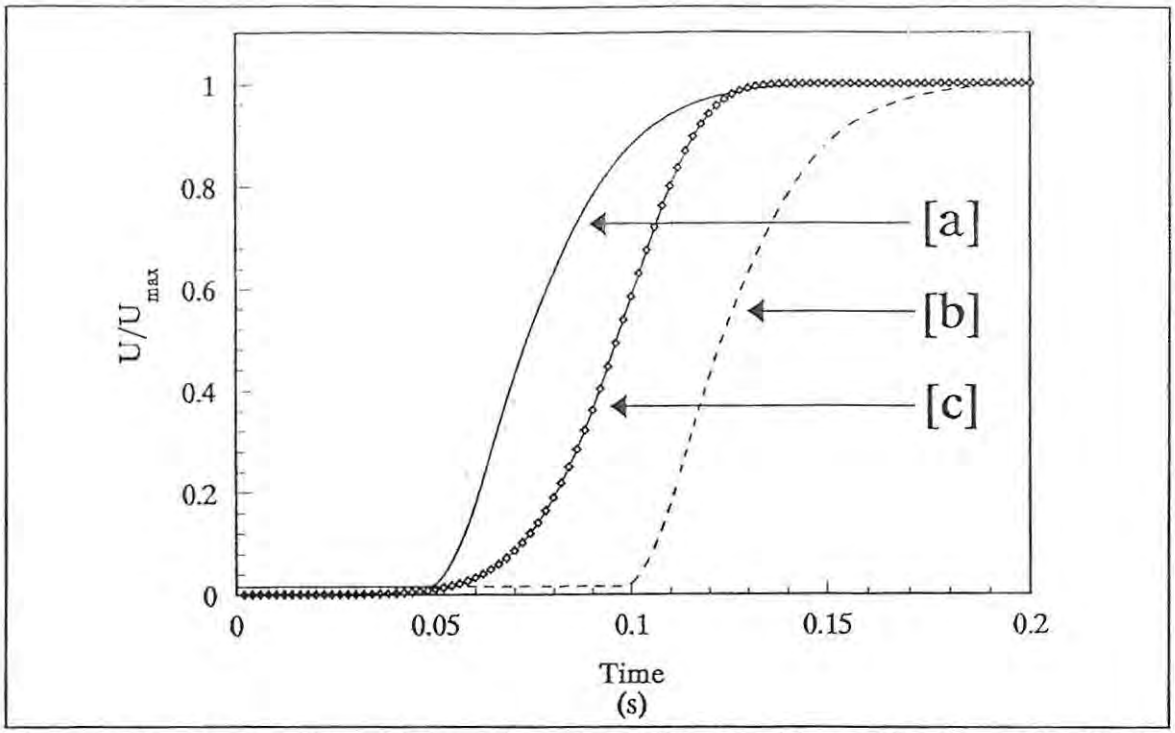

Figure 7.2: Comparison of the reference profile [c] with profiles for nodes (8) [a] and (14) [b], generated by Program I using the input data in Table 7.1.

was clear, however, that the profiles were too deceleratory in shape for what is an initially acceleratory process, and it was decided to substitute a sigmoid kinetic function for the generally used first-order rate equation (see section 3.3).

The two most commonly used sigmoid rate equations (see section 3.3) are the Prout-Tompkins equation (autocatalytic reactions) [6]:-

$$Rate = \frac{d\alpha}{dt} = k\alpha(1 - \alpha)$$

and the Johnson-Mehl-Avrami-Erofeev equation (derived from models of nucleation and growth) [5] :-

$$Rate = \frac{d\alpha}{dt} = nk(1 - \alpha)(-\ln(1 - \alpha))^{\frac{n-1}{n}}$$

n is a constant (often an integer) which is related, in the derivations, to the shape and rate

of growth of nuclei. For the purposes of this investigation, n is regarded as an empirically adjustable parameter. The effects of n on profile shape are shown in section 7.2.8.

Both equations require some additional term to enable reaction to get started and for both the initial α values throughout the column were set at 0.01. A further adjustment that had to be made, to bring the calculated profiles into the region of interest, was to increase the pre-exponential factor, **A**, from 100 s^{-1} to 500 s^{-1}.

7.2.5 **Program for Prout-Tompkins kinetics.**

Program **II** (see Appendix **II**) was devised, using the explicit method and Prout-Tompkins reaction kinetics, to produce time-temperature profiles at selected nodes (8) and (14). Burning times were calculated in the same manner as those obtained in section **7.2.4**. The input data used is given in Table **7.2**. Values used in Table **7.2** are based on those used for the previous simulations, using values from Table **7.1**. The only two

Table 7.2
Input data for Program II, for Figure 7.3.

Name	Symbol	Value	Units
Density	dens	2.2×10^6	g m^{-3}
Specific heat capacity	spht	0.60	J K^{-1} g^{-1}
Thermal conductivity	cond	0.30	J s^{-1} m^{-1} K^{-1}
Heat of reaction	q	820	J g^{-1}
Activation energy	e!	35000	J mol^{-1}
Pre-exponential factor	a	500	s^{-1}
Reaction order		1	
The length of column used	el	0.002	m
Fourier number	fo	0.20	
Biot number	biot	0.0010	
The internodal spacing	delx	0.0001	m

changes were to the value of the pre-exponential factor (100 s^{-1} to 500 s^{-1}) and the Fourier number (0.40 to 0.20). These values were chosen because they gave the closest correlation between the simulated and experimental curves.

7.2.6 Results for simulations using Prout-Tompkins kinetics.

The result of the simulation using the Prout-Tompkins kinetic model is shown in Figures **7.3**, profiles obtained at nodes (8) and (14) are compared with the experimental profile. A burning rate of 3.0 mm s^{-1} and a maximum temperature of 1474 K compared favourably with experimental values shown in Section 5. A quantitative comparison between the simulated profile and experimental profile was done using the squares of the residuals at common times :-

$$\frac{\left(\sum \left(U_s - U_e \right)^2 \right)}{N} \qquad (7.2)$$

where U_e and U_s are the experimental and simulated temperatures, respectively, and N is the number of points compared. A plot of the comparison is shown in Figure **7.4**. The calculation gave a residual of 0.000203.

7.2.7 Program for Johnson-Mehl-Avrami-Erofeev kinetics.

Program **III** (see appendix **III**) was devised to use Johnson-Mehl-Avrami-Erofeev kinetics, and give (using the explicit method) time-temperature profiles at nodes (8) and (14). The input data used are given in Table **7.3**.

7.2.8 Results of simulation using Johnson-Mehl-Avrami-Erofeev kinetics.

The profiles for nodes (8) and (14) obtained from the simulation are compared with the experimental profile in Figure **7.5**. The calculated burning rate for this profile was 3.4 mm s^{-1} and the maximum temperature was 1560 K, both values compared favourably with the experimental values of between 1.7 and 8.4 mm s^{-1} for the burning

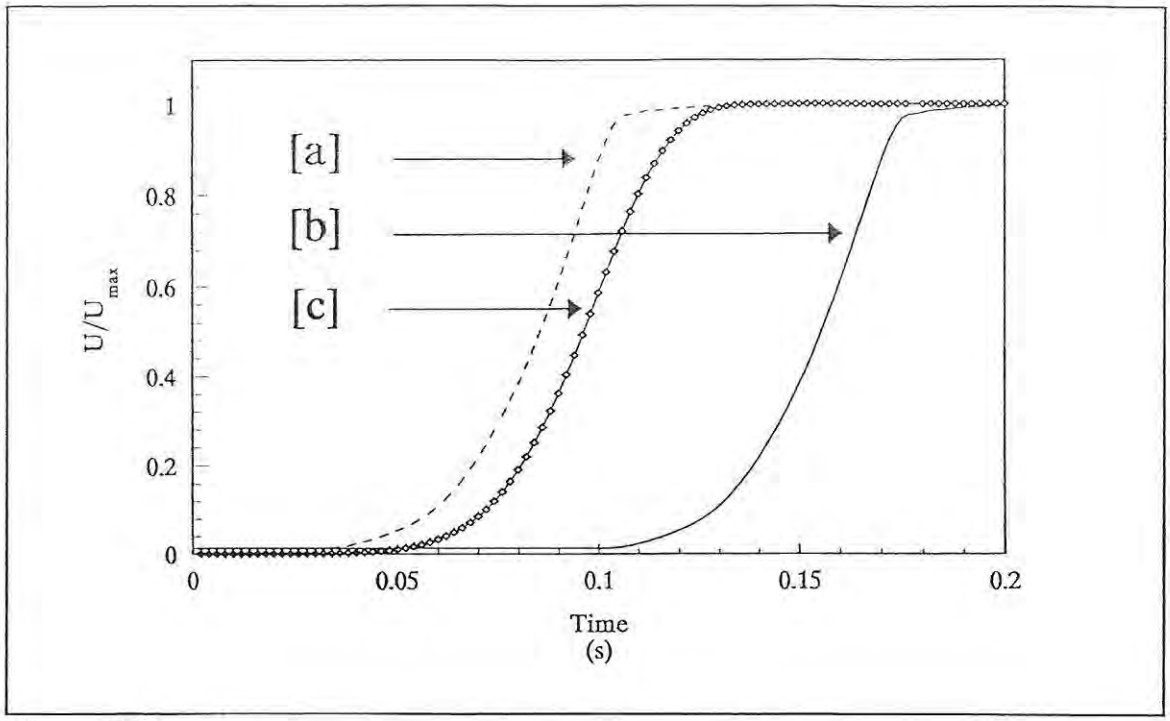

Figure 7.3: **Comparison of the reference profile [c] with profiles generated at nodes (8) [a] and (14) [b], using the Prout-Tompkins rate equation.**

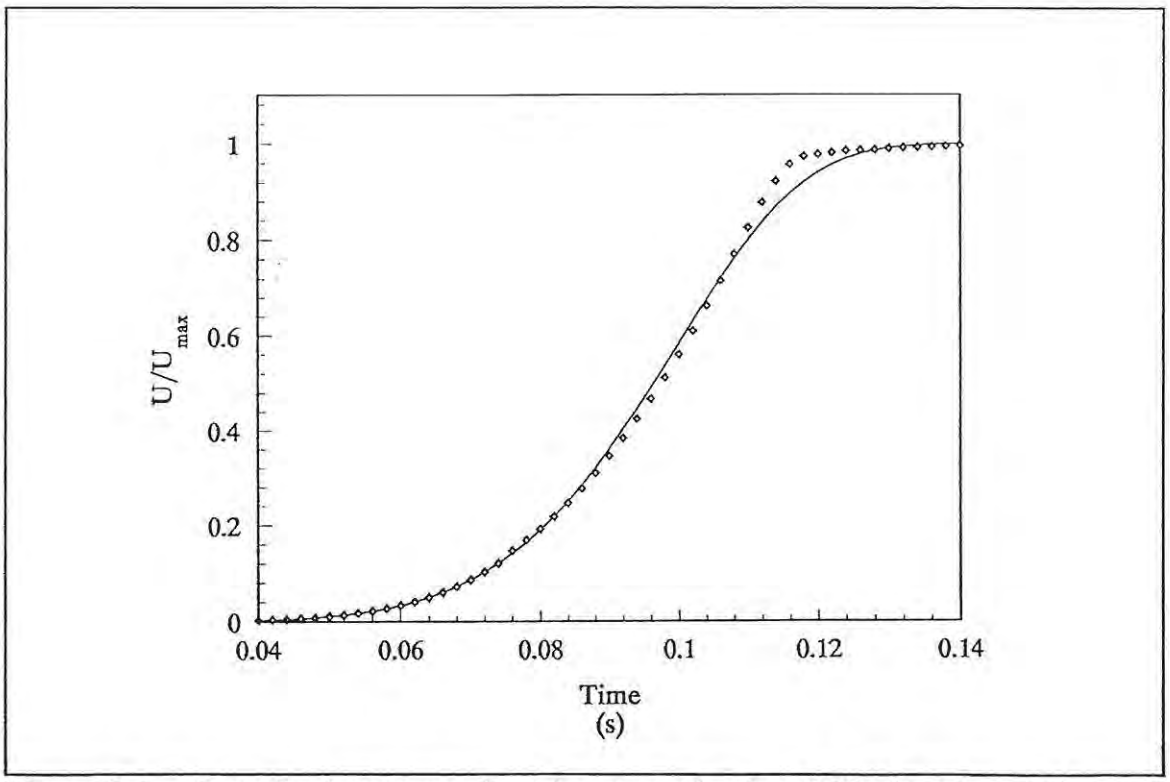

Figure 7.4: Quantitative comparison between simulated (line) and experimental (diamonds) profiles

Table 7.3
Input data for Program III, for Figure 7.7.

Name	Symbol	Value	Units
Density	dens	2.5×10^6	g m^{-3}
Specific heat capacity	spht	0.60	J K^{-1} g^{-1}
Thermal conductivity	cond	0.30	J s^{-1} m^{-1} K^{-1}
Heat of reaction	q	820	J g^{-1}
Activation energy	e!	35000	J mol^{-1}
Pre-exponential factor	a	700	s^{-1}
Reaction order	n	2	
The length of column used	el	0.002	m
Fourier number	fo	0.20	
Biot number	biot	0.0010	
The internodal spacing	delx	0.0001	m

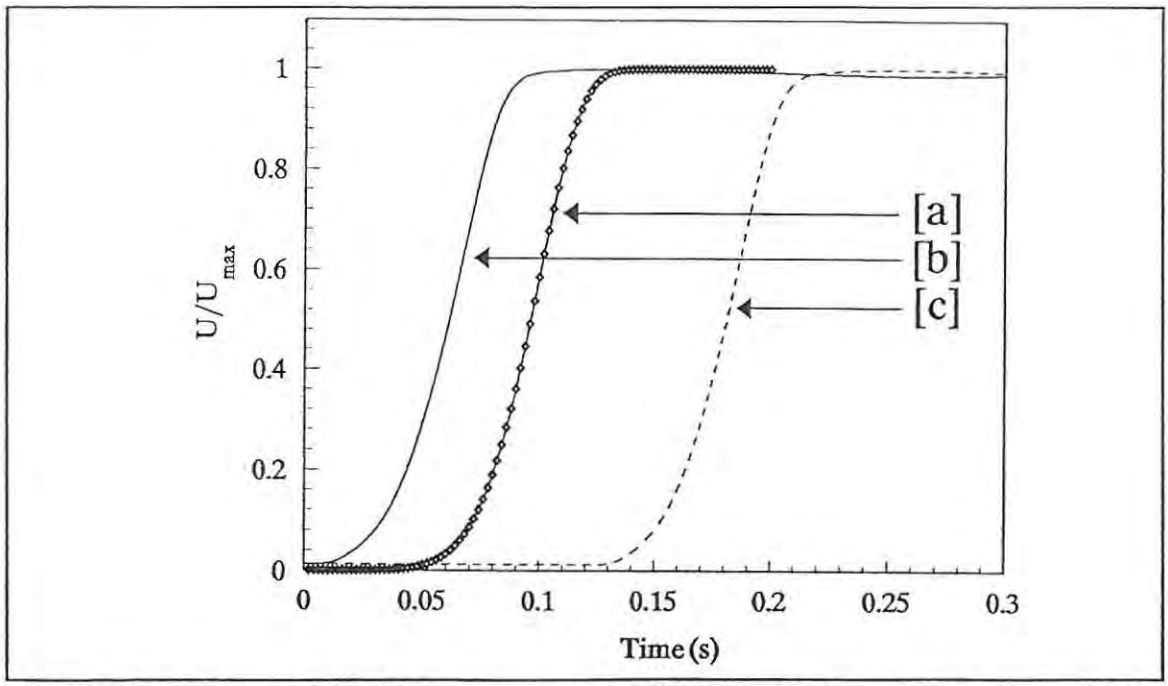

Figure 7.5: Comparison of the reference profile [a] with the profiles generated by simulation at node (8) [b] and (14) [c], using Johnson-Mehl-Avrami-Erofeev kinetics.

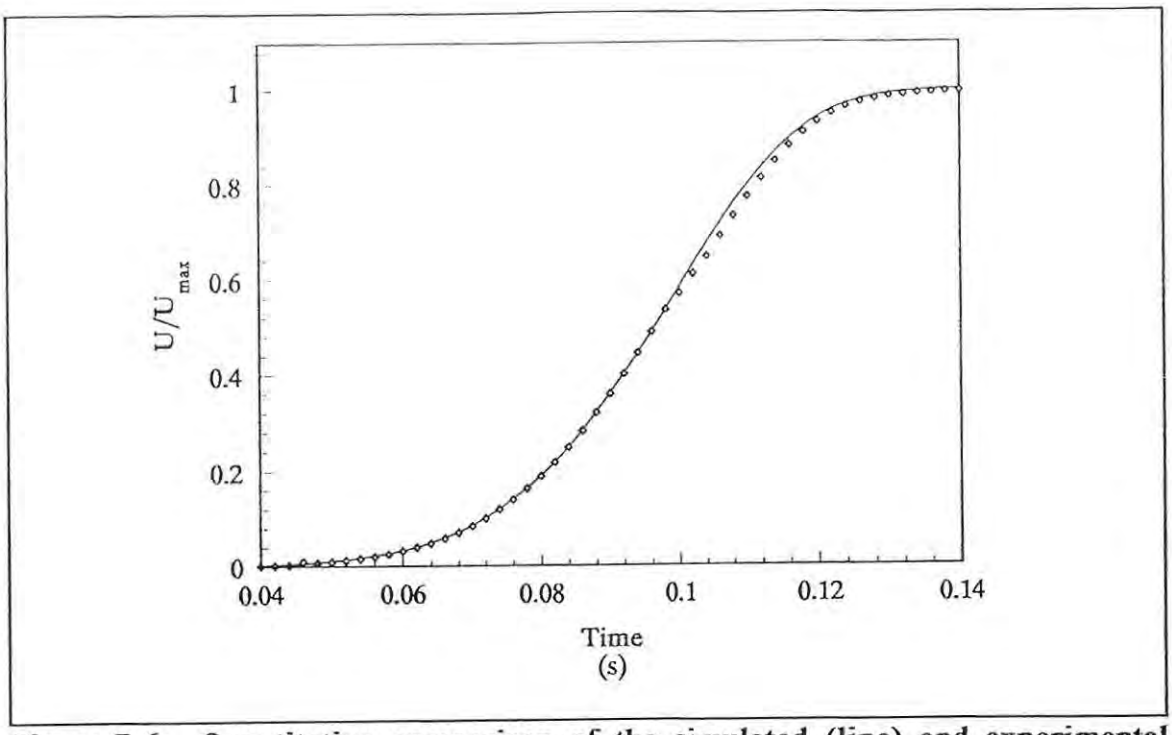

Figure 7.6: Quantitative comparison of the simulated (line) and experimental (diamond) profiles.

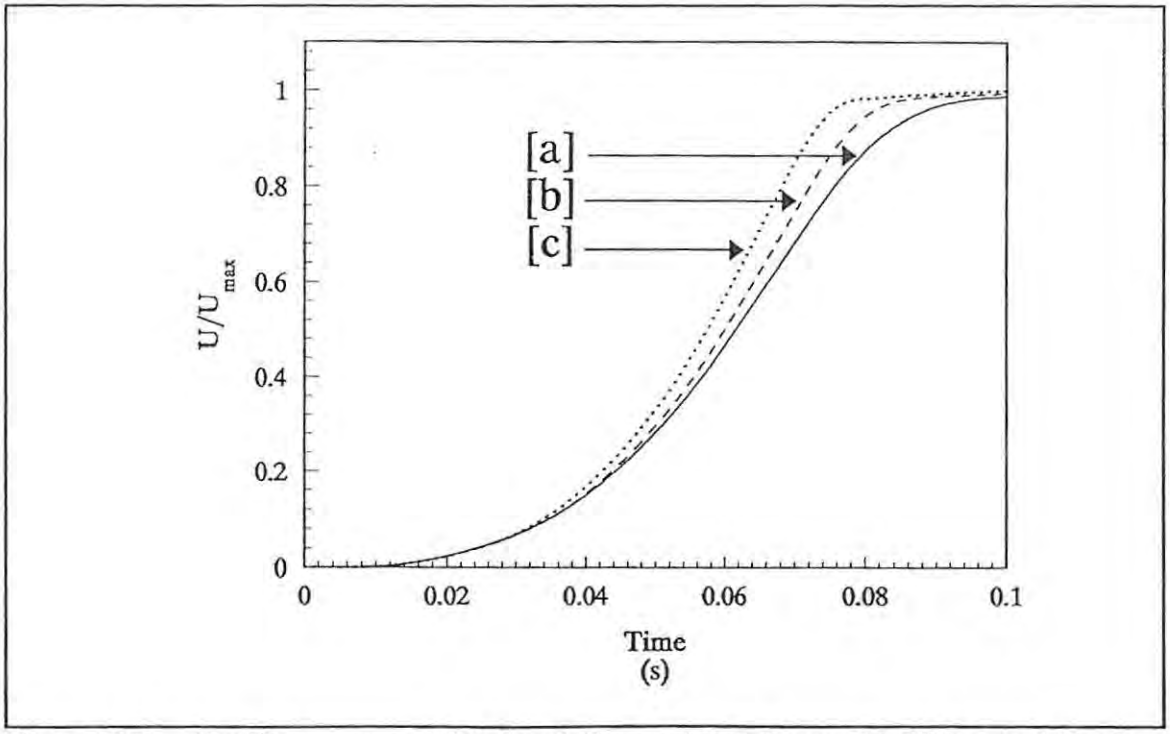

Figure 7.7: Profiles generated by simulations using Johnson-Mehl-Avrami-Erofeev kinetics, using values of *n* of 2 [a], 3 [b] and 4 [c].

rate and 1573 K for the maximum temperature. Quantitative comparison of the simulated and experimental profiles was done using Equation 7.2, and this gave the comparison shown in Figure 7.6. The calculated value for the comparison was 0.000174, which shows that there is greater correlation between the profile generated by using Johnson-Mehl-Avrami-Erofeev kinetics and the experimental profile, than there was between the Prout-Tompkins simulation and experiment.

The Johnson-Mehl-Avrami-Erofeev model requires the setting of an additional variable, **n**. Investigation into the effect of this variable on the simulated profiles yielded the results shown in Figure 7.7. As the value of n increases the profile becomes steeper and the deceleratory part of the profile becomes more abrupt. A value of $n = 2$ gave the best agreement. This rather arbitrary choice of the value of n makes the use of the simpler Prout-Tompkins kinetic model preferable.

The shapes of the profiles are in much better agreement with the experimental profile than was found for first-order kinetics and the calculated burning rate was 3.0 mm s^{-1} for the Prout-Tompkins and 3.4 mm s^{-1} for the Johnson-Mehl-Avrami-Erofeev model. Maximum temperatures of 1474 K and 1560 K were obtained, respectively.

7.3 Influence of variables.

In this section the effect on the temperature-time profile of changing certain variables within allowable ranges is examined. The variables chosen were (a) physical properties: thermal conductivity, λ, heat capacity, c, density, ρ, the Fourier number, F_o, and the Biot number, B_i, and (b) kinetic parameters: the pre-exponential factor, **A**, and the activation energy, **E**. All simulations were done using the first-order kinetic model. To allow for the examination of the effect of varying a specified parameter on the maximum temperature, U_{max} was chosen as the maximum for the set of simulations done in the investigation of effect of the specified parameter.

7.3.1 The influence of physical properties.

7.3.1.1 Thermal conductivity, λ.

Changing the value of thermal conductivity, λ, from 0.22 (λ for pure Sb) to 0.4 W m^{-1} K^{-1} (λ for pure $KMnO_4$) resulted in an increase in burning rate (1.9 to 3.4 mm s^{-1}), and also an increase in the cooling rate (shown by the steeper gradient of the curve in the cooling zone in Figure **7.8**) after combustion. The maximum temperature did not change significantly. The increasing burning rate
is also evident through the decrease in rise time of the profile (section **4**). Experimentally the burning rate increases with increasing proportion of Sb present in the composition and this also corresponds with an increase in the thermal conductivity of the pyrotechnic composition. So the resulting increase in the burning rate of the simulated system corresponds with that found experimentally.

7.3.1.2 Heat capacity, *c*.

Changing the value of heat capacity from 0.2 (pure Sb) to 0.75 J K^{-1} g^{-1} (pure $KMnO_4$) resulted in dramatic changes in both the maximum temperature (from 3050 K to 1300 K respectively) and the burning rates (3.8 mm s^{-1} to 0.9 mm s^{-1}) as shown in Figure **7.9**. This result is to be expected since the amount of energy generated by reaction is held constant while the heat capacity is increased.

7.3.1.3 Density, ρ

Changing the value of the density used from 3.5 g cm^{-3} (pure $KMnO_4$) through to 6.7 g cm^{-3} (pure Sb) resulted in the profiles shown in Figure **7.10**. These profiles showed that with decreasing density there was a decrease in both the maximum temperature and the burning rate. Heat transfer through a less dense material is, in general, slower than in a material of higher density, this would account for the slowing

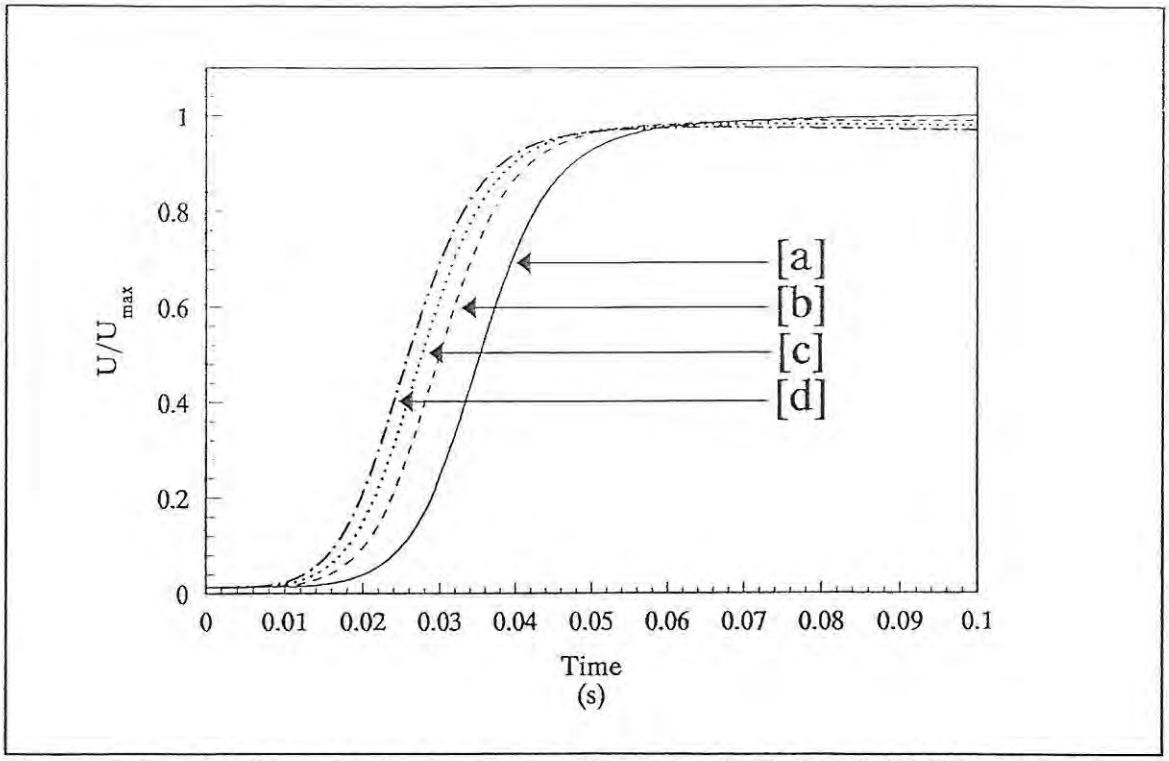

Figure 7.8: Profiles obtained by using the values 0.22 [a], 0.30 [b], 0.35 [c] and 0.40 [d] W m^{-1} K^{-1} for the thermal conductivity, λ.

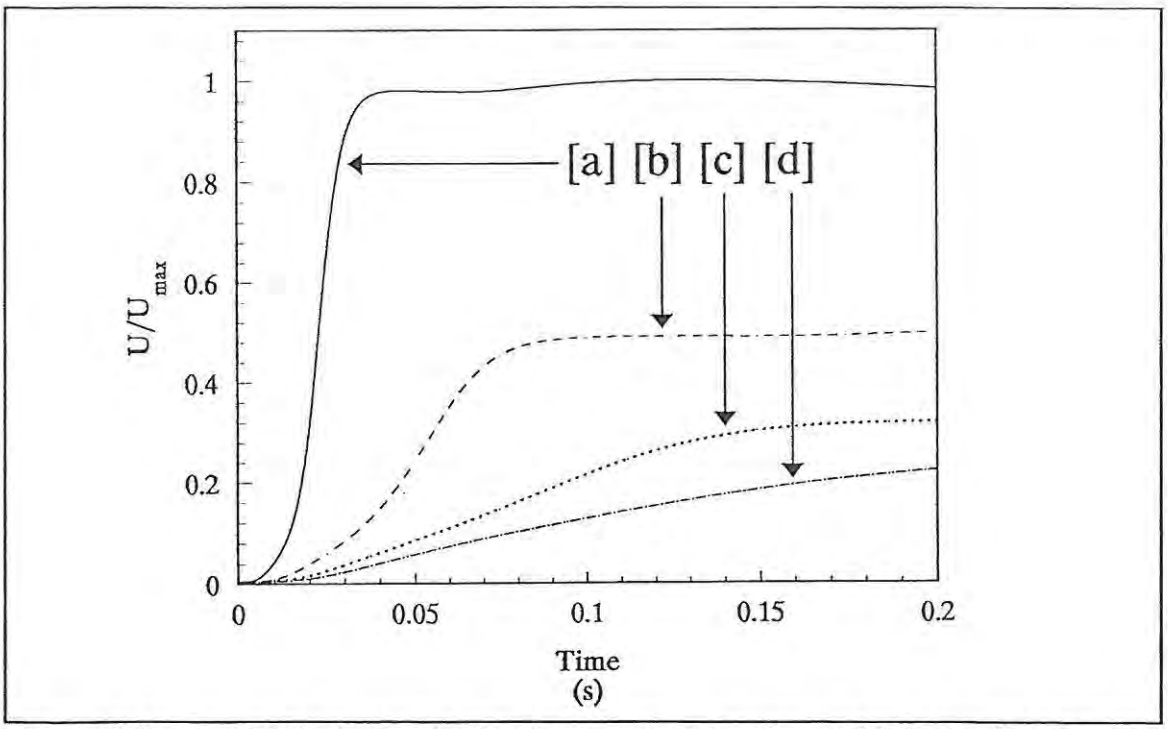

Figure 7.9: Profiles obtained using heat capacity values of 0.2 [a], 0.4 [b], 0.6 [c] and 0.75 [d] J K^{-1} g^{-1}.

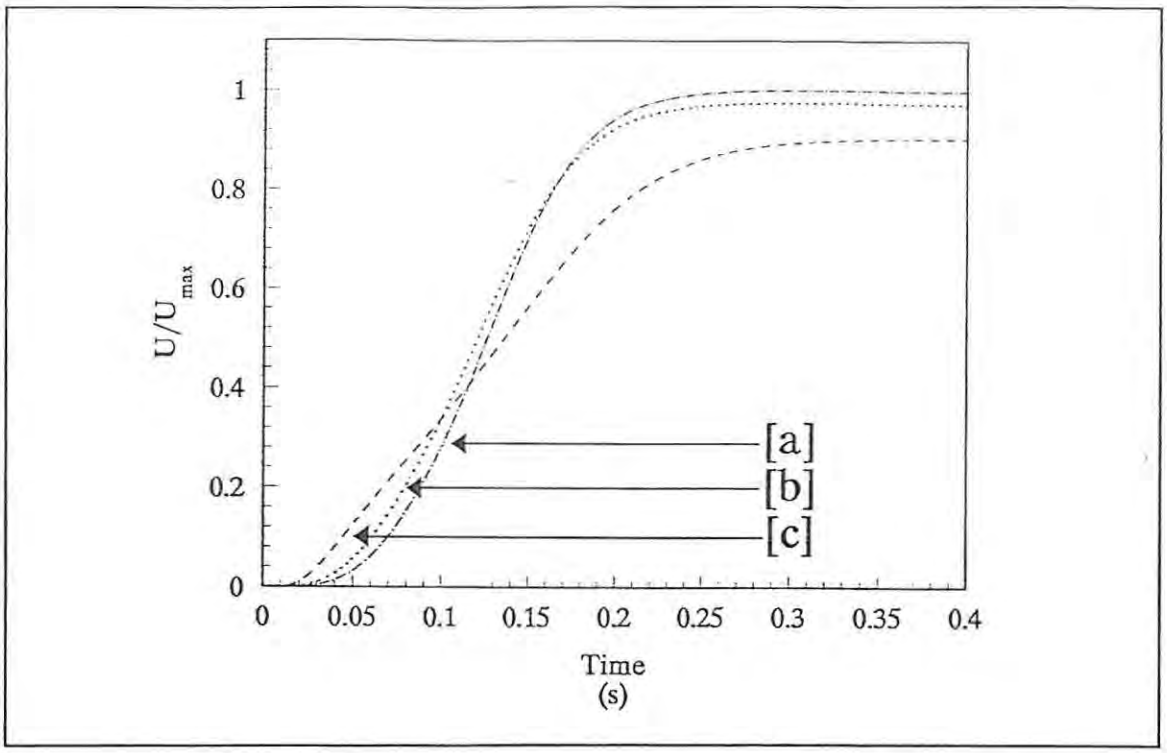

Figure 7.10: Profiles obtained using density values of 6.7 [a], 5.5 [b] and 3.5 [c] g cm^{-3}

of the burning rate. Changing the composition of the Sb/$KMnO_4$ system from 50 % Sb to 30 % Sb results in a decrease in the burning rate (Table 5.1) corresponding to the decrease in density.

7.3.1.4 Fourier number, F_o.

Changing the Fourier number between the values of 0.4 and 0.15 resulted in the profiles shown in Figure 7.11. It should be noted that the simulation failed for values of the Fourier number of 0.12 or less, due to the reaction not being propagated down the column. With decreasing Fourier number there is an increasing resistance to heat being transferred down the column and hence slower rise times (and burning rates) and lower maximum temperatures were obtained.

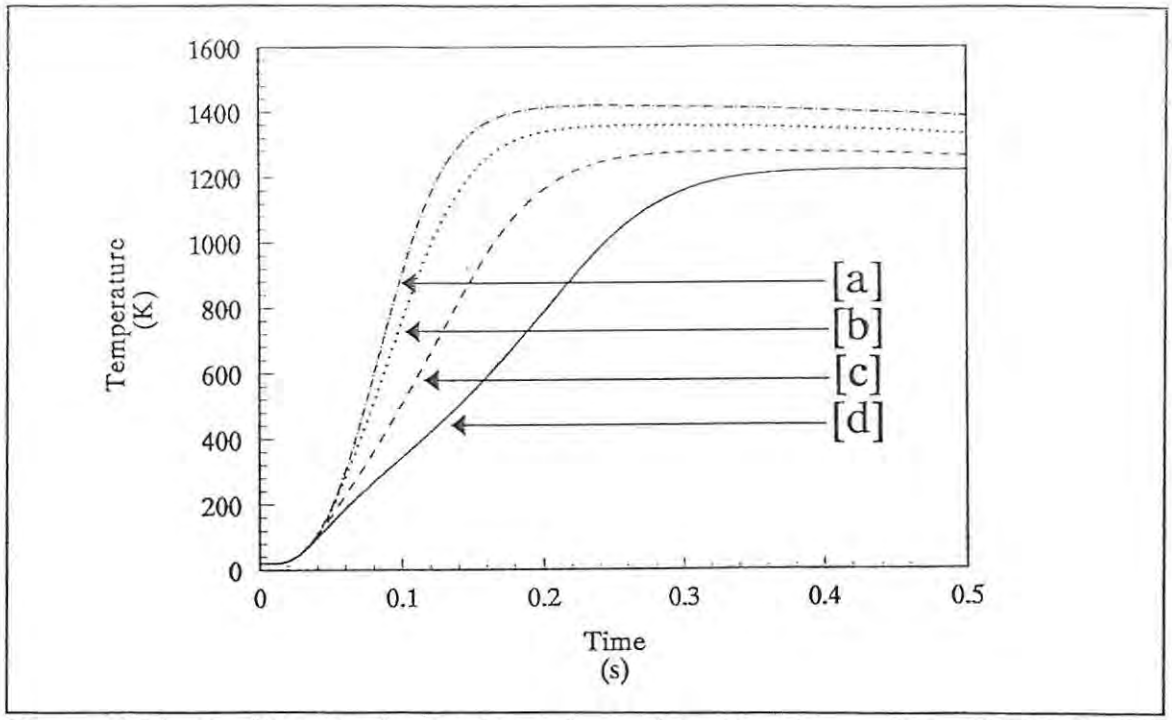

Figure 7.11: Profiles obtained using values of the Fourier number of 0.4 [a], 0.3 [b], 0.2 [c] and 0.15 [d].

7.3.1.5 Biot number, B_i.

The Biot number gives an estimate of the rate of heat loss at the ends of the column. The profiles obtained when varying the Biot number between 0 and 0.012 are shown in Figure 7.12. Values or 0.015 and above lead to a failure of combustion down the column, due to the rate of heat loss at the end being too great to allow for enough heat to be transferred down the column for combustion. Curves [a] and [b] show the effect of "reflected" heat from the right-hand end of the column, due to the rate of heat loss through the end of the column being less than the rate of heat transfer through the column. The right hand end of the column will therefore have a net positive heat flow and this will cause the temperature of the end nodes to increase, so affecting the nodes further down the column.

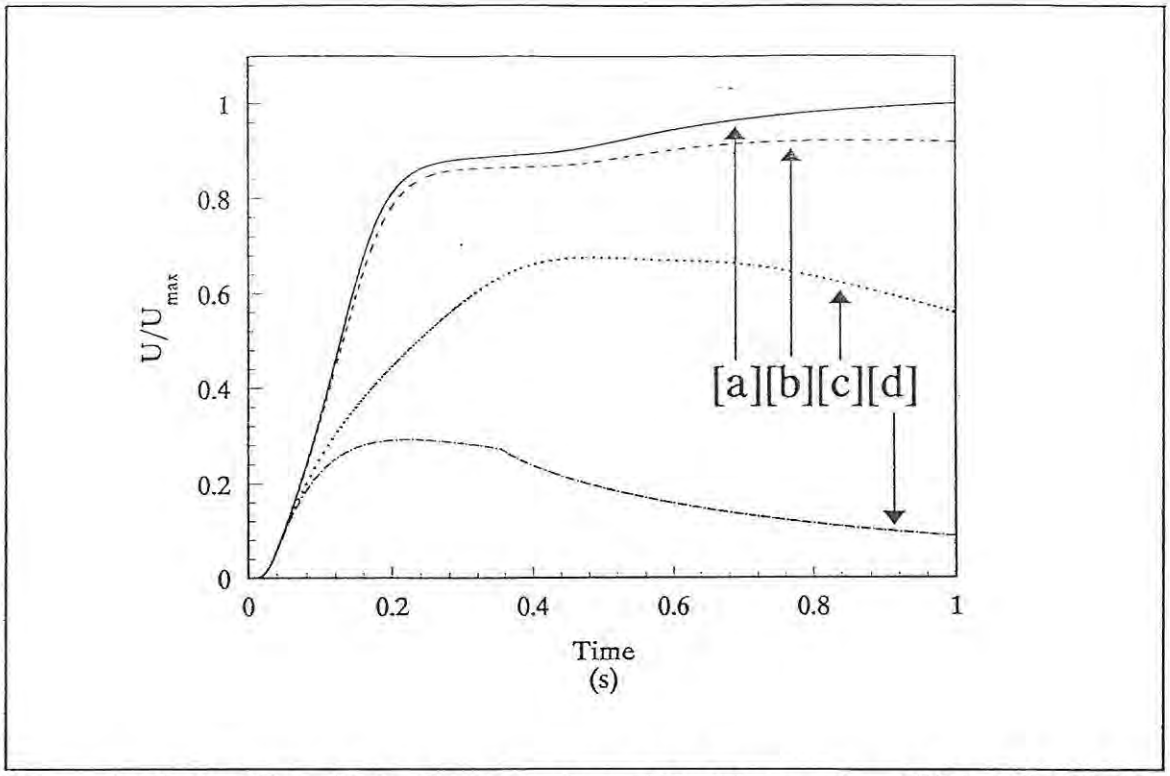

Figure 7.12: Profiles obtained using values of the Biot number of 0 [a], 0.001 [b], 0.01 [c] and 0.012 [d].

7.3.2 The influence of kinetic parameters.

7.3.2.1 The pre-exponential factor, A.

A series of simulations were done varying the value of **A** from 100 s^{-1} to 2000 s^{-1}, while keeping E constant at 35 kJ mol^{-1}, and the resulting temperature-time profiles are shown in Figure **7.13**. Increasing the value of **A** increases both the burning rate (0.9 to 7.5 mm s^{-1}) and the maximum temperature (1394 to 1575 K). An increase in the value of **A** causes an increase in the rate coefficient (following the Arrhenius equation), and it follows that for a simple "order-of-reaction" model there will be an increase in the rate of change of the reaction, and hence an increase in the calculated burning rate.

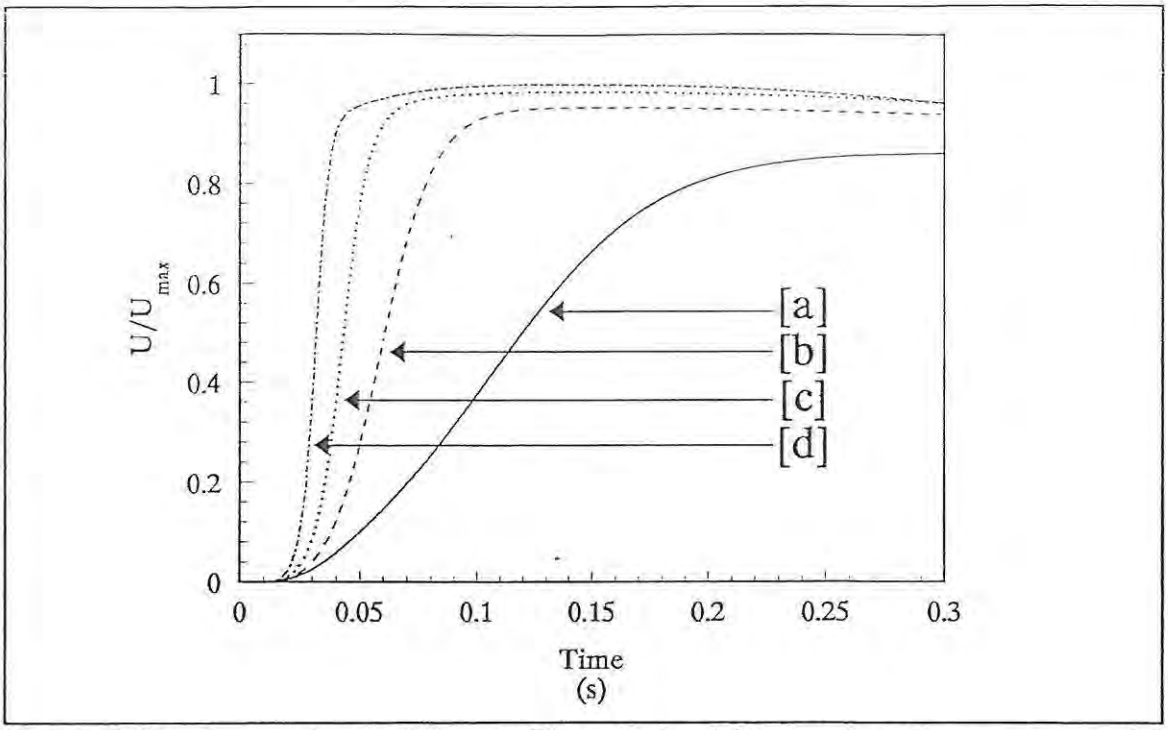

Figure 7.13 Comparison of the profiles obtained by varying the pre-exponetial factor, A, using values of 100 s^{-1} [a], 750 s^{-1} [b], 1000 s^{-1} [c] and 2000 s^{-1} [d].

7.3.2.2 The activation energy, E.

Decreasing the activation energy, E, from 35 kJ mol^{-1} to 20 kJ mol^{-1}, while keeping the value of A constant at 750 s^{-1} (see Figure 7.14) causes an increase in the burning rate (0.3 to 2.4 mm s^{-1}) with little change in the maximum temperature. Using the same reasoning as in Section 7.3.2.1 above, it follows that an increase in the value of E will cause a decrease in the rate coefficient and hence a corresponding decrease in the calculated burning rate, as is shown in Figure 7.14.

7.4 Summary and conclusions.

A one-dimensional finite difference approach has been used to model combustion. The calculated temperature-time profiles were compared with the experimental profiles obtained, for the 30% Sb/$KMnO_4$ pyrotechnic composition. Kinetic parameters and

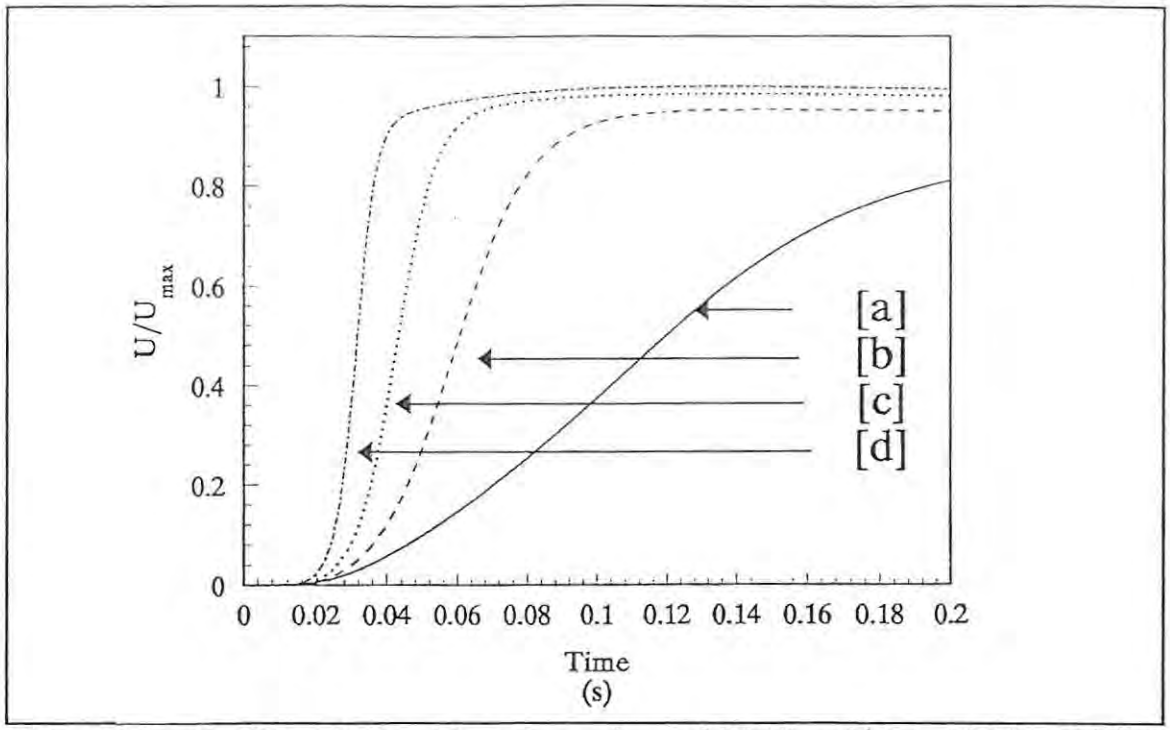

Figure 7.14: Profiles obtained by using values of 35 kJ mol^{-1} [a], 30 kJ mol^{-1} [b], 20 kJ mol^{-1} [c] and 15 kJ mol^{-1} [d] for the activation energy, E.

values of physical properties used in the simulations were altered within limits based on extremes of values for pure fuel, or pure oxidant for physical properties, and more arbitrary units for kinetic parameters. Wherever possible simulated trends were compared with experimental trends.

Three kinetic models for the combustion reaction were investigated :-

i) Use of first-order kinetics gave acceptable correlation between simulated and experimentally obtained burning rates and maximum temperatures, but the shapes of the simulated curves were found to be too deceleratory to model accurately an initially acceleratory process such as combustion;

ii) Use of autocatalytic (Prout-Tompkins) kinetics also gave acceptable correlation between experimental and simulated values of burning rate and maximum temperatures. The overall shape of the curve, gave a closer approximation to the experimental profile than simulations using first-order kinetics. The value of the pre-exponential factor, **A**, had to be increased (10 to 500 s^{-1}) to get an acceptable burning rate. It should be noted, however, that the values of **A** obtained by kinetic analysis of experimental

temperature-time profiles are based on the assumption of first-order kinetics [5]. The rate equation does not apply for $\alpha = 0$, and so α has to be set to a small initial value. This initial value greatly affects the burning rate, and for values of $\alpha < 0.01$ the rate of change of α was too small to generate enough heat to cause the required increase in reaction rate. A value of $\alpha = 0.01$ gave acceptable burning rates.

iii) An alternative acceleratory model (Johnson-Mehl-Avrami-Erofeev kinetics) also gave acceptable correlation between experimental and simulated burning rates and maximum temperatures. The shape of the curve approximated that of the experimental profile even better than the profiles generated by the Prout-Tompkins model (see section **7.8.2**). However, this second model had a further adjustable parameter, n, a value for which had to be chosen rather arbitrarily (see section **7.8.1**). The value of **A** also had to be increased (10 to 700 s^{-1}) and the initial value of α was set at 0.01.

The relative simplicity of the Prout-Tompkins equation and the good results obtained when using it in a simulation, suggested that this model should be investigated further when the simulation was done using two-dimensional finite element models.

8. TWO-DIMENSIONAL FINITE-ELEMENT SIMULATIONS.

8.1 Background to Finite-Element Methods. (FEM).[40,41]

8.1.1 Introduction.

The Finite-Element Method (FEM) is a numerical analysis technique for obtaining approximate solutions to a wide variety of engineering problems. It was originally developed to study mechanical stresses in complex airframe structures, but it has been extended to a broad field of applications. The underlying principle of the FEM is its ability to solve problems described by complex boundary shapes. Since its inception, the FEM has been found to be equally effective in nonstructural problems, particularly those in heat transfer and fluid dynamics.

The problem domain is partitioned into a finite number of four node-quadrilateral elements interconnected at their nodal points, see Figure 8.1, i.e. a finite element mesh for the problem is constructed. In the FEM, a partial differential equation is reduced to

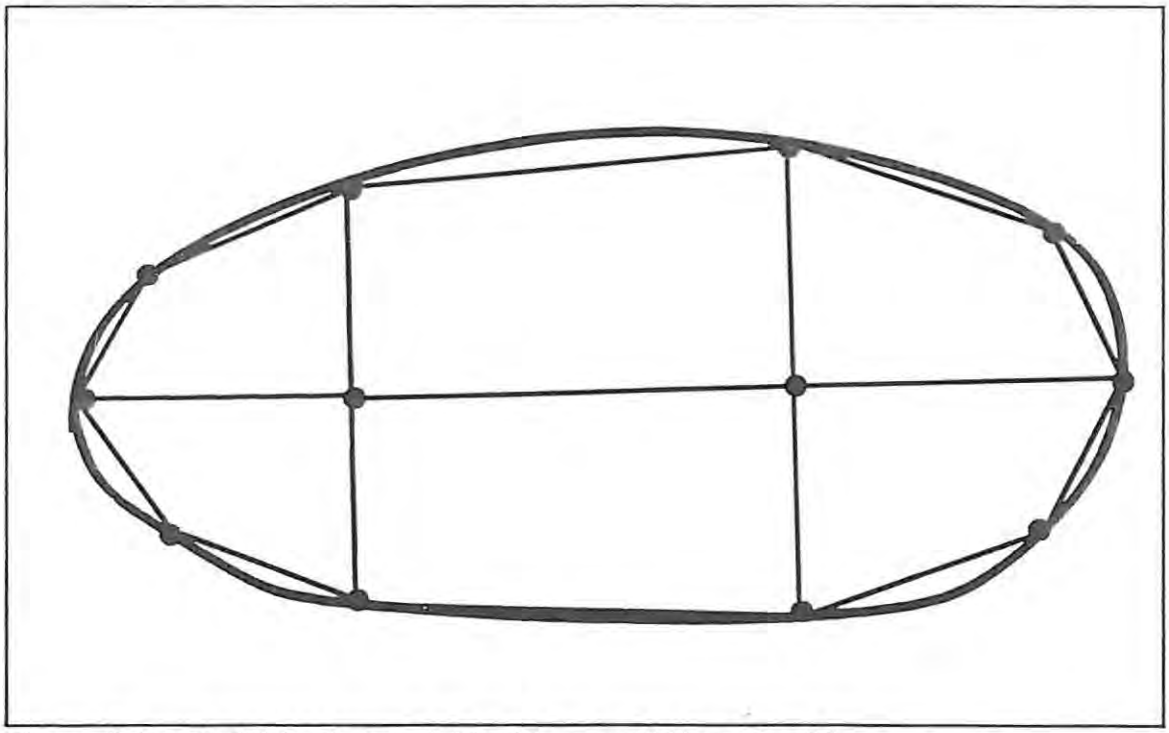

Figure 8.1: Solid body overlaid with a quadrilateral grid.

a finite system of ordinary differential equations, which is then solved by matrix solution techniques.

8.1.2 Conduction of heat in an orthotropic solid

The differential equation of conduction of heat in a two-dimensional solid Ω is given by :-

$$\rho c\frac{\partial T}{\partial t} = \frac{\partial}{\partial x}[k_x\frac{\partial T}{\partial x}] + \frac{\partial}{\partial y}[k_y\frac{\partial T}{\partial y}] + q_g \quad in \quad \Omega \tag{8.1}$$

where ρ is the density, c the heat capacity, t the time, q_g the heat generation, k_i the thermal conductivity in the direction i and T is the temperature. The solid is bounded by surface Γ which is subjected to the boundary condition :-

$$k_x\frac{\partial T}{\partial x}n_x + k_y\frac{\partial T}{\partial y}n_y + \beta T = \gamma \ on \ \Gamma \tag{8.2}$$

where n_i is a directional cosine of the outward normal vector in the direction i and ß is a thermal coefficient. The surface uses the initial condition, which specifies the temperature distribution at time zero, being :-

$$T = T(x,y) \ at \ t = t_0 \tag{8.3}$$

Equations (**8.1**) to (**8.3**) represent the strong form of a boundary value problem to be solved for the temperature field within the solid.

8.1.3 Finite element formulation

A weak form of this boundary value problem is obtained by requiring each side of equation (**8.1**) to be satisfied in an average sense [41] :-

$$\iint_{\Omega} w\rho c\frac{\partial T}{\partial t}dxdy = \iint_{\Omega} w[\frac{\partial}{\partial x}k_x\frac{\partial T}{\partial y} + \frac{\partial}{\partial y}k_y\frac{\partial T}{\partial y}]dxdy + \iint_{\Omega} wq_g dxdy \qquad (8.4)$$

The weight function, **w**, is any function of **x** and **y** that is sufficiently well behaved that the integrals make sense. Integrating the first term on the right side of equation (8.4) by parts, results in a weak form of the boundary value problem.

time dependency

$$\iint_{\Omega} w\rho c\frac{\partial T}{\partial t}dxdy = \qquad (8.5)$$

heat conduction

$$- \iint_{\Omega} [\frac{\partial w}{\partial x}k_x\frac{\partial T}{\partial x} + \frac{\partial w}{\partial y}k_y\frac{\partial T}{\partial y}]dxdy$$

natural boundary condition

$$+ \int_{\Gamma} w[k_x\frac{\partial T}{\partial x}n_x + k_y\frac{\partial T}{\partial y}n_y]d\,\Gamma$$

internal heat generation

$$+ \iint_{\Omega} wq_g dxdy$$

Notice the appearance of the "natural" boundary condition term in equation (8.5) resulting from the integration-by-parts operation. Several forms of the boundary condition equation (8.2) will now be substituted for the natural boundary condition term. Equation (8.2) can be rewritten as :-

$$k_x\frac{\partial T}{\partial x}n_x + k_y\frac{\partial T}{\partial y}n_y = \gamma - \beta T \qquad (8.6)$$

By convention, heat flow is positive in the direction of the surface outward normal vector. A flux (or Neumann type) boundary condition can be represented by specifying

$$\beta = 0$$

$$\gamma = -q_f \qquad \text{(FLUX B.C.)} \qquad (8.7)$$

in equation (8.6). A convection (or Robin type) boundary condition can be represented by specifying :-

$$\beta = h_c$$
$$\gamma = h_c T_\infty \qquad \text{(CONVECTION B.C.)} \qquad (8.8)$$

in equation (8.6). Equation (8.8) can also be used for a radiation boundary condition by introducing a radiant-heat-transfer coefficient $\mathscr{F}$.

$$h_r = \sigma \mathscr{F} (T_1 + T_2)(T_1^2 + T_1^2) \qquad \textit{(RADIATION B.C.)}$$

where σ is the Stefan-Boltzmann constant. The forced (or Dirichlet type) boundary condition in which the temperature is specified on the boundary, is imposed on the final system of equations by a penalty method.

If a flux is applied on the boundary Γ_f, heat transfer occurs by convection on the boundary Γ_c. Using equations (8.6) - (8.8), equation (8.6) becomes :-

time dependency
$$\iint_\Omega w \rho c \frac{\partial T}{\partial t} dxdy =$$

heat conduction
$$- \iint_\Omega [\frac{\partial w}{\partial x} k_x \frac{\partial T}{\partial x} + \frac{\partial w}{\partial y} k_y \frac{\partial T}{\partial y}] dxdy$$

flux b.c.
$$- \int_{\Gamma_f} w q_f \, d\Gamma_f \qquad (8.9)$$

$$+ \int_{\Gamma_c} w h_c T_\infty d\, \Gamma_c$$

convection b.c. $- \int_{\Gamma_c} wh_c T \, d\,\Gamma_c$

internal heat generation. $+ \iint_{\Omega} wg_g dxdy$

Galerkin's method consists of seeking an approximate solution to equation (8.9). This proceeds by assuming a trial (shape) function expansion for T,

$$T = \sum_{i=1}^{n} N_i T_i = N\Theta \tag{8.10}$$

where n is the number of nodes assigned to the shape, and T_i are the discrete nodal temperatures. The weighting function is taken as:-

$$w = N_i \tag{8.11}$$

Using the relationships (8.10) and (8.11) in equation (8.9) results in :-

$$[\iint_{\Omega} N_i \rho c \; N \; dxdy]\{\frac{\partial \Theta}{\partial t}\} = [- \iint_{\Omega} \nabla^T N_i K \nabla N \; dxdy]\{\Theta\}$$

$$- \int_{\Gamma_f} N_i q_f \, d\Gamma_f + \int_{\Gamma_c} N_i h_c \theta_\infty d\Gamma_c - [\int_{\Gamma_c} N_i h_c N d\Gamma_c]\{\Theta\} \tag{8.12}$$

$$+ \iint_{\Omega} N_i q_g dxdy \quad (i=1,2,....,n)$$

or a set of discrete equations of the form :-

$$[C]\{\dot{\Theta}\} + [H]\,\{\Theta\} = \{F\}$$

with

$$[C_{ij}] = \int\int_{\Omega} N_i \rho c N_j dxdy$$

$$[H_{ij}] = \int\int_{\Omega} \nabla^T N_i K \nabla N_j dxdy + \int_{\Gamma_c} N_i h_c N_j d\Gamma_c$$

$$\{F_i\} = \int\int_{\Omega} N_i q_g dxdy - \int_{\Gamma_c} N_i q_f d\Gamma_f + \int_{\Gamma_c} N_i h_c T_\infty d\Gamma_c$$

The finite element method provides a technique for spatial discretization of the body and construction of shape functions, $\mathbf{N}_i$, for the numerical solution of equation (8.12). Let the domain, Ω, be partitioned into a finite number of four node-quadrilateral elements interconnected at their nodal points, see Figure (8.2). This achieves the spatial discretization and the required is then :-

$$[C] = \sum_e [C_{ij}^e] = \sum_e \int\int_{\Omega e} N_i \rho c N_j dxdy$$

(8.13)

$$[H] = \sum_e [H_{ij}^e] = \sum_e \int\int_{\Omega e} \nabla^T N_i k \nabla N_j dxdy + \int_{\Gamma_c^e} N_i h_c N_j d\Gamma_c \qquad \begin{matrix} i=1,2,3,4 \\ j=1,2,3,4 \\ e=1,\ldots,n \end{matrix}$$

$$\{F\} = \sum_e \{F_i^e\} = \sum_e \int\int_{\Omega e} N_i q_g dxdy - \int_{\Gamma_f^e} N_i q_f \, d\Gamma + \int_{\Gamma_c^e} N_i h_c T_\infty d\Gamma_c$$

for substitution into equation (8.12).

A finite element mesh for the problem is demonstrated, and then a corresponding set of shape functions. In constructing the shape functions, the coordinates are changed to map the given into a bi-unit square. This standardizes the subsequent integration of equations (8.13). Mappings of the form :-

$$x(\xi,\eta) = \sum_{i=1}^{4} N_i(\xi,\eta)x_i^e$$

$$y(\xi,\eta) = \sum_{i=1}^{4} N_i(\xi,\eta)y_i^e$$

are used and the shape function is defined as :-

$$N_i(\xi,\eta) = \tfrac{1}{4}(1 + \xi_1\xi)\ (1 + \eta_1\eta)$$

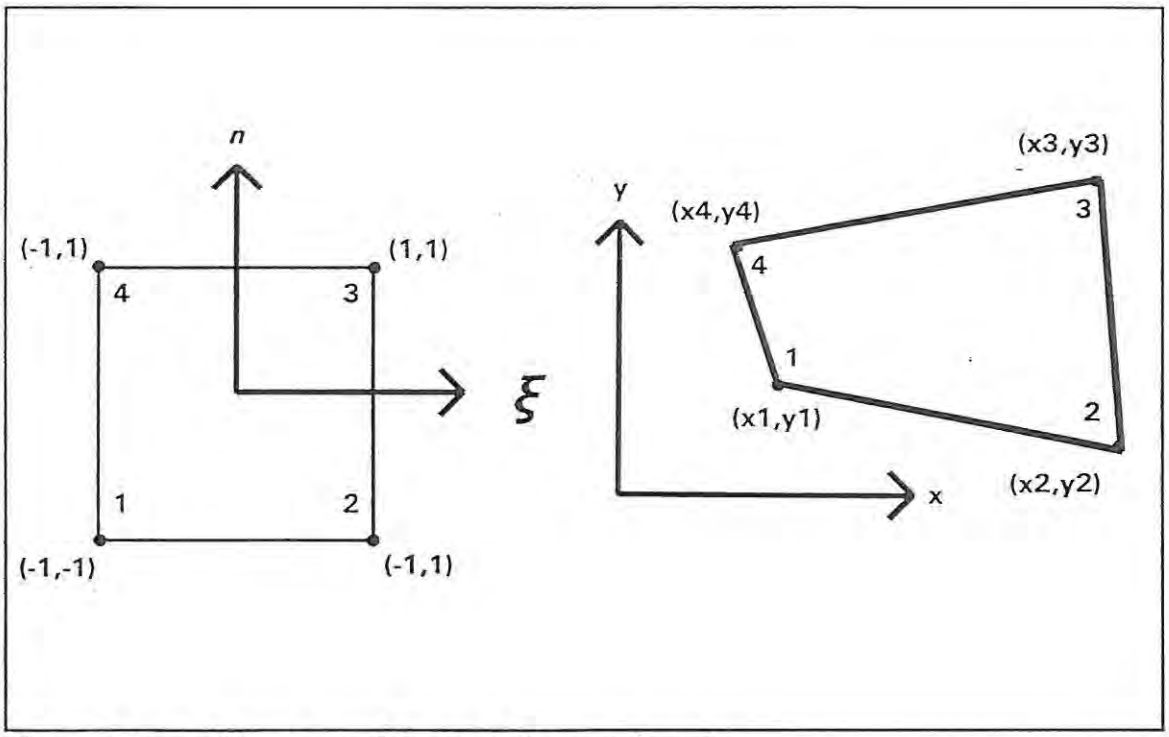

Figure 8.2: Bilinear quadrilateral element domain.

which relate points in the bi-unit square (ξ,η coordinate system) to coordinates of a point in Ω^e (x,y coordinate system), see Figure (8.2). The temperature must also be interpolated by these same shape functions (i.e. the isoparametric concept).

$$T(\xi,\eta) = \sum_{i=1}^{4} N_i(\xi,\eta) T_i^e$$

Equations (8.13) are now written as functions of the new variables ξ and η, that is, the integrands are expressed in terms of ξ and η, and $dxdy$ is replaced by $d\xi d\eta$ times the absolute value of the Jacobian J. In general,

$$\int\int_{\Omega} f(x,y)dxdy = \int_{-1}^{1}\int_{-1}^{1} f[x(\xi,\eta),y(\xi,\eta)]|J|d\xi d\eta$$

where

$$J = \begin{bmatrix} \frac{\partial x}{\partial \xi} & \frac{\partial x}{\partial \eta} \\ \frac{\partial y}{\partial \xi} & \frac{\partial y}{\partial \eta} \end{bmatrix}$$

The equations (8.13) are integrated numerically by using a second-order Gaussian quadrature in each direction. In general :-

$$\int_{-1}^{1}\int_{-1}^{1} g(\xi,\eta)d\xi d\eta = \sum_{l=1}^{4} g(\xi_l,\eta_l)W_l$$

where

I	ξ_I	η_I	W_I
1	$-1/\sqrt{3}$	$-1/\sqrt{3}$	1
2	$1/\sqrt{3}$	$-1/\sqrt{3}$	1
3	$1/\sqrt{3}$	$1/\sqrt{3}$	1
4	$-1/\sqrt{3}$	$1/\sqrt{3}$	1

Upon integration of equations (8.13) for each element, the element equations are assembled to form the matrix equation (8.12). This equation is solved for the temperature field.

8.1.4 Time integration scheme

The time integration of equation (8.12) is carried out using a generalized trapezoidal method. This method has been shown by Hughes [42] to be unconditionally stable for nonlinear problems. This method consists of the following family of algorithms:-

Find $\mathbf{T}_n$, $\mathbf{n} \in \{0,1,\ldots,n\}$, such that :-

$$C_{n+\alpha}\dot{T}_{n+\alpha} + H_{n+\alpha}T_{n+\alpha} = F_{n+\alpha} \tag{8.14}$$

$$T_{n+1} = T_n + \Delta t\dot{T}_{n+\alpha} \quad , \tag{8.15}$$

$$T_0 = T \quad ,$$

where

$$C_{n+\alpha} = C(T_{n+\alpha}\ ,\ t_{n+\alpha}) \quad ,$$

$$H_{n+\alpha} = H(T_{n+\alpha}\ ,\ t_{n+\alpha}) \quad ,$$

$$T_{n+\alpha} = (1-\alpha)T_n + \alpha T_{n+1} \quad , \tag{8.16}$$

$$F_{n+\alpha} = (1-\alpha)F_n + \alpha F_{n+1} \quad ,$$

$$\dot{T}_{n+\alpha} = (1-\alpha)T_n + \alpha T_{n+1} \quad ,$$

$$t_{n+\alpha} = (n+\alpha)\ \Delta t \quad .$$

Equations (**8.15**) and (**8.16**) can be rephrased as

$$\dot{T}_{n+\alpha} = \frac{1}{\Delta t}(T_{n+1} - T_n)$$

$$T_{n+\alpha} = T_n + \alpha(T_{n+1} - T_n)$$

respectively. Substituting these equations into equation (**8.14**) yields :-

$$\left[\frac{C_{n+\alpha}}{\Delta}t + \alpha H_{n+\alpha}\right]\{T_{n+1} - T_n\} = \{F_{n+\alpha} - H_{n+\alpha}T_n\} \tag{8.17}$$

The solution progresses with time by first solving equation (**8.17**) for the incremental temperature change vector $\{T_{n+1} - T_n\}$ and then updating the temperature. In nonlinear problems, $\boldsymbol{C}$, $\boldsymbol{H}$ and $\boldsymbol{F}$ may be functions of T and thus iteration must be used to solve equation (**8.17**). The parameter α is taken to be in the interval [0,1].

8.2 The Finite-Element code TOPAZ [43]

8.2.1 Introduction

TOPAZ is a two-dimensional implicit finite-element computer code, developed by Lawrence Livermore Laboratories, originally used for heat transfer analysis, but has now been adapted to include electrostatic and magnetostatic problems. TOPAZ solves for transient or steady-state temperature fields on two-dimensional planar or axisymmetric geometries. It handles a number of time and temperature dependent boundary conditions, including temperature, flux, radiation and convection.

The code has been modified to handle chemical reaction kinetics, and this modification makes the code suitable for modelling pyrotechnic devices. Initial changes involved reprogramming the heat generation routine of the TOPAZ program to accommodate a simple temperature independent first-order expression, $\mathbf{K(1-\alpha)}$, where **K** is a temperature independent constant. TOPAZ forms part of a series of codes, amongst which DYNA, DYNA3D and NIKE, are better known. TOPAZ uses versions of the mesh generation code MAZE, and a post-processor ORION, which allows the output to be displayed as fringe or contour plots, and time-temperature profiles of individual nodes within the problem space to be calculated.

8.2.2 **Hardware and software**

The TOPAZ91 [43] program is written in FORTRAN, and is compiled to run under the VAX VMS operating system. VMS version 5.3 is currently being used on a DIGITAL micro-VAX 3100. Communication with the VAX is done via a four core telephone cable from the COM1 port of a 86486-DX/33 MHz micro-computer (INTEL, with OAK sVGA 512Kb screen, 4 Mb RAM), to the EMULEX Performance 4000 ethernet server.

Reflection 4+ [44] is used as the emulator, running at a baud rate of 38400 and a terminal type of VT400-7, with 8 data-bits and no parity bits. Future communication will probably involve a direct connection to the ethernet. Hardcopies were made on an

```
6 NOFRAME LPOFF PPOFF          :
LD 1 LP 2 0 10 0 0             :
LD 2 LP 2 0 0 10 0             :
LD 3 LSTL 1 0.1 0              :Line definitions
LD 4 LSTL 1 0.2 0              :
LD 5 LSTL 1 0.3 0              :
LD 6 LSTL 1 0.4 0              :
LD 7 LSTL 2 0 0.1              :
LD 8 LSTL 2 0 3                :
PART 1 2 5 7 1 2 30 Y          :
PART 1 7 3 8 1 58 10 Y         :Part definitions
PART 3 7 4 8 1 58 10 Y         :
PART 4 7 5 8 1 58 -10 3 Y      :
PART 5 2 6 8 2 60 -10 0.3 Y    :
ASSM                           :Assemble parts and grids
MG 2 3 MG 2 4                  :Merge Pyrotechnic parts
SLN 1 4 1                      :Slideline def, type 4 TCR 1
SLBP 2 1                       :Slideline between parts 1&4
SLN 2 4 1 SLBP 1 5             :Slideline between parts 1&5
SLN 3 4 1 SLBP 2 5             :Slideline between parts 2&5
TUNI 2                         :Temperature units °C
STEP 0                         :Fixed time step
STAR 0 TERM .2 Delt .0001      :Start 0, end 0.2, Δt .0001
TMPM 1                         :Max temperature change
BWMO 1                         :Bandwidth optimized by MAZE
ANAL 1                         :
P 1 TIC 1 93 671               :Initialize starter to 671K
P 2 TIC 94 1922 300            :Pyrotechnic column at 300K
P 5 TIC 1923 2593 300          :Stainless-steel at 300K
PLTI .0001 PRTI .1             :Plot and print times
TITLE                          :
OPEN CHANNEL                   :
WBCD TOPAZ2D                   :Make output for TOPAZ2D
TMAT 1                         :Material 1
STARTER                        :Name
DEN 2.4                        :Density
MT 5                           :Material type pyrotechnic
CP 1 .157638                   :Heat capacity
CON1 1 .0005517                :Thermal conductivity
Q 257.9                        :Heat of reaction
ACT 2.9378                     :Activation energy
PRE 580                        :Pre-exponential factor
TIG 671                        :Ignition temperature
LAM 1                          :Order of reaction
TMAT 2                         :Material 2
STAINLESS STEEL                :
DEN 7.800                      :
MT 1                           :Material type Isotropic
CP 1 0.122 CON1 1 0.032        :
END                            :End
```

Figure 8.3: MAZE command file.

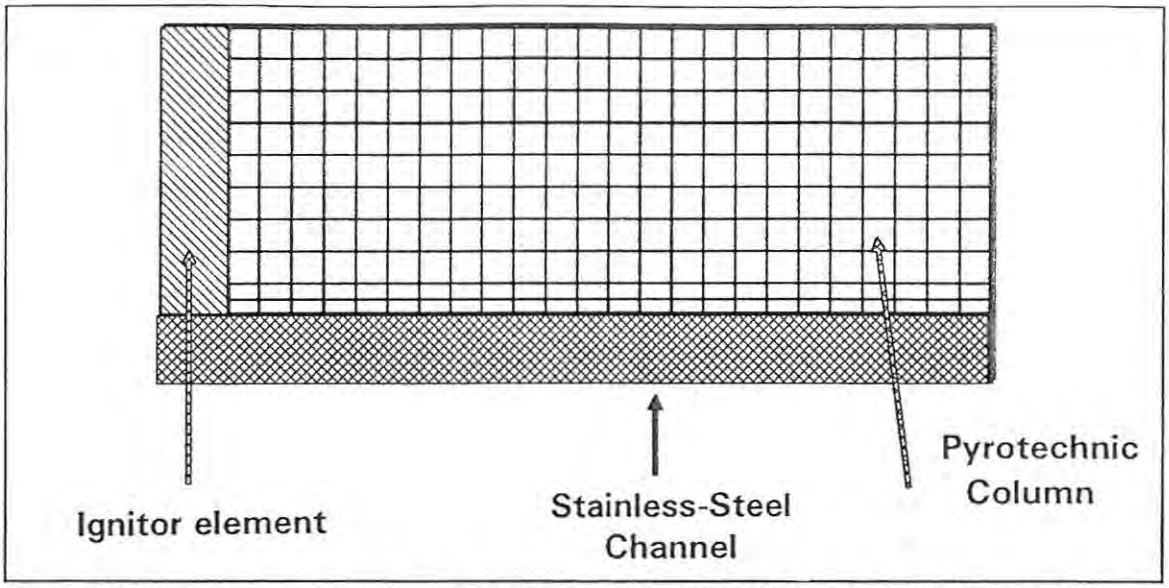

Figure 8.4: Finite element mesh generated by MAZE for the simulated channel. The channel is symmetrical, so only half of the channel is generated.

were made on an HP500C deskjet.

The pre-processor, MAZE92 [45], also written in FORTRAN, converts a simple set of instructions, typed in by the user or as a file, into a form that TOPAZ91 can utilize. An example of such a set of commands in given in Figure **8.3**. These commands generate the mesh shown in Figure **8.4**. The **TUNI I** command controls what units the simulation is going to use. In all our simulations, **I** was set to 2 meaning that the following units were to be used:- density (g cm^{-3}), thermal conductivity (cal s^{-1} cm^{-1} K^{-1}), heat capacity (cal g^{-1} K^{-1}), reaction exothermicity (cal g^{-1}), activation energy (kcal mol^{-1}), ignition temperature (K) and pre-exponential factor (s^{-1}). The output file from MAZE92 is used as input for TOPAZ91.

The post-processor, ORION92 [46], is used to produce graphical representations of the resultant data. A contour or fringe plot gives a picture of the temperature distribution with in the column and its surroundings, for a given time in the experiment, an example of the commands used is given in Figure **8.5**.

An example of the type of output which can be obtained is given in Figure **8.6**. This figure shows the temperature gradient throughout the column, in the form of contours of uniform temperature represented by arbitrarily assigned colours. The effect

```
6                       :Terminal type
TIME       0.1          :Look at system when time = 0.1
RCVA                    :Reflect plot around the vertical
FRIN 20 2 1 2           :Give fringe plot of the temperature
                        :(20) distribution of 2 materials 1
                        :and 2.
```

Figure 8.5: Command file for ORION to generate a fringe plot at time 0.1 s.

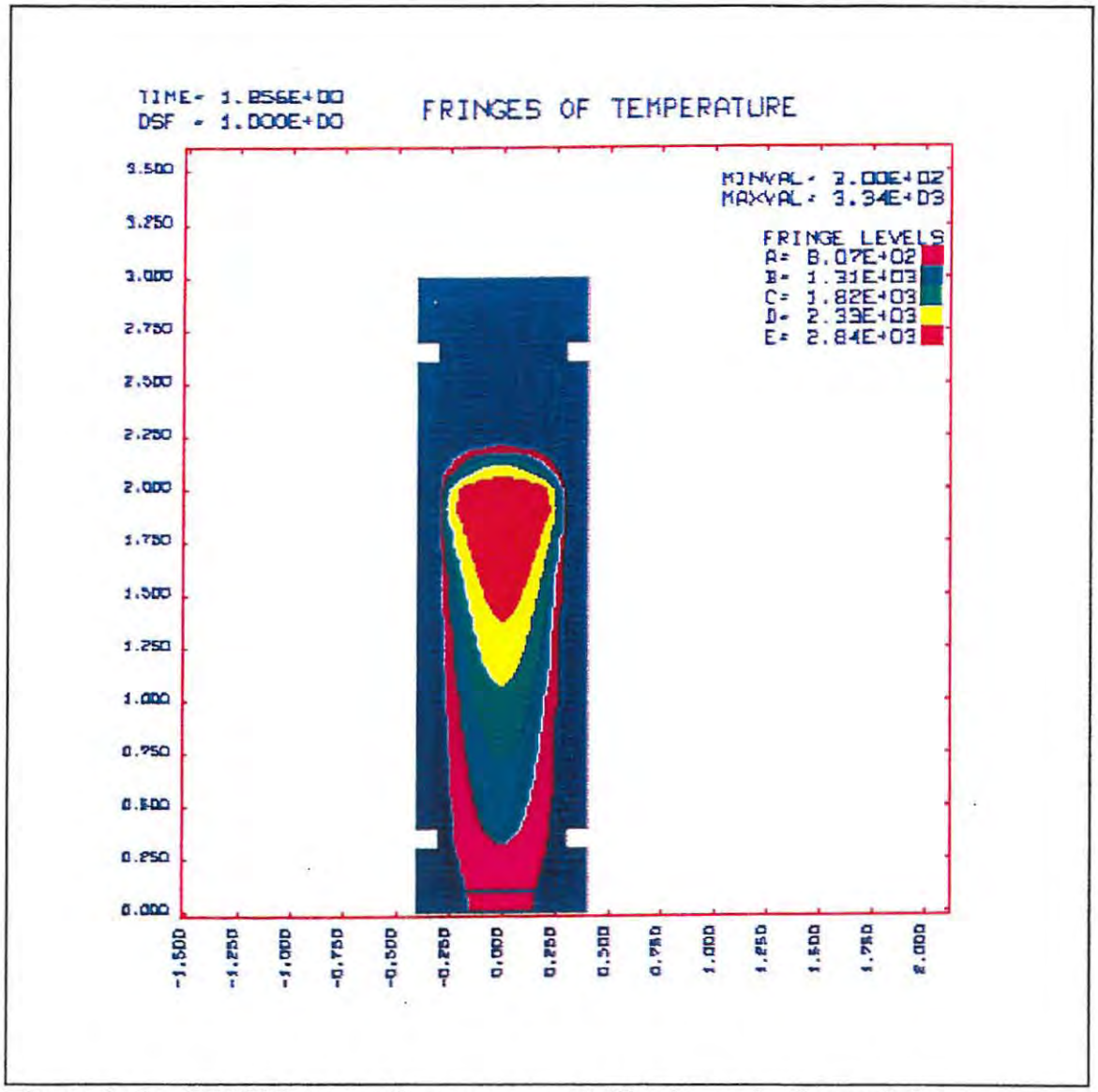

Figure 8.6: ORION output from command file shown in figure 8.5.

```
6                'Terminal type
PHS  2           'Enter phase II command set
NODE 2 140 150 'Look at two nodes 140 and 150
GATHER           'Gather all the temperature time history
                 of the two nodes 'defined above
COLUMN           'Output file must be in column format
PRNT             'Output all data used to make graphs in
                 NTIME command
NTIME 7 2 140 150        'Draw a graph of temperature (7)
                          'for two nodes (140 and 150)
```

Figure 8.7: Command file for ORION to give temperature-time profiles of nodes 140 and 150 (will also save the output in a file, ORNOUT.DAT, for further manipulation by Lotus 123 spreadsheet).

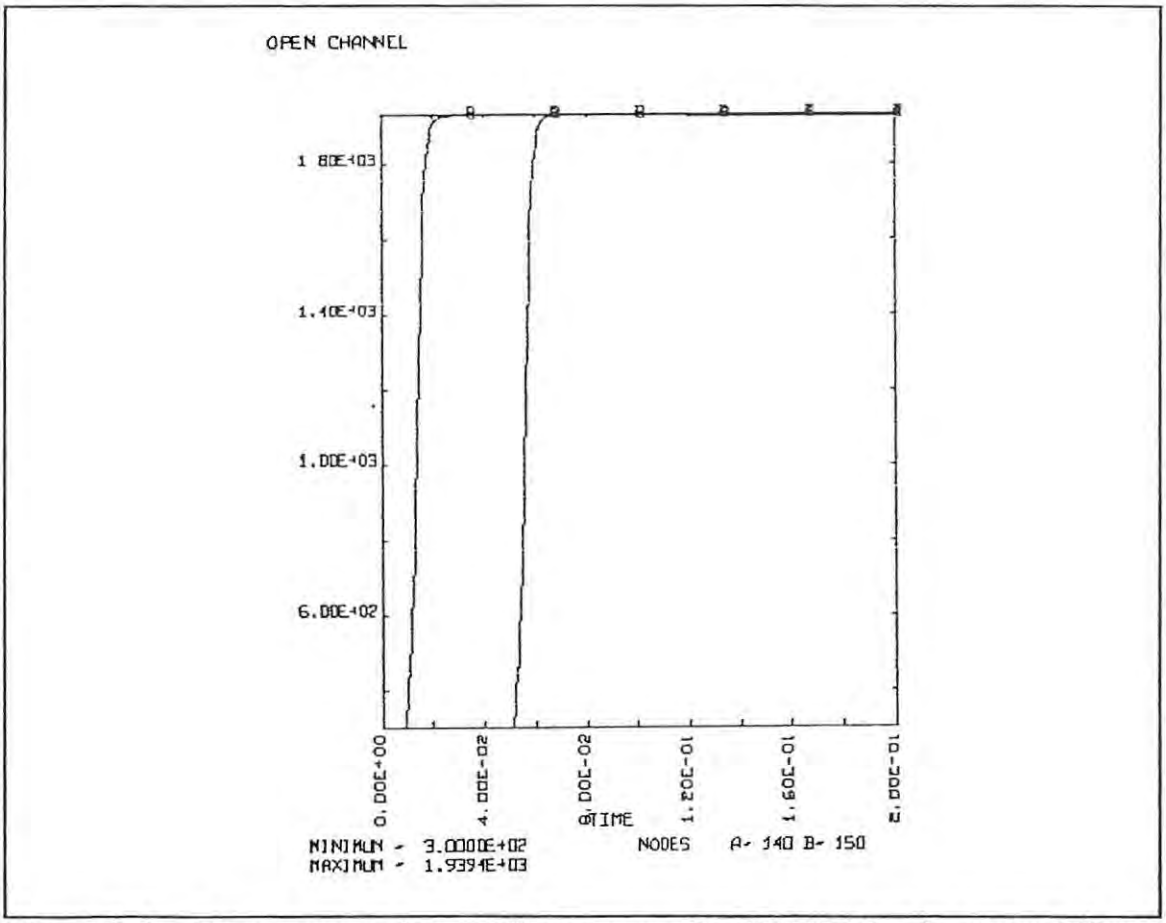

Figure 8.8: Temperature-time profile generated by ORION for the nodes 140 and 150 using the command file shown in figure 8.7.

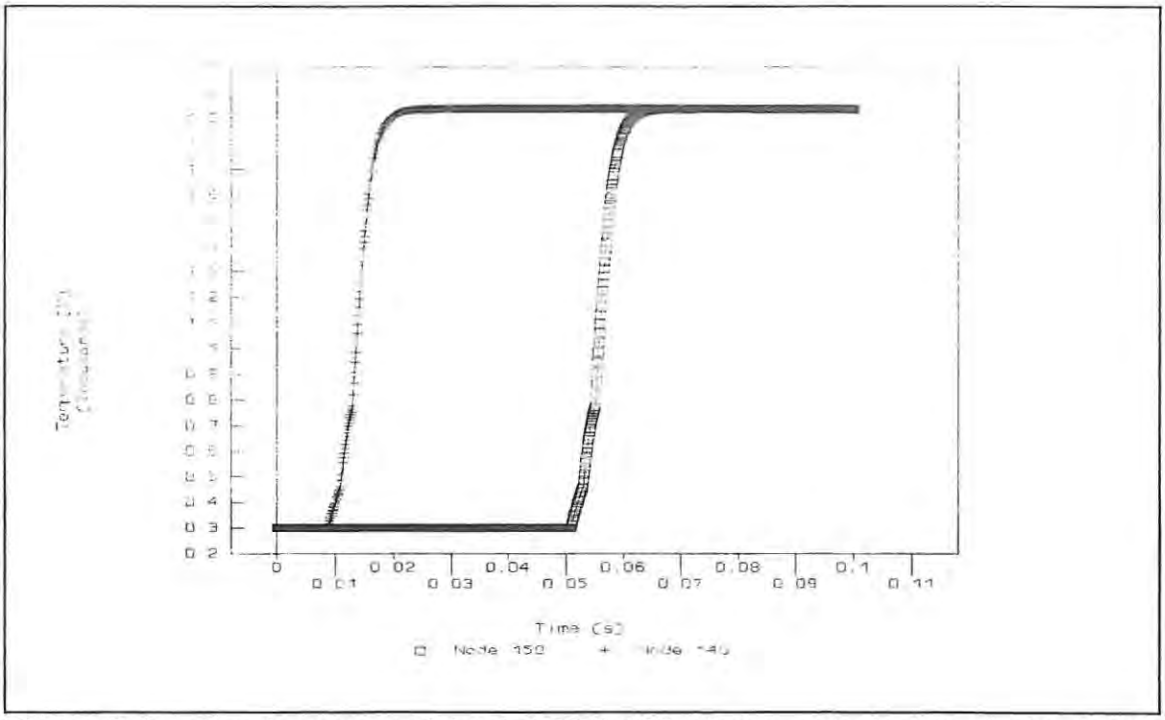

Figure 8.9: Graph generated by LOTUS 123 after manipulation of the output from ORION after executing the command file shown in Figure 8.7.

of cooling of the sides of the column on the internal temperature of the reacted column can be seen. The metal casing (the two slits used for the timing of the reaction in the experimental work, were included), shows up as a uniform (blue) colour, with no obvious temperature gradient within it. This is because the extremes of the temperature range, from the hot internal combustion zone to the cool casing, are too large to allow for greater definition at the lower end of the temperature scale.

The two nodes (140 and 150) were chosen because they lie along the central axis of the simulated column, and are far enough apart to give acceptable accuracy in the measurements of buring rate, while being far enough from the ends of the column not to be affected by any distrubances that occur there.

Temperature-time graphs can be produced for specific nodes, over the experimental time range, and examples of the commands and output are given in Figures **8.7** and **8.8**. The data output files produced by ORION92 for the temperature-time graphs were usually transferred to a Lotus 123 spreadsheet [47] for further manipulation, to analyze for burning rates and for the production of higher quality graphs, as shown in

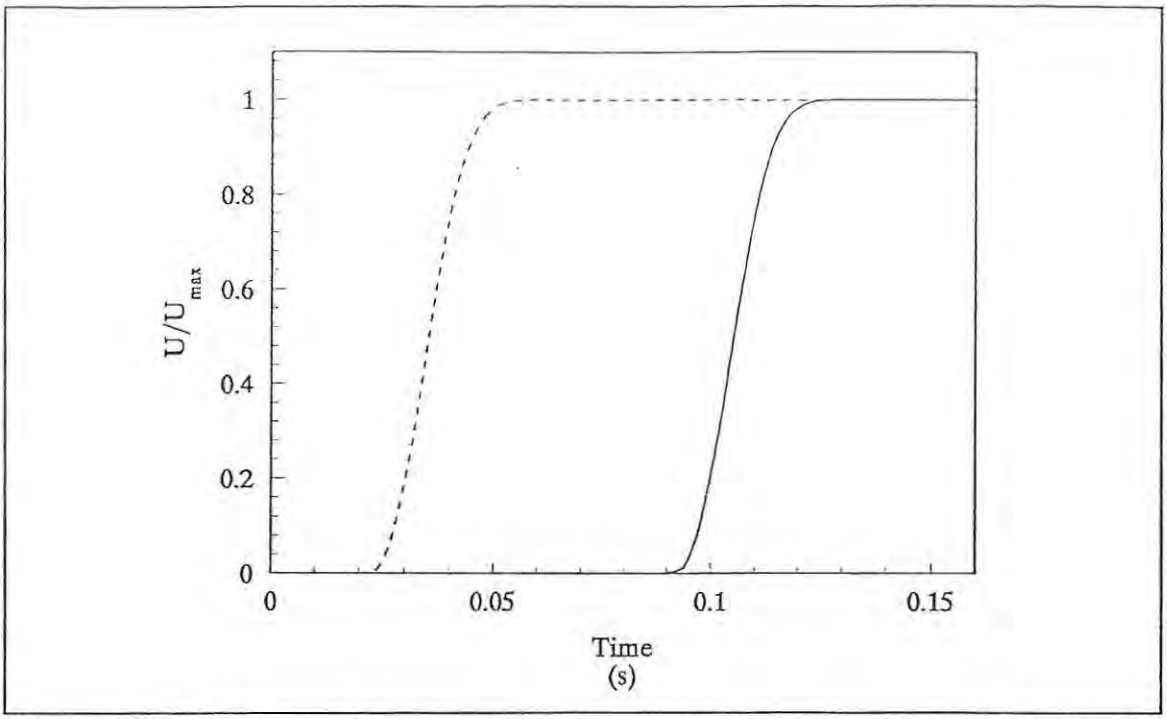

Figure 8.10: Further enhancement of the graph shown in Figure 8.9, by the program GRAFTOOL.

Figure 8.9. The graphs could be further enhanced by importing them into the graphing program GRAFTOOL [48], to give the results shown in Figure 8.10.

If two parts of a body are placed in contact, a considerable resistance to heat flow from one part to the other may exist. This thermal contact resistance (TCR), is a function of the physical properties of the contacting materials, the surface conditions and finish, the contact pressure, and the presence of a fluid or vacuum in the gap between the surfaces. TOPAZ uses the following algorithm to couple the finite element heat transfer equations between two parts through a contact resistance across a gap, which can be of zero thickness, between the contacting surfaces. The gap thickness is factored out of the conductance matrix and is incorporated into a contact resistance term. This allows for zero gap thickness in both reality (perfect thermal contact) and for numerical processing (the two contacting surfaces have the same spatial coordinates). A value has to be input for the TCR between the composition and the container. For the initial simulations, this was set to 1.

8.3 TOPAZ simulation of the Sb/$KMnO_4$ reference system.

8.3.1 Introduction.

An essential first step was to determine the set of input parameters for the simulation which would give good agreement between the simulated temperature profiles and burning rates and those measured experimentally. Beck [15,25,26] has summarized his experimental results for the 30% Sb (plant grade < 53 μm)/$KMnO_4$ compositions (Table **8.1**). Beck also reported that decreasing the particle size of the fuel (< 6 μm) increased the burning rate from 2.5 mm s^{-1} to 8.2 mm s^{-1} and the effective thermal conductivity (calculated from $1/t_r = \rho c v^2/\lambda$) 2.8 to 4.0 W m^{-1} K^{-1} (9.6 x 10^{-3} cal s^{-1} cm^{-1} K^{-1}). Beck's simulations using TOPAZ [25] assumed adiabatic combustion and used the parameters given in Table **8.2**. These values resulted in a profile with T_{max} = 1610 °C and v = 10.1 mm s^{-1} which where both too high (see Table **8.1**). Decreasing the value of **Q** to 220 cal g^{-1} resulted in a simulated profile with T_{max} = 1130 °C and v = 4.3 mm s^{-1} which is closer to the experimental values shown in Table **8.1**.

When Arrhenius parameters were introduced (n = 0.67, E_a = 4.8 kcal mol^{-1}, **A** = 94 s^{-1}), the resulting profile had T_{max} = 1910 °C and v = 2.8 mm s^{-1}. When an ignition temperature was not used and E_a = 8.25 kcal mol^{-1} and **A** = 506 s^{-1}, T_{max} increased further to 2230 °C. Decreasing the time step to 1 ms caused a further increase in T_{max} to 3250 °C (v still at about 2.3 mm s^{-1}) and this trend was attributed to a problem with the TOPAZ code. Warren [49] also used Beck's experimental results to model the behaviour of the Sb/$KMnO_4$ systems in containers of different thermal diffusivities. She used the non-Arrhenius version (see above) and obtained excellent agreement between the simulation (T_{max} = 1177 °C, v = 2.7 mm s^{-1}) and experimental (T_{max} = 1200 °C, v = 2.9 mm s^{-1}) by using the experimental results from Beck's PhD thesis as input. Changes in the thermal diffusivity of the channel material from 0.03 cm^2 s^{-1} (stainless steel) to 1.14 cm^2 s^{-1} (copper) were predicted to be accompanied by increases in the burning rate from 2.3 mm s^{-1} to 3.0 mm s^{-1}. Experimental values increased only slightly from 2.0 mm s^{-1} to 2.3 mm s^{-1}.

Table 8.1
Experimental results for 30% Sb (< 53 μm)/$KMnO_4$ compositions.

T_{max}	1200 ± 60 °C	1473 ± 60 K
v (burning rate)	2.2 ± 0.3 mm s^{-1}	
Q (combustion energy)	720 - 920 J g^{-1}	172 - 220 cal g^{-1}
c (reactant heat capacity)	0.58 - 0.61 J K^{-1} g^{-1}	0.14 - 0.15 cal K^{-1} g^{-1}
c (product heat capacity)	0.50 - 1.20 J K^{-1} g^{-1}	0.12 - 0.29 cal K^{-1} g^{-1}
ρ (density)	2.5 ± 0.2 g cm^{-3}	
λ (thermal conductivity)	0.3 ± 0.1 W m^{-1} K^{-1}	7.0 x 10^{-4} cal s^{-1} cm^{-1} K^{-1}
E_a (activation energy)	34.5 kJ mol^{-1}	8.25 kcal mol^{-1}
A (pre-exponential factor)	506 s^{-1}	

Table 8.2
Input parameters for the TOPAZ simulations done by Beck [25].

Time step	20 ms	
Q	1090 J g^{-1}	260 cal g^{-1}
λ	0.3 W m^{-1} K^{-1}	7.0 x 10^{-4} cal s^{-1} cm^{-1} K^{-1}
c	0.59 J K^{-1} g^{-1}	0.14 cal K^{-1} g^{-1}
T_i (ignition temperature)	290 °C	560 K

Table 8.3

Summary of results obtained by Warren [49] for the sensitivity of T_{max} and v to changes in input parameters (non-Arrhenius version of TOPAZ).

		T_{max} /K	v / mm s^{-1}
Thermal conductivity, λ / cal s^{-1} cm^{-1} K^{-1}			
reference	6.7×10^{-4}	1600	2.96
low	2.0×10^{-4}	1500	2.08
high	1250×10^{-4}	1470	22.7
Heat output, Q /cal g^{-1}			
reference	315	1710	3.53
low	248	1390	2.14
high	405	2080	5.85
Kinetic factor, A / s^{-1}			
reference	94	1600	2.96
low	50	1640	1.94
high	600	1920	11.34

Warren [49] also reports the results of tests done on the sensitivity of T_{max} and v to changes in some of the input parameters: the thermal conductivity (λ), the heat output (Q), and the factor A in the non-Arrhenius version of TOPAZ (above). These results are

condensed in Table 8.3.

8.3.2 Trial simulations.

An initial set of input parameters (Table 8.4) was drawn up, based on the experiences of Beck, using the Arrhenius version of TOPAZ. The column of pyrotechnic mixture was defined as being 30 mm long and 6 mm wide, and having a 1 mm thick stainless-steel channel surrounding it, as shown in Figures 4.1 and 8.4. 30 nodes were defined down the length of the column and 15 across. Thus the internodal separation down the column is 1 mm. The comparison of the profile obtained using the input parameters in Table 8.4 with the experimental profile is shown in Figure 8.11 (over 300 ms) and Figure 8.12 (over 12 s). The burning rates were : experimental 2.2 $\pm$ 0.3 mm s^{-1} and simulation 3.87 mm s^{-1}; T_{max} was : 1473 $\pm$ 60 K, experimental and 1908 K, simulation.

Agreement between simulation and experimental is not good, when all the input variables possible are matched with experimental values. One variable for which there is no information from experiment, is the thermal contact resistance (TCR), between the

Table 8.4
Values of parameters used in the initial simulation.

Density, ρ (measured)	2.52 g cm^{-3}
Heat capacity, c (calculated, see Table 5.4)	1.41 x 10^{-1} cal g^{-1} K^{-1}
Reaction exothermicity, **Q**	220 cal g^{-1}
Activation energy, E_a	8.25 kcal mol^{-1}
Pre-exponential factor, **A**	94 s^{-1}
Ignition temperature	560 K
Order of reaction, n	0.67
Thermal conductivity, λ	7.0 x 10^{-4} cal s^{-1} cm^{-1} K^{-1}

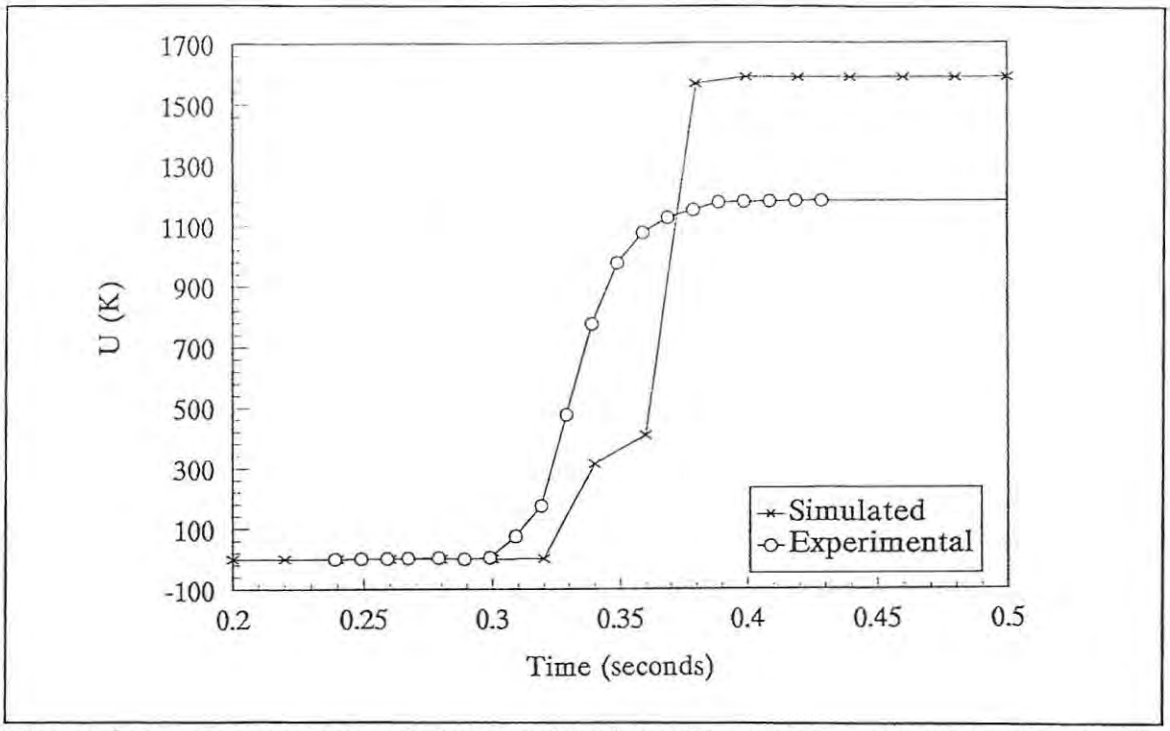

Figure 8.11: Comparison of the simulated profile and the experimental profile over 300 ms.

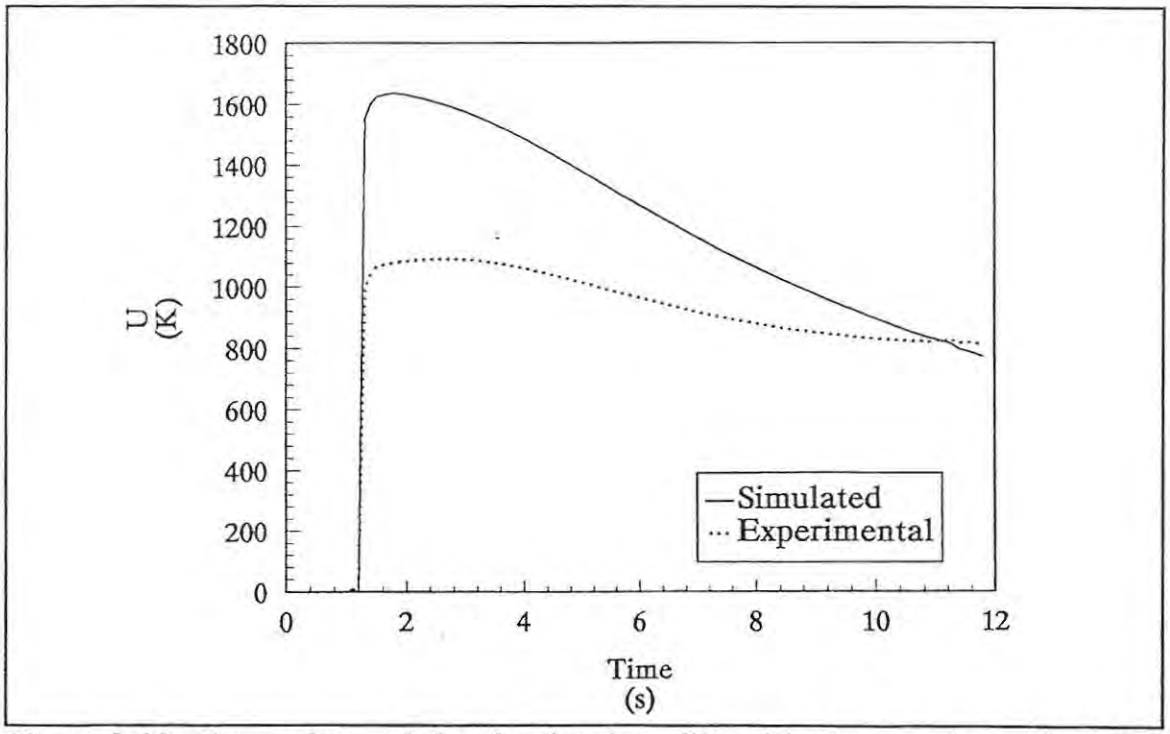

Figure 8.12: Comparison of the simulated profile with the experimental profile over 12 seconds.

composition and container. In the above simulation, the TCR was set to 1. Beck assumed adiabatic behaviour i.e. TCR is set to zero (no heat transfer between the pyrotechnic column and the stainless-steel channel). The current version of TOPAZ requires a non-zero value for the TCR and the lowest non-zero value acceptable by the program is 1×10^{-5}. Discussions with TOPAZ experts at ICL could not give us a physical meaning for the value of the TCR. The value was chosen on the grounds that previous studies had used a value of this magnitude.

In an attempt to make the agreement between the simulated and experimental profiles closer, several of the variables where altered within their given experimental ranges. Some degree of success was attained, but it became apparent that due to the number of variables involved some formalized approach to variation was needed, this approach is described below (section **8.3.3**).

8.3.3 **Variation of parameters.**

In an attempt to improve agreement between simulation and experiment, studies were made of the general trends produced in the burning rate and maximum temperature on varying some of the main parameters about their reference values.

For a *fixed-system*, the burning rate (and maximum temperature) depends mainly upon composition, particle-size and compaction. In TOPAZ there are no direct variables representing composition, so influences on the burning rate and the maximum temperature must arise from changes in one or more of the following : density, heat capacity, thermal conductivity, heat of reaction and the kinetic parameters.

For a *fixed system of fixed composition*, changes in the burning rate and maximum temperature can arise from varying the particle-size and/or the degree of compaction. There is no direct variable representing particle-size, so one would need to look at density and thermal conductivity. Heat capacity, heat of reaction and the kinetic parameters should not change significantly.

As a first trial variation, thermal conductivity, λ, was chosen and the effects on T_{max} and v of varying λ from 0.1 to 10 times the reference value of 7.0×10^{-4} cal s^{-1} cm^{-1}

K^{-1} are compared in Table 8.5 with some values obtained by Warren [49] using the non-Arrhenius version of TOPAZ where the reaction rate was described by the simple first-order expression $K(1 - \alpha)$. Values of K between 30 and 110 s^{-1} were used to give reasonable agreement with experimental profiles [50]. T_{max} values are lower and closer to experiment in the non-Arrhenius version. Burning rates are similar.

To investigate the effect of varying all the possible parameters on the burning rate and the maximum temperature of the system, would require a very large number of calculations. A way to decrease the number of calculations is to use multivariate non-linear programming. Central composite design (section 6.2) was applied in two sets of simulations, using a fixed system of fixed composition (30% $Sb/KMnO_4$). As discussed

Table 8.5
Comparison of varying λ on T_{max} and v in both the Arrhenius and non-Arrhenius versions of TOPAZ.

	Arrhenius		non-Arrhenius	
Thermal Conductivities / 10^{-3} cal s^{-1} cm^{-1} K^{-1}	Maximum Temperature / K	Burning Rate / mm s^{-1}	Maximum Temperature / K	Burning rate / mm s^{-1}
7.00	1823	5.00		
6.00	1832	5.00	1605	6.88
4.50	1847	5.00		
3.50	2285	3.81		
1.40	2163	4.21	1640	3.83
1.00	2261	4.00		
0.70*	1908*	3.87*	1600*	2.96*
0.45	2254	4.00		
0.07	2768	4.32		
0.06	2817	4.44		

* reference values.

Table 8.6
Fixed parameters used in multivariate experiments.

$Sb/KMnO_4$	30% Sb
Heat Capacity	1.35×10^{-1} cal g^{-1} K^{-1}
Reaction Exothermicity	220 cal g^{-1}
Activation Energy	4.8 kcal mol^{-1}
Pre-exponential Constant	94 s^{-1}
Ignition Temperature	560 K
Concentration Dependence (order)	0.67

Table 8.7
Burning rates and maximum temperatures obtained in response to variations of density and thermal conductivity.

	FACTORS				RESPONSES	
Design Point	X_1	Density g cm^{-3}	X_2	Thermal Conductivity cal s^{-1} cm^{-1} K^{-1} 10^{-4}	Burning rate mm s^{-1}	Maximum Temperature K
6	1.41	4.00	0.00	7.45	3.81	2398
1	1.00	3.67	1.00	8.97	4.21	2483
2	1.00	3.67	-1.00	5.93	4.10	2377
5	0.00	2.85	0.00	7.45	4.00	2214
8	0.00	2.85	1.41	9.60	4.27	2165
9	0.00	2.85	-1.41	5.30	4.10	2278
3	-1.00	2.03	1.00	8.97	4.00	2268
4	-1.00	2.03	-1.00	5.93	4.10	2911
7	-1.41	1.70	0.00	7.45	4.00	2250

ref. value 2.22 g cm^{-3}, 6.70×10^{-4} cal s^{-1} cm^{-1} K^{-1} [25]

in section 8.3.3 above, the **fixed values** were heat capacity; heat of reaction; and the kinetic parameters as shown in Table 8.6. The variables in study 1 were : x_1, density; and x_2: thermal conductivity. Two sets of responses were calculated : burning rate, v and maximum temperature, T_{max}.

The range of densities was from 1.70 g cm^{-3} (the density of $KMnO_4$ powder alone), to 4.00 g cm^{-3} (density of antimony powder alone). The thermal conductivities ranged from 5.3 x 10^{-4} cal s^{-1} cm^{-1} K^{-1} (for $KMnO_4$ powder) to 9.6 x 10^{-4} cal s^{-1} cm^{-1} K^{-1} [25].

The burning rates and maximum temperatures obtained in simulations in response to the variations of density and thermal conductivity are given in Table 8.7. To illustrate these results, the program GRAFTOOL [48] was used to draw scatter plots of the points obtained in Table 8.7 (see Figures 8.13 and 8.14). More useful information is obtained by converting these scatter plots into 27 x 27 point surfaces (as shown in Figures 8.15 and 8.16). Surface regressions were then carried out on the two surfaces and the response surface for each run was obtained from the calculated polynomial expression (see Figures 8.17 and 8.18). The regression computes up to 25 coefficients in a two-variable Maclaurin power series. The calculated surface is described by a polynomial of the form :

$$z = a00 + a01y + a02y^2 + a10x + a11xy + a12xy^2 + a20x^2 + a21x^2y + a22x$$

Tables 8.8 and 8.9 give the calculated values for the polynomial shown above.

The results of the above experiment show that the parameters chosen give maximum temperatures which are much higher than the experimental value (usually around 1200°C) and the burning rates are also faster (experimental 2.2 mm s^{-1}).

The trends shown in Figures 8.15 and 8.16 are interesting :

(a) the changes in the two responses : burning rate, v, and maximum temperature, T_{max}, (with changes in the input factors : thermal conductivity, λ, and density, ρ) do not follow a related pattern.

(b) Changes in T_{max} are much greater (e.g. 2200 → 2800 K is 27%) than in v (4.00 → 4.25 mm s^{-1} is 6%).

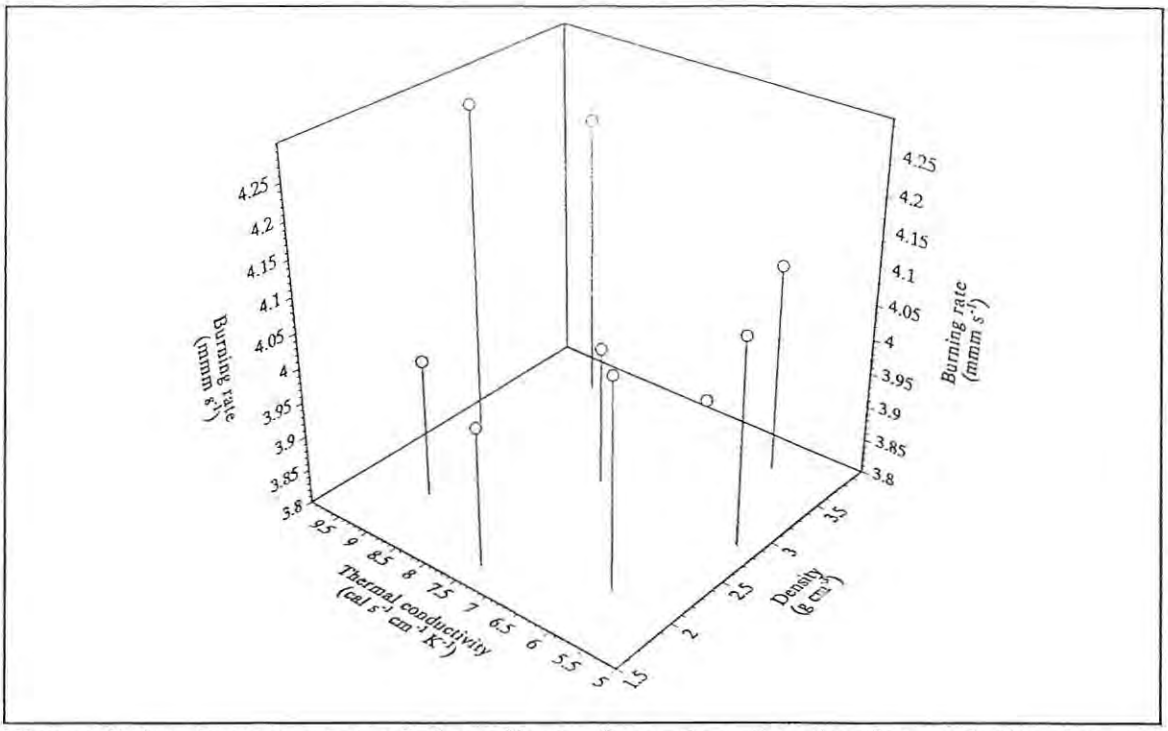

Figure 8.13: Scatter plot of the effect of varying the density and the thermal conductivity on the burning rate.

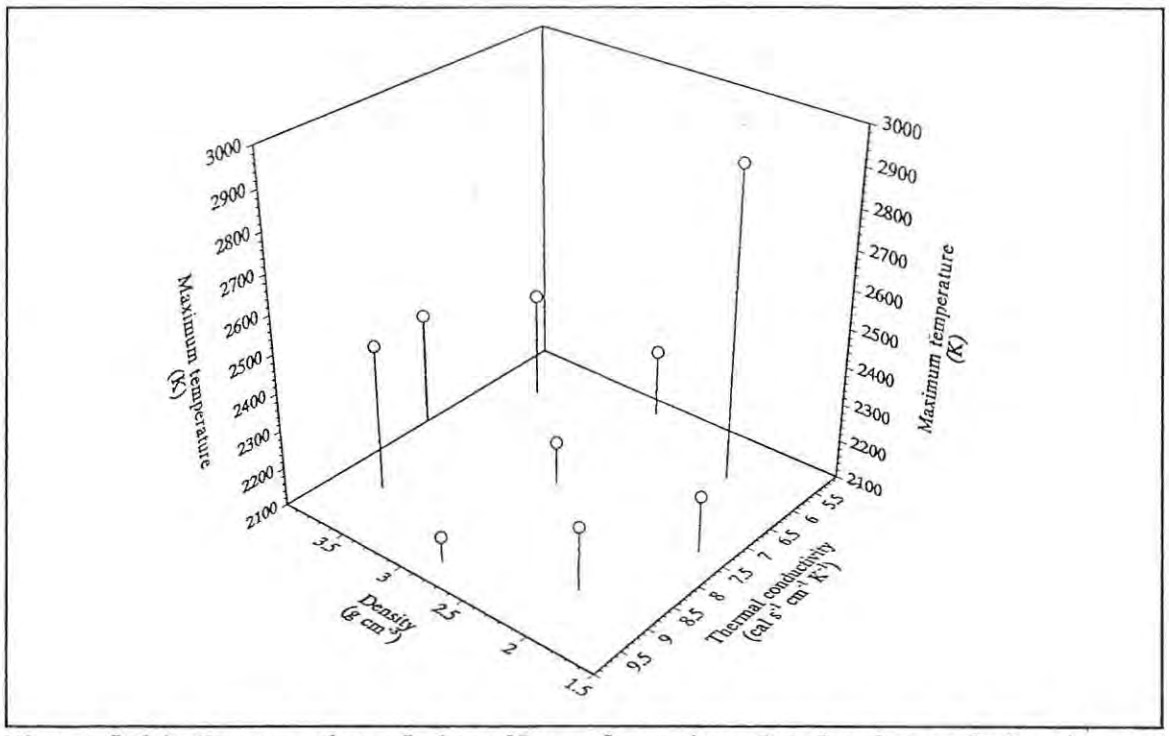

Figure 8.14: Scatter plot of the effect of varying the density and the thermal conductivity on the maximum temperature.

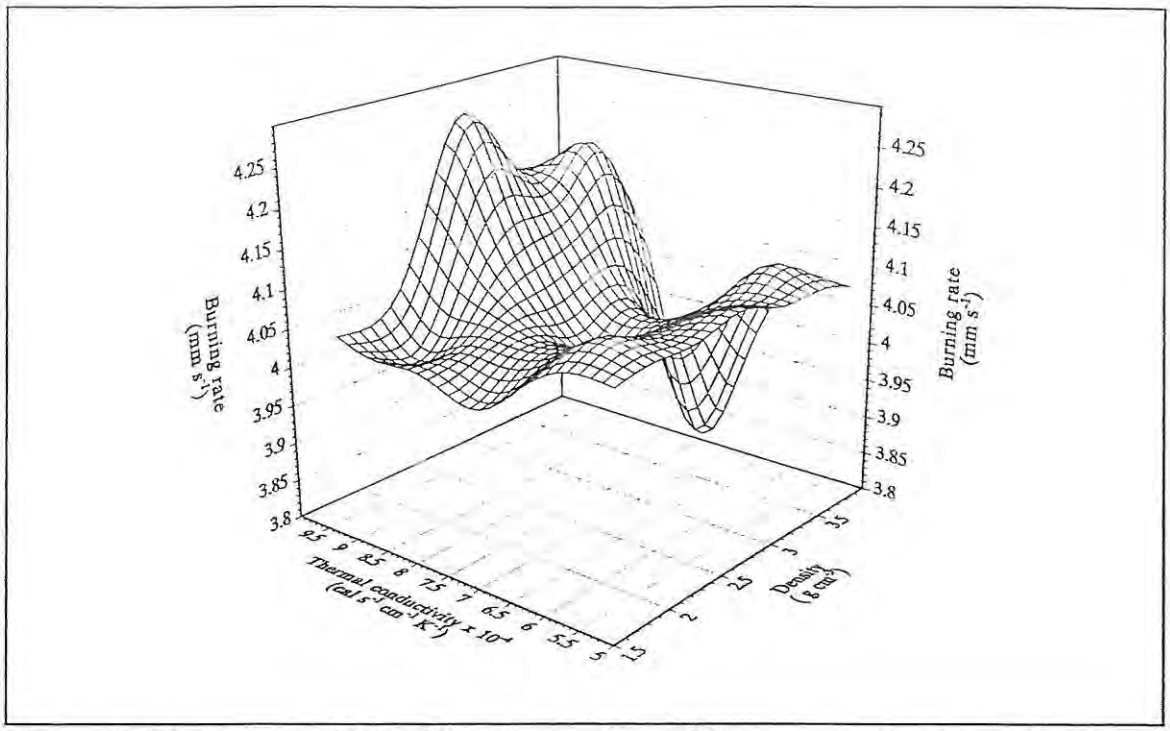

Figure 8.15: Generated 27 x 27 point surface of the scatter plot shown in Figure 8.13.

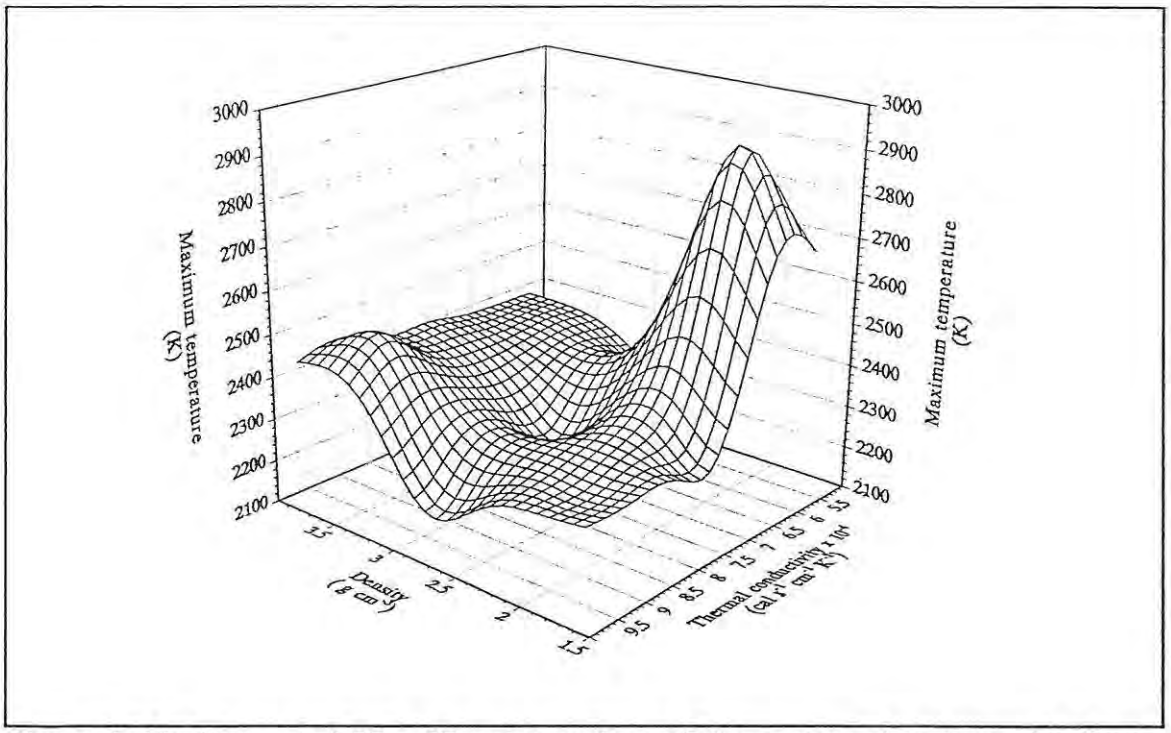

Figure 8.16: Generated 27 x 27 point surface of the scatter plot shown in Figure 8.14.

Table 8.8
Regression coefficients computed for burning rate.

a00	3.290
a01	0.340
a02	-0.035
a10	0.696
a11	-0.274
a12	0.027
a20	0.022
a21	0.004
a22	-0.001

Table 8.9
Regression coefficients computed for maximum temperature.

a00	17477.20
a01	-3432.94
a02	199.63
a10	-8351.62
a11	1886.41
a12	-111.89
a20	1170.51
a21	-265.47
a22	16.18

(c) T_{max} reaches its highest values in the approximate centre of both the λ and the ρ ranges, decreasing sharply to relative plateaus towards the extremes of the ranges. There does not seem to be an immediate physical explanation of this behaviour and this result should perhaps be treated with caution in view of the reports (Beck) of exaggerated T_{max} values generated by this code.

(d) The burning rates, v, show increases at high thermal conductivities and high densities as would be expected from the increased heat transfer. The detailed fluctuations of the surface may be artefacts. The lowering of the burning rate predicted at high density and intermediate conductivities is unusual and will be investigated further.

The central composite design is a useful means of investigating the effects of simultaneous variation of two parameters with an acceptable minimum number of simulations.

8.3.4 Further simulation.

On the basis of the experience gained from the trial simulations (**8.3.2**) and the trends shown in the variation of parameters (**8.3.3**), a modified set of values of the input parameters was chosen for the simulation of the reference system, 30% Sb (plant grade)/$KMnO_4$, as shown in Table **8.10**. All the values are within the experimentally found ranges for such data, however the pre-exponential factor was found to be too high, giving unrealistic profiles, and so a lower value was chosen. These values where used as input for a TOPAZ simulation and a comparison of the simulated profile with the experimental profile is shown in Figure **8.17**.

The sum of the squares of the residual temperature differences at common times, Equation (**8.18**), was used as a means of comparing two profiles :-

$$\frac{\left(\sum \left(T_s - T_e\right)^2\right)}{N} \qquad \textbf{(8.18)}$$

where T_s is the simulated temperature;

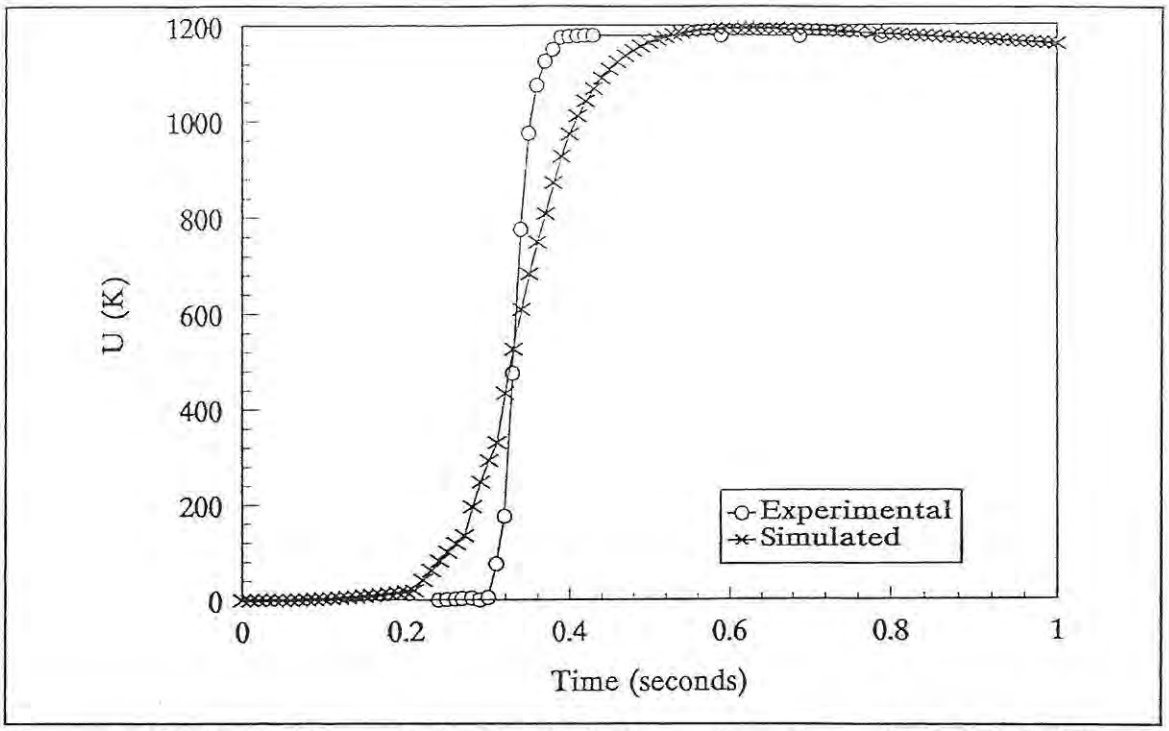

Figure 8.17: Comparison of simulated (using values shown in Table 8.10) and experimental time - temperature profiles, for the 30% Sb/$KMnO_4$ system.

T_e is the experimental temperature;

and N is the number of points used in the comparison.

Since the zero of the time scales in the experimental temperature profiles is arbitrary, the simulated and experimental profiles were made to coincide at $U = \frac{1}{2}U_{max}$. An example of the use of equation (8.18) to optimize one of the parameters, the pre-exponential factor, **A**, is shown in Figure 8.20.

An aspect of the TOPAZ simulation which is a cause for some concern is the inverted segmental curvature of the rise region. This is discussed further below.

It is very important to note that not only must the simulated and experimental temperature profiles coincide as closely as possible, but there must also be agreement between the experimental and simulated burning rates. The simulated burning rate is obtained by determination of the time interval between corresponding temperatures on the profiles at nodes separated by a known distance. According to the theory (section 4.2) the burning rate, v, and the rise-time, t^*, of the temperature profile are related via equation (8.19) :-

Table 8.10
The values chosen for the simulation of a "reference system".

	value	units*	SI values value	units
ρ (density)	2.55	g cm^{-3}	2550	kg m^{-3}
c (average heat capacity)	0.14	cal K^{-1} g^{-1}	0.59	J K^{-1} g^{-1}
λ (reactant thermal conductivity)	7.0 x 10^{-4}	cal s^{-1} cm^{-1} K^{-1}	0.29	W K^{-1} m^{-1} s^{-1}
Q (combustion energy)	172	cal g^{-1}	0.72	kJ g^{-1}
E_a (activation energy)	8.25	kcal mol^{-1}	34.5	kJ mol^{-1}
A (pre-exponential factor) (initial value)	25.0	s^{-1}		
A (pre-exponential factor) (best value)	14.9	s^{-1}		
n (order of reaction)	1			
T_{ign} (ignition temperature)	560	K		

* Note: the units given are those required for input to TOPAZ.

$$t^* = \frac{\lambda}{\rho c v^2} = \frac{D}{v^2} \qquad (8.19)$$

although agreement between t^* values from the experimental profiles and the experimental burning rates is generally not good and has been explained [24] as arising from the effective values of D or λ being different from those predicted from the properties of the reactants.

For the values given in Table **8.10**, the simulated burning rate is more than ten times greater than the experimental value, see Table **8.11**. To slow down the simulated burning rate, the effect of the kinetic parameters was investigated. A central composite design experiment was done varying the pre-exponential factor, **A**, and the activation

Table 8.11
Comparison of experimental results (Sb/$KMnO_4$ system) with simulated results, using input values shown in Table 8.10.

	Maximum temperature /(K)	Burning Rate /mm s^{-1}
Experimental	1473	2.20
Simulated (Table **8.10**)	1528	26.63

Table 8.12
Parameters for a central composite design experiment in which the pre-exponential factor,A, and activation energy, E, were varied.

Pre-exponential factor/ s^{-1}	Activation energy/ kcal mol^{-1}	Maximum temperature/ K	Burning rate/ mm s^{-1}
21.66	17.24	1528	5.00
21.66	3.76	1528	5.00
5.34	17.24	1497	1.32
5.34	3.76	1497	1.32
13.50	10.50	1526	3.13
25.00	10.50	1528	5.00
2.00	10.50	1488	0.56
13.50	20.00	1528	2.78
13.50	1.00	1528	3.13

energy, E. The parameters used were taken from Tables **8.10** and **8.12**. The results are also given in Table **8.12**. These results were plotted in two surface plots (Figures **8.18** and **8.19**) and it can be clearly seen from the surfaces generated that there is a very planar relationship. The effect of changing the value of **A** is very marked, especially on

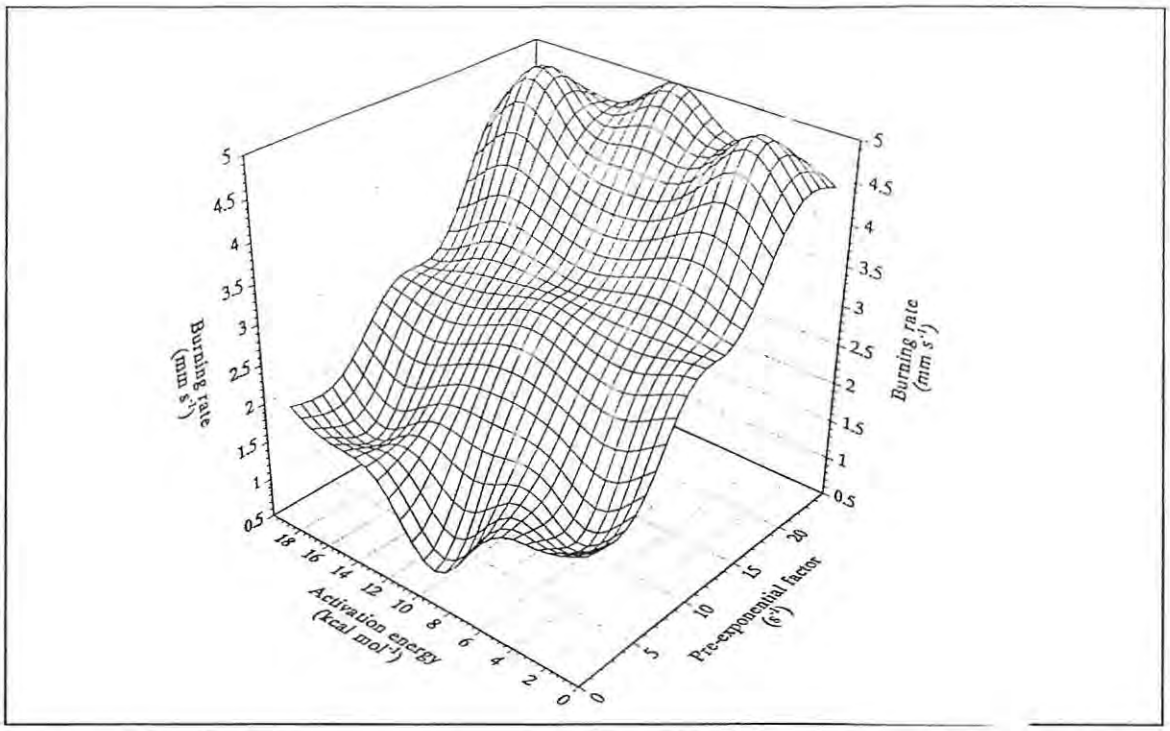

Figure 8.18: Surface plot showing the effect of varying the activation energy, E, and the pre-exponential factor, A, on burning rate.

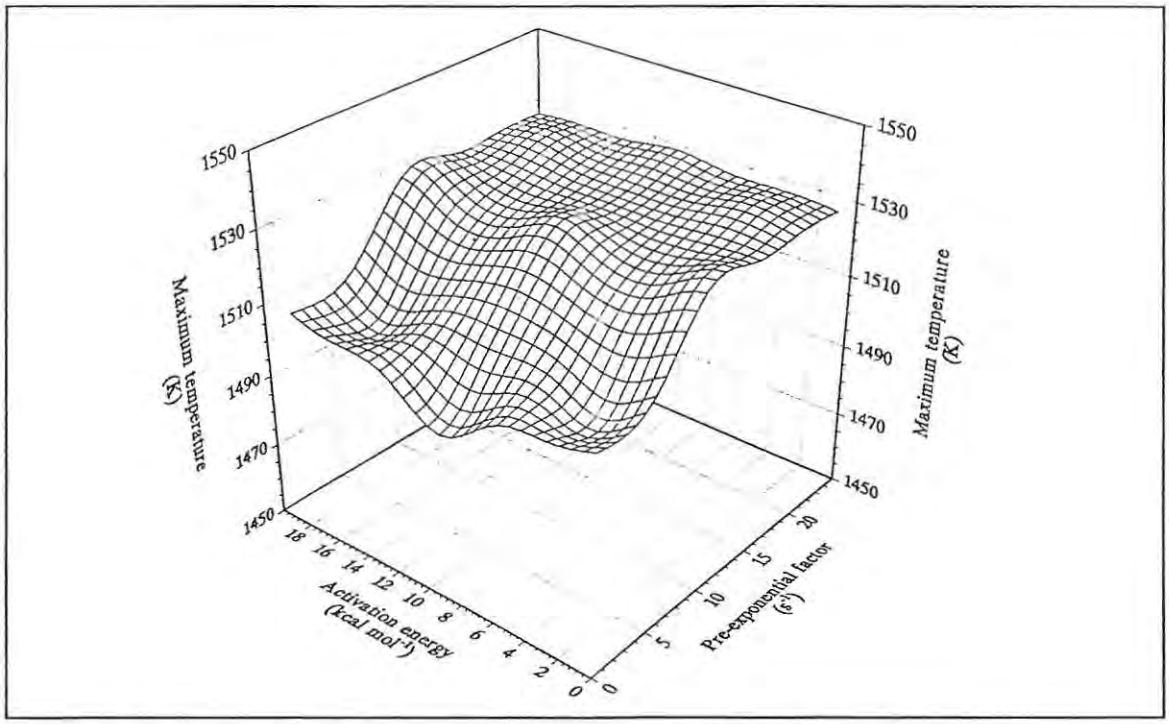

Figure 8.19: Surface plot showing the effect of varying the activation energy, E, and the pre-exponential factor, A, on the maximum temperature.

Table 8.13
Results of changing the pre-exponential factor, A, between 25 and 4 s^{-1}.

Pre-exponential factor (A) /s^{-1}	Sum of the squares of the residual temperatures	Burning Rate /mm s^{-1} from internodal times	Burning Rate /mm s^{-1} from profile rise times
25	58723	7.58	3.55
20	27391	5.77	2.75
15	11451	5.00	2.32
10	22486	3.30	1.60
5	48122	2.11	1.46
4	60456	2.00	1.28

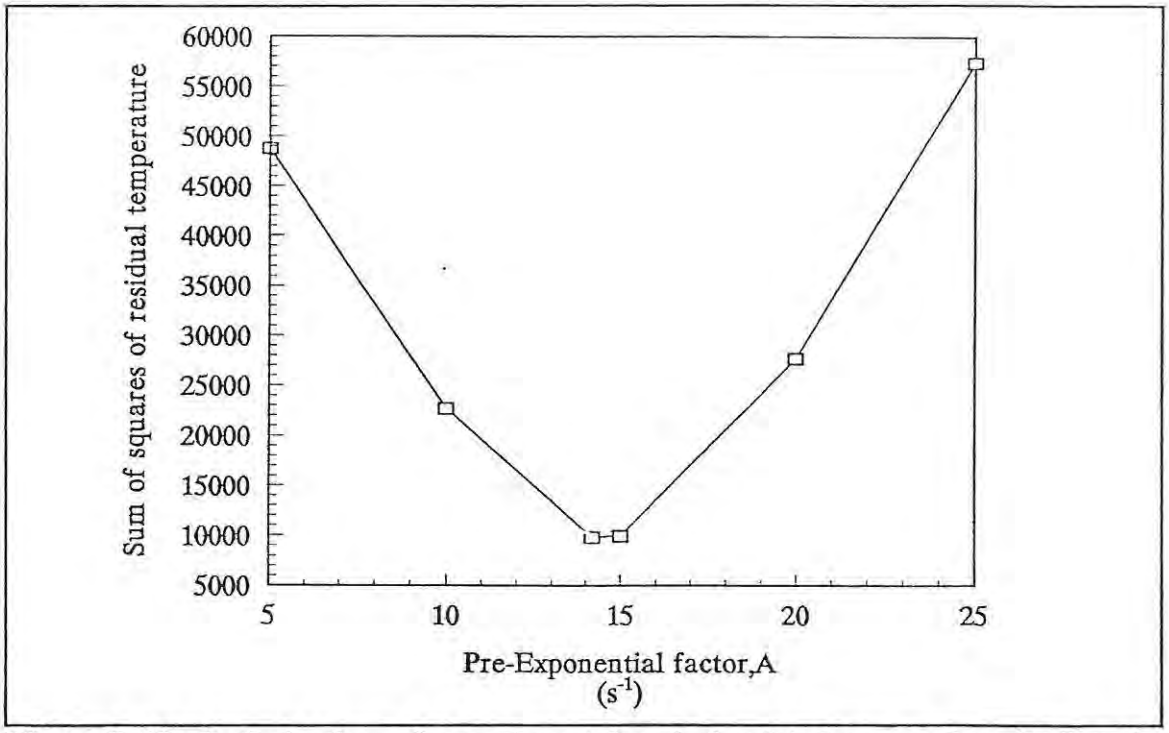

Figure 8.20: Optimization of experimental and simulated curves by altering the pre-exponential factor, A.

the burning rate. The lower the value of A, the lower the burning rate (changing A from 25 s^{-1} to 2^{-1} decreases the burning rate from 5.00 mm s^{-1} to 0.56 mm s^{-1}). The effect of the value of A on the maximum temperature is less significant, with only a marginal reduction in the value of the maximum temperature at low values of A. The activation energy is shown to have no significant effect on either the burning rate or the maximum temperature. Further more precise simulations which involved altering only the pre-exponential factor between 25 and 2 s^{-1} gave the results shown in Table **8.13** and Figure 8.21.

An example of the determination of the rise-time, t^*, from one of the simulated profiles (A=14.2 s^{-1}) is shown in Figure **8.22**. The inverted segmental curvature of the rise period of the TOPAZ simulation, referred to earlier, results in an irregular plot of ln U against t.

The graph of ln U versus time gives gradients

$$\frac{d\ln U}{dt} = 71.08 \ \ to \ \ 23.81 \ s^{-1}$$

$$\therefore \ v = 3.77 \ \ to \ \ 2.18 \ mm \ s^{-1}$$

A burning rate of 4.81 mm s^{-1} was obtained by direct measurement of the time taken for the temperature at two nodes a known distance apart to reach a temperature of ½U. Both values compare favourably with previous work [25], of 2.2±0.3mm s^{-1}.

8.3.5 Discussion.

The aim of this section (8.3) was to model, as accurately as possible, the combustion of the Sb/$KMnO_4$ pyrotechnic system, when it is burnt in an open channel, using the two-dimensional finite-element code TOPAZ. Using experimental and kinetic data from previous research done on this system, profiles were calculated. Initially these profiles did not correlate very well with the experimental profiles, but with some further

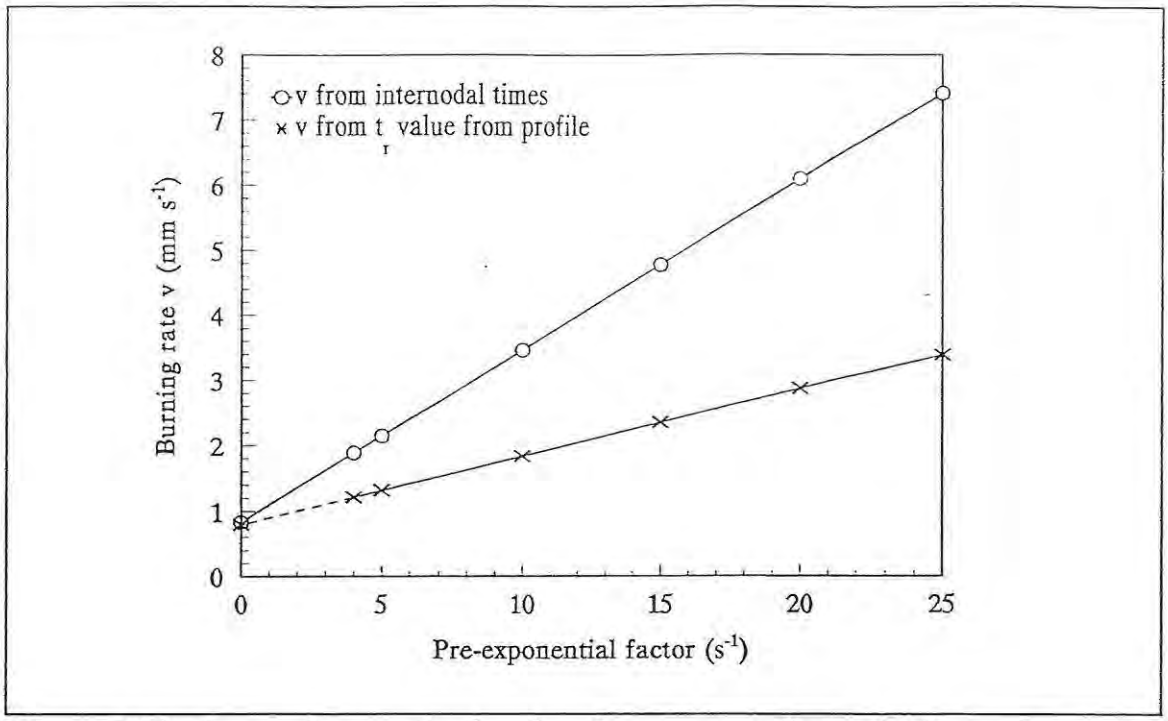

Figure 8.21: Comparison of the burning rates obtained from internodal calculations with those calculated from the rise times of the profiles. (Averaged values used in both cases.)

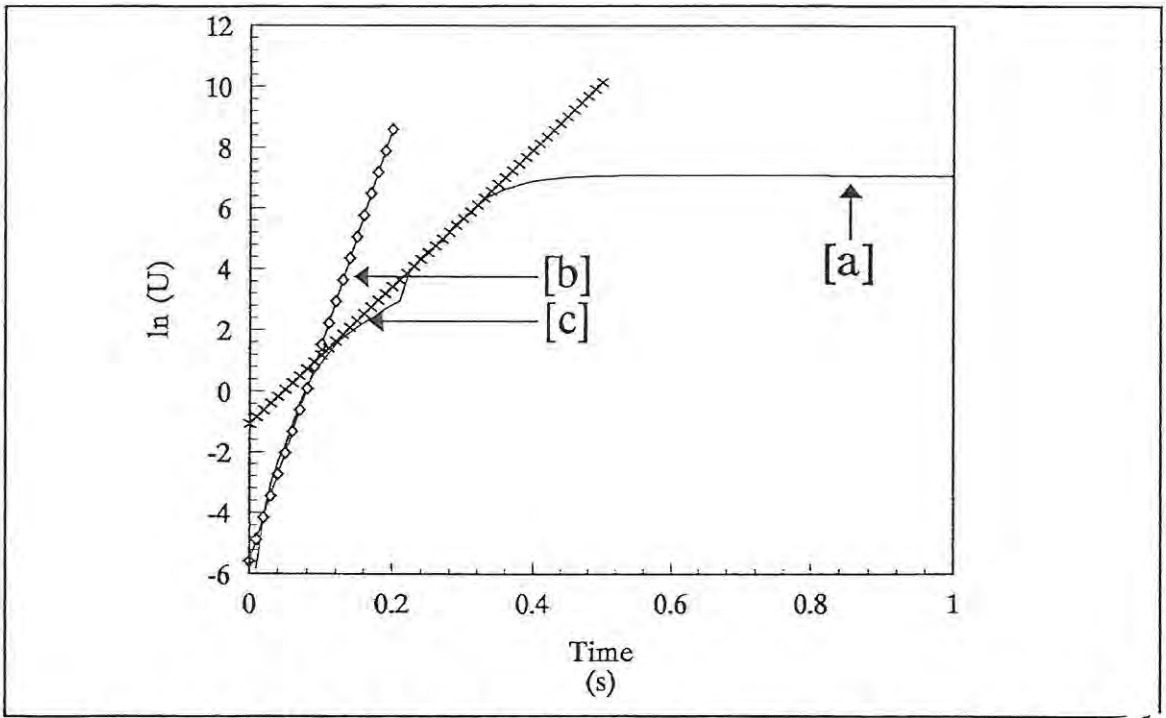

Figure 8.22: Plot of ln U vs time for the Sb/ $KMnO_4$ simulation (using A = 14.2s^{-1}), used for calculating the rise time, where [a] is the calculated profile, [b] and [c] are the two possible extremes of gradient of the rise time region.

investigation into the effects of various parameters, acceptable correlation of burning rates and maximum temperatures was attained, as shown in Figure 8.21. The usefulness of the central composite design (explained in Section 6.2) for varying two parameters at the same time while keeping the number of simulations to a minimum, was demonstrated.

Table 8.14
Values for 50% tungsten/potassium dichromate pyrotechnic composition.

			SI values	
	value	units*	value	units
ρ (density)	2.40	g cm^{-3}	2400	kg m^{-3}
c (average heat capacity)	0.1576	cal K^{-1} g^{-1}	0.66	J K^{-1} g^{-1}
λ (reactant thermal conductivity)	5.52×10^{-4}	cal s^{-1} cm^{-1} K^{-1}	0.23	W K^{-1} m^{-1} s^{-1}
Q (combustion energy)	257	cal g^{-1}	1.08	kJ g^{-1}
E_a (activation energy)	2.94	kcal mol^{-1}	12.3	kJ mol^{-1}
A (pre-exponential factor) (initial value)	580	s^{-1}		
A (pre-exponential factor) (best value)	300	s^{-1}		
n (order of reaction)	1			
T_{ign} (ignition temperature)	671	K		

* Note: units given are those required for input to TOPAZ

8.4 TOPAZ simulation of the $W/K_2Cr_2O_7$ system.

8.4.1 Introduction.

As a check on the simulations of the $Sb/KMnO_4$ reference system, similar procedures were applied to simulation of the $W/K_2Cr_2O_7$ system, for which results of extensive experimental and theoretical study by Boddington and Laye [24] are available. The composition chosen for the simulation was 50% $W/K_2Cr_2O_7$ and the input parameters are listed in Table 8.14.

Comparison of the experimental values in Table 8.14 with those in Table 8.10 (for 30% $Sb/KMnO_4$) show that values of ρ and c for the two systems are similar, values of Q, A and T_{ign} are larger and values of λ and E_a are smaller for the $W/K_2Cr_2O_7$ system.

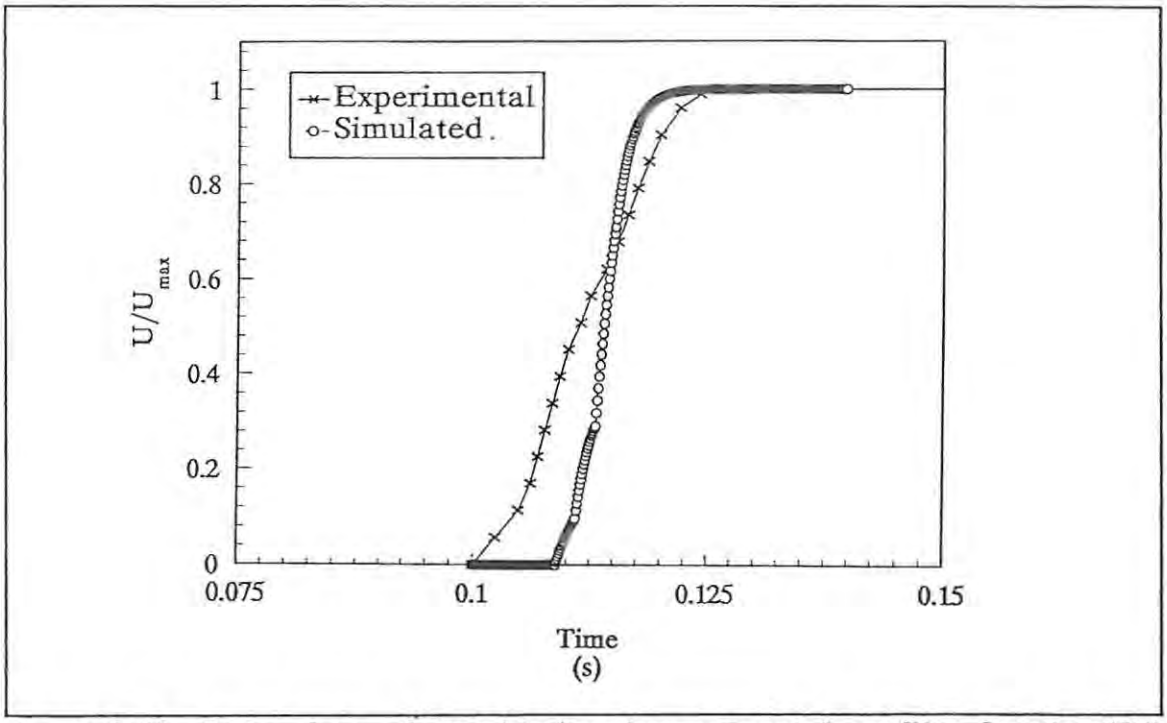

Figure 8.23: Comparison of simulated and experimental profiles for the 50% $W/K_2Cr_2O_7$ system, using a pre-exponential factor of 580 s^{-1}.

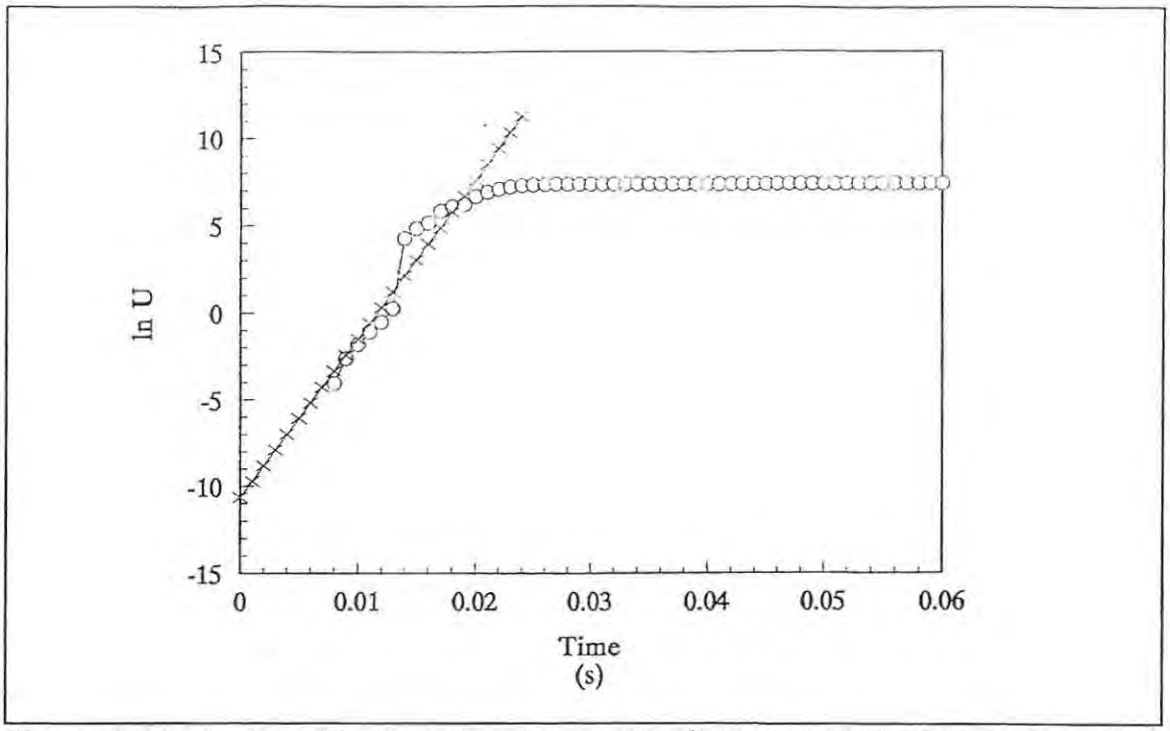

Figure 8.24 A plot of ln U vs time (A = 580 s^{-1}) for the 50% W/$K_2Cr_2O_7$ system used to calculate the rise time.

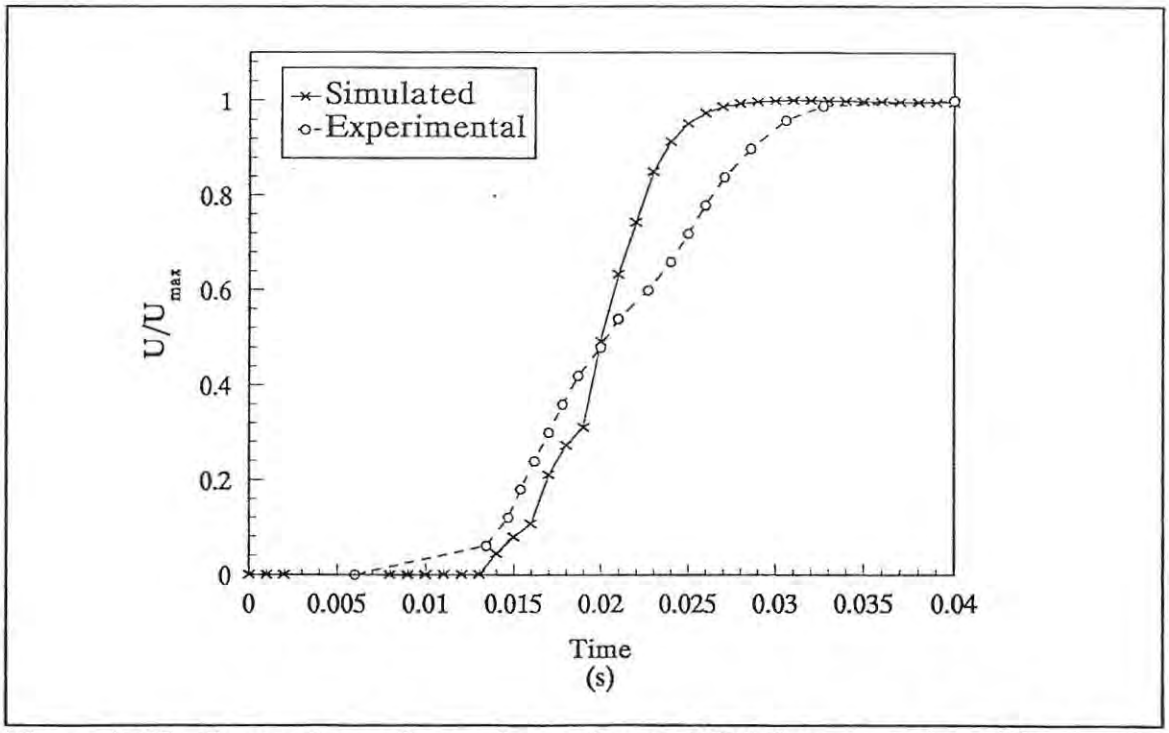

Figure 8.25: Comparison of experimental and TOPAZ generated profiles for the 50% W/$K_2Cr_2O_7$ system, using a pre-exponential factor of 300 s^{-1}.

8.4.2 TOPAZ simulation.

The values in Table **8.14** (taking the initial value for the pre-exponential factor) gave the profile shown in Figure **8.23** compared with an experimental profile. The value of d (ln U) /dt for the first part of the plot, shown in Figure **8.24**, is 5279 s^{-1} which gives a burning rate of 27.75 mm s^{-1}, and a maximum temperature of 1937 K, compared with experimental values of 12.1 $\pm$ 4.9 mm s^{-1} and 2070 K.

Some fine tuning was achieved by setting the pre-exponential factor to 300 s^{-1} which gave a burning rate of 11.53 mm s^{-1} and a maximum temperature of 1973 K which is in the acceptable range. A comparison between the simulated and experimental profiles is shown in Figure **8.25**.

8.5 Discussion.

The starting points of these studies are the experimental temperature-time profiles recorded for two different pyrotechnic compositions :

(a) 30% $Sb/KMnO_4$ and

(b) 50% $W/K_2Cr_2O_7$.

These experimental profiles had been analyzed by the researchers involved to extract the kinetic and thermodynamic parameters characteristic of the system. The profile for system (a) (Figure **8.12**), compared to that for system (b) (Figure **8.25**) shows that combustion of the $Sb/KMnO_4$ composition has a lower value of U_{max} during combustion (~1200 K compared to ~1650 K for $W/K_2Cr_2O_7$) and that the rise to U_{max} occurs over a longer time scale (~100 ms compared to ~25 ms for $W/K_2Cr_2O_7$).

Comparison of the reported kinetic and thermodynamic parameters for the two systems (Tables **8.1** and **8.14**) shows that the two systems have similar densities, specific heat capacities and thermal conductivities (all measured at ambient temperature). The $W/K_2Cr_2O_7$ system has a higher reaction heat output per gram (257 cal against 172 cal) and, on the assumption of first-order kinetics, has a lower activation energy (2.94 kcal mol^{-1} against 8.25 kcal mol^{-1}) and higher pre-exponential factor (580 → 300 s^{-1} against 25 → 15 s^{-1}).

When the parameters extracted from the experimental profiles were used as input for TOPAZ, the profiles produced were broadly similar to the originals. The reaction kinetics used within TOPAZ are of the same form (i.e. general order-of-reaction type, rate equation and Arrhenius temperature dependence) as used in the kinetic analyses of experimental profiles.

In the analysis of experimental profiles, the burning rate v, only appears indirectly in the rise time, t_r, of the profile (see section 4) and the agreement between values of v calculated from experimental values of t_r ($1/t_r = D/v^2$) and measured burning rates is generally not good. Agreement between the values of v, calculated from corresponding points on TOPAZ profiles separated by a known internodal spacing, and experimental burning rates was not good, but the calculated v was found to be very sensitive to the value used for the Arrhenius pre-exponential factor, **A**. Adjustment of the value of **A** could be used to produce a value of v in agreement with experiment, without significant changes to the other features of the simulated profile. The pre-exponential factor, **A**, is notoriously the kinetic parameter with the greatest uncertainty, since it appears as the intercept of the linearly extrapolated Arrhenius plot at $\mathbf{1/T = 0}$ (i.e. $T = \infty$) which is far beyond the range of experimental measurements. **A** also tends to accumulate various constant terms by default.

Studies described in section **8.3.3** examined the influence of the two physical parameters, the thermal conductivity, λ, and the density, ρ, on the burning rate v, and the maximum temperature, T_{max}. The maximum temperature reaches its highest value in the approximate centre of both the thermal conductivity and the density ranges examined (Figure **8.14**) and decreases sharply to relative plateaus towards the extremes of the ranges. TOPAZ tends to exaggerate the value of the maximum temperature (this has also been commented on previously by Beck [50]). The burning rate, v, showed increases at high thermal conductivities and high density, (Figure **8.13**), as would be expected from the increased heat transfer.

One aspect of the TOPAZ profiles which is of particular concern is the series of deceleratory segments making up the initial "rise" region of the profiles. This precludes very good matching of calculated with experimental profiles. This feature could have its origins in the definition of the finite element mesh used, or the time steps used in the

calculation, but may also be a consequence of the deceleratory reaction kinetic model used in allowing for heat generation in TOPAZ. The influence of the kinetic model is examined in the next section.

The effect of the mesh size on the profiles generated was investigated as far as possible. TOPAZ, running on a VAX system, is limited in the number of elements in the mesh which it can use. Initially a column was defined using a grid of 15 by 30. Grids of 30 by 60 and 60 by 120 were also investigated, with the latter being found to be too big for this version of TOPAZ to handle. Comparison of both the profile shape and the values of the burning rate and maximum temperature produced by using the two sets of grids were similar, with the smaller grid giving less precision in its results. It was descided to use the 30 by 60 grid definition of the column as the standard, because it gave a good compromise between the time taken for calculation and the precision and reproduciblity of the results.

9. THE INFLUENCE OF THE CHOICE OF KINETIC MODEL ON THE SHAPES OF TEMPERATURE PROFILES.

9.1 Introduction.

Temperature profiles simulated using the finite-difference model and a first-order rate equation were far more deceleratory than the corresponding experimental profiles (Figure 5.1). A marked improvement in comparability was obtained when sigmoid-type rate equations (specifically the Prout-Tompkins equation : $\mathbf{d\alpha/dt = k\ \alpha(1 - \alpha)}$, characteristic of autocatalysis, and the Johnson-Mehl-Avrami-Erofeev equation: $\mathbf{d\alpha/dt = n\ k(1 - \alpha)(-\ln(1 - \alpha))^{(n-1)/n}}$, characteristic of processes based on formation and growth of product nuclei) were used in place of the first-order equation, as shown in Figures 7.3 and 7.5.

The parameters extracted from the experimental profiles for the two reference systems are compared in Table 9.1 with the parameters used in the TOPAZ and finite-difference simulations to give best agreement with experiment. The TOPAZ simulations, as shown by comparison with the simpler finite-difference simulations, are probably hampered by the limited choice of reaction kinetic equations used. The possibility of modifying the appropriate section of TOPAZ (see Figure 9.1) was investigated.

The code (written in VMS Fortran) uses the expression **dd = -(con(m)**cde) *fexp*dt** to calculate the amount of heat generated due to reaction. This expression uses $\mathbf{con(m)^{cde}}$ to give order-of-reaction kinetics (and specifically first-order kinetics when cde = 1).

9.2 Use of Prout-Tompkins (autocatalytic) kinetics.

Substitution of the first-order reaction kinetics by Prout-Tompkins kinetics involves the code changes shown in Figure 9.2. The Prout-Tompkins system equation cannot operate from values of $\alpha = 0$ or, in this case, **con(m)** = 1. So additional modifications had to be made to set the initial concentration value to slightly less than 1 (i.e. 0.9999).

Table 9.1
Input parameters required for TOPAZ and finite difference models to give the best match of simulated profiles with experimental profiles.

Symbols	Extracted Parameters	TOPAZ	Finite Difference	units
		30% $Sb/KMnO_4$ System		
ρ	2500	2550	2500	kg m^{-3}
c	0.58 - 1.20	0.59	0.60	J K^{-1} g^{-1}
λ	0.3 $\pm$ 0.1	0.29	0.30	J s^{-1} m^{-1} K^{-1}
Q	0.72 - 0.92	0.72	0.82	kJ g^{-1}
E_a	34.5	34.5	35.0	kJ mol^{-1}
A	506	14.9	100	s^{-1}
n	0.66	1	1	
T_{ign}	560	560	200	K
		50% $W/K_2Cr_2O_7$ System		
ρ	2400	2400		kg m^{-3}
c	0.66 $\pm$ 0.07	0.66		J K^{-1} g^{-1}
λ	0.23 $\pm$ 0.01	0.23		J s^{-1} m^{-1} K^{-1}
Q	1.08 $\pm$ 0.05	1.08		kJ g^{-1}
E_a	12.3 $\pm$ 2.6	12.3		kJ mol^{-1}
A	580	300		s^{-1}
n	1.7	1		
T_{ign}	671	671		K

```
c*************************************************
subroutine reaction1(m,atemp,value,con,del,wt)
c*************************************************
c     calculates heat evolution in reacting materials
c     with arrhenius kinetics and ignition temperature
c*************************************************
      common /chem/ nel,time,dt
      common /reac/ qdsx,edsx,zdsx,tig,cde
      dimension con(1),del(1)
      if (atemp.lt.tig) then
      value=0.0
      goto 10
      endif
      rt=1.9872*atemp
      fexp=zdsx*exp(-edsx/rt)
      dd=-(con(m)**cde)*fexp*dt
      ddwm=wt*dd
      if ((ddwm+del(m)+con(m)).lt.0.0) ddwm=-con(m)-
1del(m)
      del(m)=del(m)+ddwm
      value=-qdsx*ddwm/(dt*wt)
 10   continue
      return
      end
```

Figure 9.1: Subroutine reaction1 from TOPAZ code.

The modification was done to a subroutine conin (Figure **9.3**).

Trials using the input parameters given in Table **9.1** for both the Sb/$KMnO_4$ and W/$K_2Cr_2O_7$ systems gave the profiles shown in Figures **9.4** and **9.5**. Both of the profiles in Figure **9.4** and **9.5** show distinct steps approximately midway through the profile. This step was eliminated by increasing the initial value of α from 0.0001 to 0.01. Profiles obtained by using the parameters in Table 1 are given in Figures **9.6** and **9.7**. The calculated profiles are compared with the experimental profiles.

```
c*************************************************
subroutine reaction1(m,atemp,value,con,del,wt)
c*************************************************
c     calculates heat evolution in reacting materials
c     with arrhenius kinetics and ignition temperature
c      Modified for Prout-Tompkins approach
c*************************************************
      common /chem/ nel,time,dt
      common /reac/ qdsx,edsx,zdsx,tig,cde
      dimension con(1),del(1)
      if (atemp.lt.tig) then
      value=0.0
      goto 10
      endif
      rt=1.9872*atemp
      fexp=zdsx*exp(-edsx/rt)
c Modification
      dd=-(con(m)*(1-con(m))*fexp*dt
      ddwm=wt*dd
      if ((ddwm+del(m)+con(m)).lt.0.0) ddwm=-con(m)-
1del(m)
      del(m)=del(m)+ddwm
      value=-qdsx*ddwm/(dt*wt)
 10   continue
      return
      end
```

Figure 9.2: Modification of subroutine reaction1, of TOPAZ code, to use Prout-Tompkins reaction kinetics.

```
c*******************************************************
     subroutine conin(km,con,mtype,numel)
c*******************************************************
c*   subroutine to initialise reactant concentrations
c*   Modified for Prout-Tompkins reaction kinetics
c*******************************************************
     dimension km(5,1),con(1),mtype(2,1)
     do 10 i=1,numel
  10    con(i)=0.0
     do 20 i=1,numel
     matn=km(5,i)
     if (mtype(1,matn).le.4 goto 20
     con(i)=0.9999
  20 continue
     return
     end
```

Figure 9.3: Modification to subroutine conin of TOPAZ code to allow for Prout-Tompkins reaction kinetics to occur.

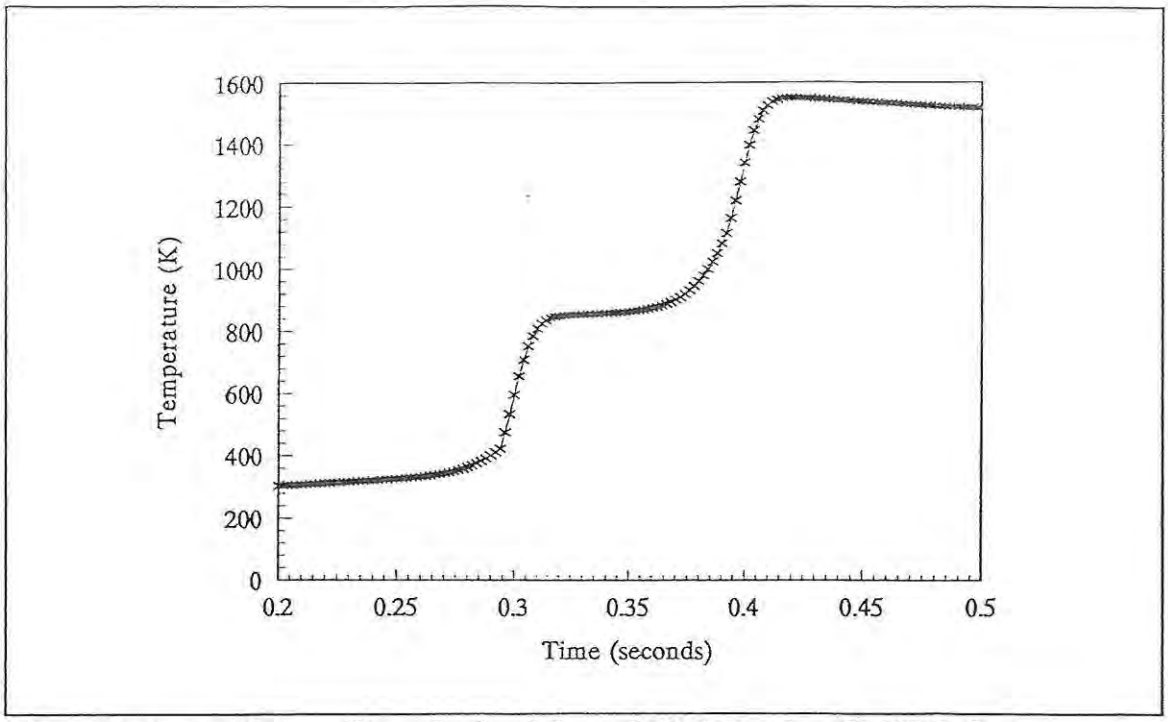

Figure 9.4: Initial profiles obtained from TOPAZ using Sb/$KMnO_4$ parameters and Prout-Tompkins reaction kinetics.

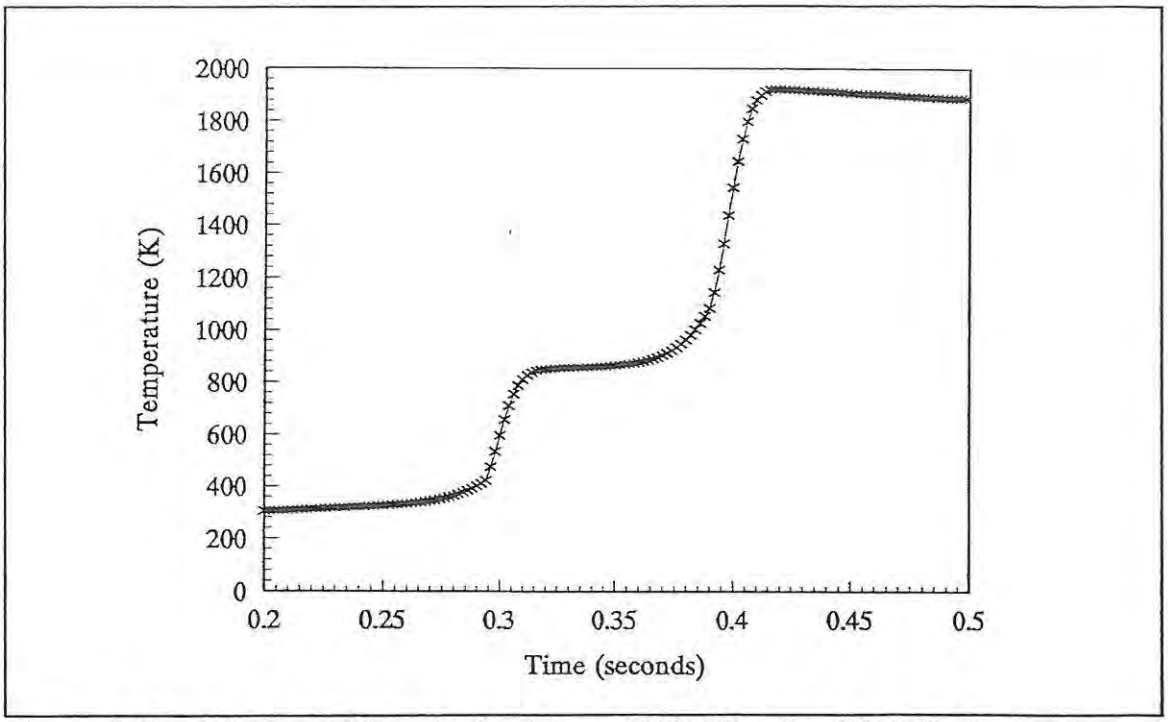

Figure 9.5: Initial profiles obtained from TOPAZ using W/$K_2Cr_2O_7$ parameters and Prout-Tompkins reaction kinetics.

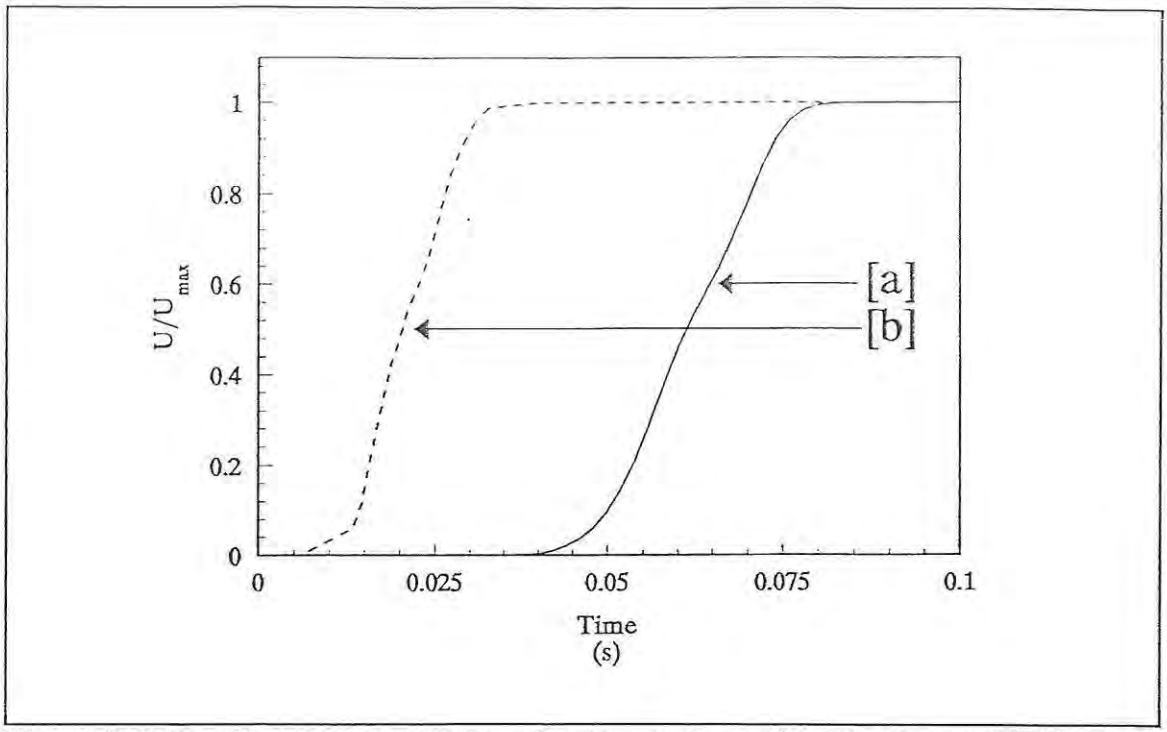

Figure 9.6 Profiles at node 140 [a] using Prout-Tompkins kinetics and W/$K_2Cr_2O_7$ input parameters, compared to the experimental profile [b].

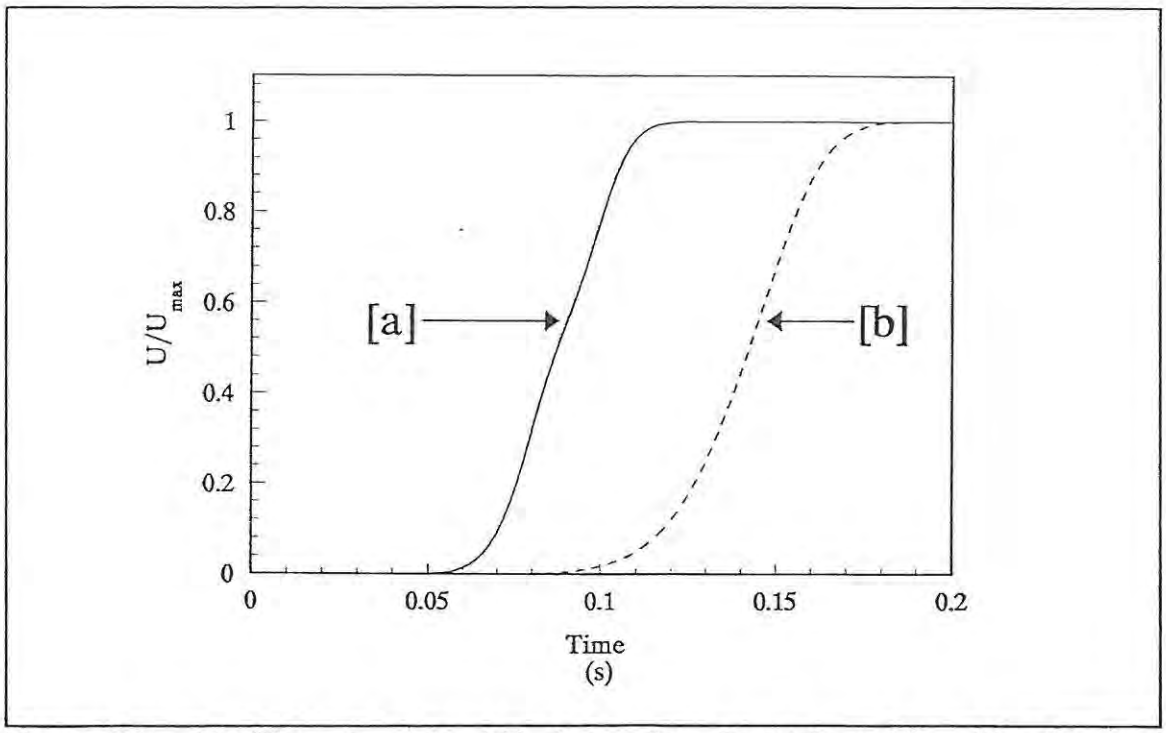

Figure 9.7: Profiles at node 140 [a] using Prout-Tompkins kinetics and Sb/$KMnO_4$ input parameters, compared with the experimental profile [b].

9.3 Johnson-Mehl-Avrami-Erofeev kinetics.

Substitution of the first-order kinetics by Johnson-Mehl-Avrami-Erofeev kinetics involved the programming changes shown in Figure 9.8. As was found for the Prout-Tompkins kinetic model, the value of **con()** had to be set to 0.99. Profiles obtained using this model and the input parameters shown in Table 9.1 for simulations of the $Sb/KMnO_4$ and the $W/K_2Cr_2O_7$ systems are shown in Figures 9.9 and 9.10.

The shape of the profile changed with increasing value of ***n*** (Figure 9.11).

```
c*****************************************************
      subroutine reaction1(m,atemp,value,con,del,wt)
c*****************************************************
c     calculates heat evolution in reacting materials
c     with arrhenius kinetics and ignition temperature
c     Modified for Prout-Tompkins approach
c*****************************************************
      common /chem/ nel,time,dt
      common /reac/ qdsx,edsx,zdsx,tig,cde
      dimension con(1),del(1)
      if (atemp.lt.tig) then
      value=0.0
      goto 10
      endif
      rt=1.9872*atemp
      fexp=zdsx*exp(-edsx/rt)
c Modification
c Prevent taking the log of 0 or negative number
      if (con(m).le.0) then
      dd = 0
      else
      dd=-(2*(1-con(m))*(-ln(1-con(m)))**0.5)*fexp*dt
      endif
      ddwm=wt*dd
      if ((ddwm+del(m)+con(m)).lt.0.0) ddwm=-con(m)-
1del(m)
      del(m)=del(m)+ddwm
      value=-qdsx*ddwm/(dt*wt)
 10   continue
      return
      end
```

Figure 9.8: Modification of subroutine reaction1, of TOPAZ code, to use Johnson-Mehl-Avrami-Erofeev reaction kinetics.

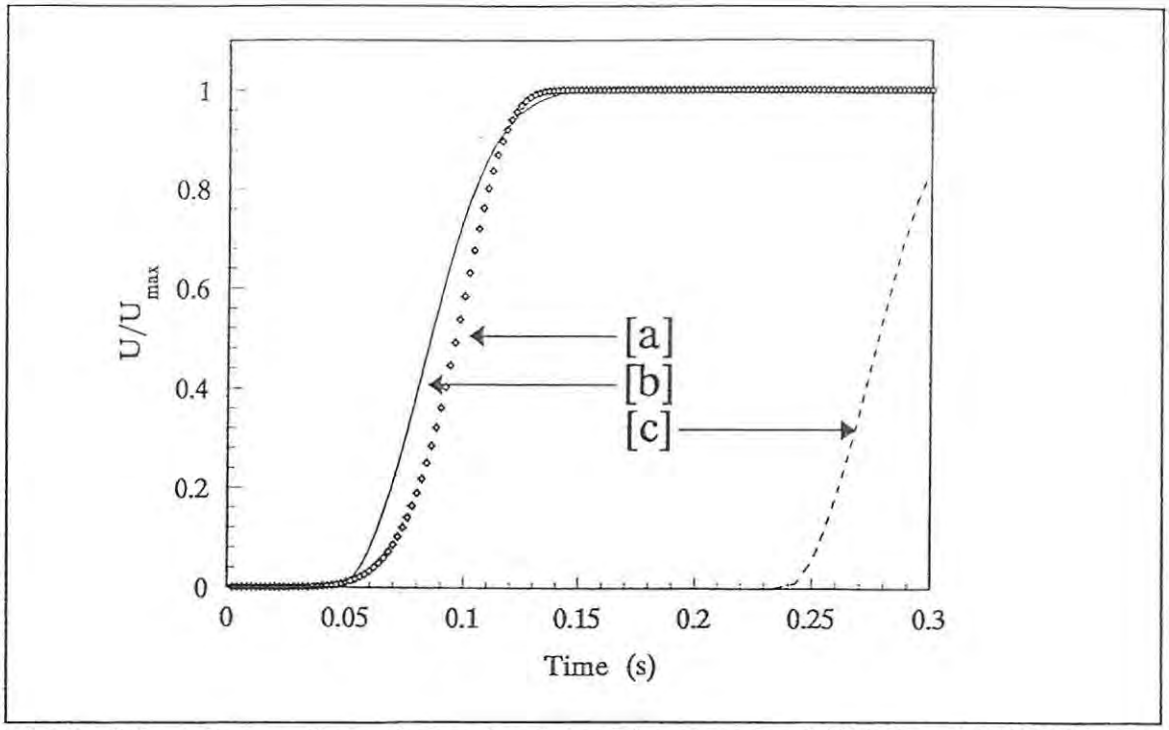

Figure 9.9: Comparison of simulated profiles at nodes 140 [a] and 150 [b] using Avrami kinetics and $Sb/KMnO_4$ input parameters, with the experimental profile [c].

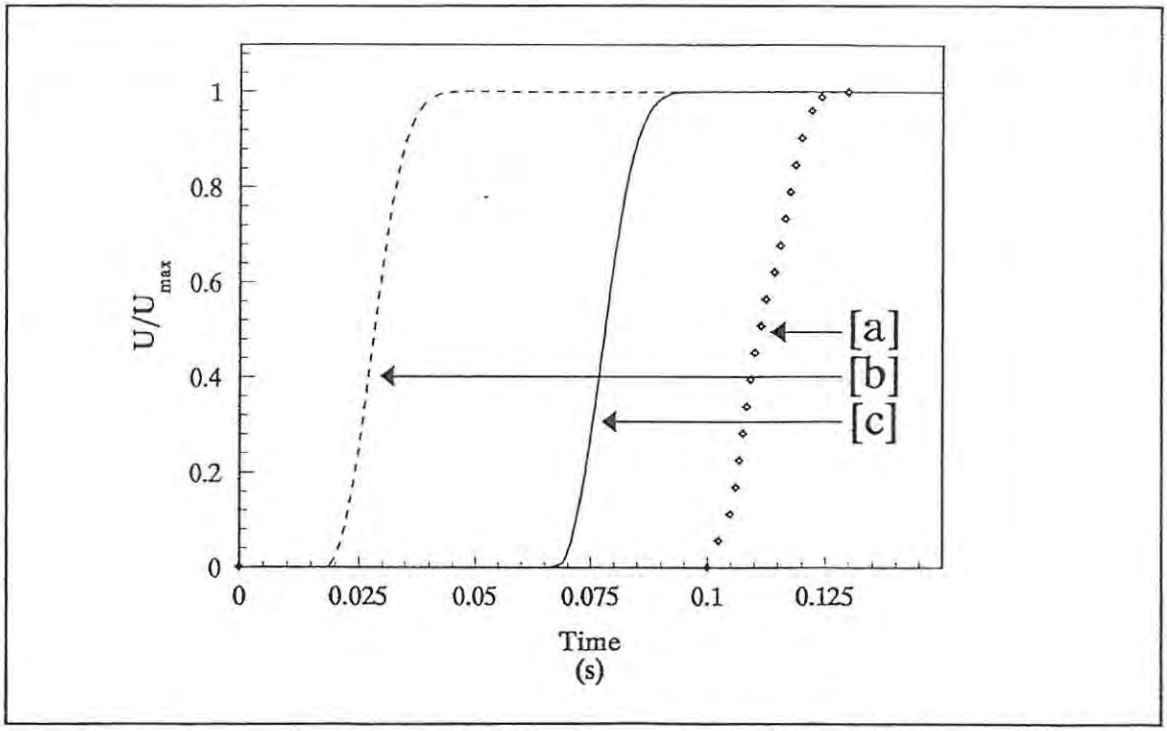

Figure 9.10: Comparison of simulated profiles of nodes 140 [a] and 150 [b], using Avrami kinetics and $W/K_2Cr_2O_7$ input parameters comppared with the experimental profile [c].

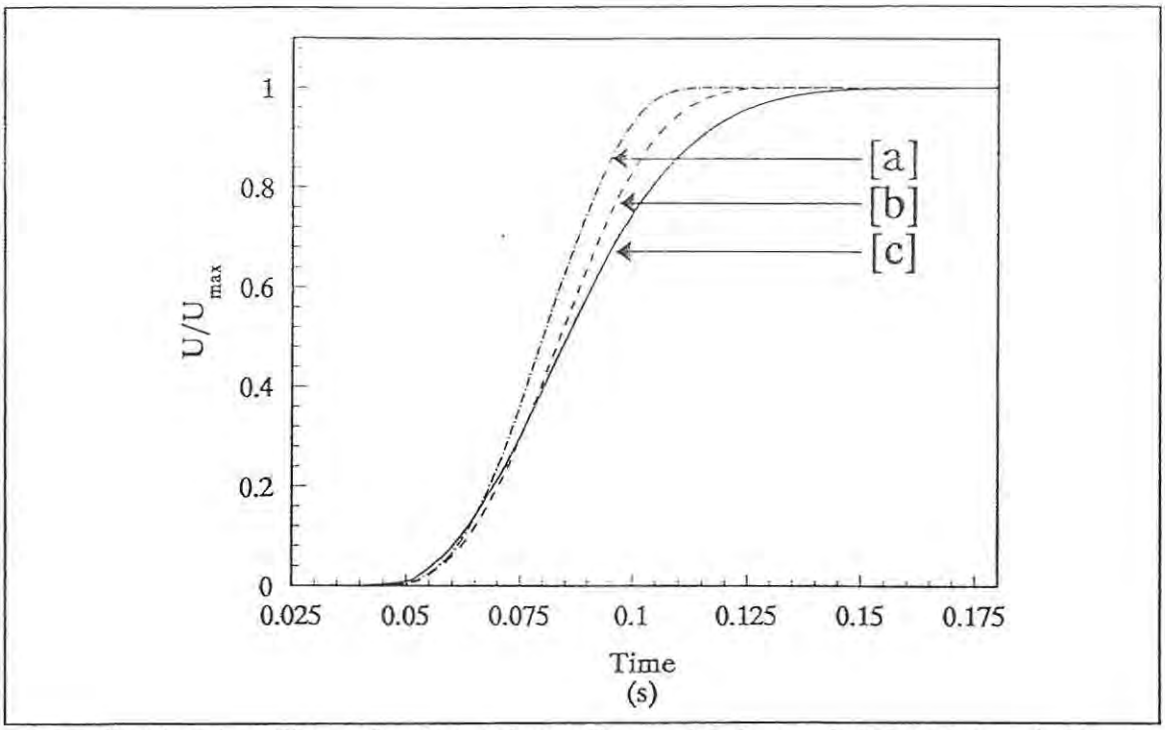

Figure 9.11: The effect of using values of n = 4 [a], n= 3 [b] and n = 2 [c], on the profiles generated using Avrami kinetics.

Both the acceleratory and deceleratory regions became more marked at higher values of *n*.

9.4 Conclusions.

By investigating additional kinetic models, other than the simple first-order kinetic model used in the TOPAZ program, it was hoped to achieve a better correlation between the experimental and the simulated profiles. Of the two kinetic models investigated, the Johnson-Mehl-Avrami-Erofeev kinetic model appears to be more promising. However, both models introduce further variables to an already complex system, thus decreasing the ease of obtaining precision in the results obtained.

Time constaints prevented further, more detailed investigation into alternative kinetic models, and this is an area for further investigation.

10 PARTICLE PACKING AND ITS INFLUENCE ON PYROTECHNIC COMBUSTION.

10.1 Introduction.

Hao and Tanaka [51] have shown that in a binary mixture of solids A and B, if the particles of A and B are assumed to be uniformly spherical with radii, r_A and r_B, and molar densities (mol m^{-3}), ρ_A and ρ_B, respectively, and if the initial amounts of A and B (in moles) are m_{A0} and m_{B0}, the total number of contact points between the two kinds of spheres, for this specified amount of mixture, is

$$N_R = XY/Z$$

where $X = [3(1 - \epsilon_A)\, m_{A0} / (\pi\, \rho_A\, r_A^3)]$

$Y = [(1 + R_r + 2\gamma)^2\{2R_r + (1 + R_r)\gamma\}^2]$

$Z = [(1 + \gamma)(R_r + \gamma)^2\{3(R_r + \gamma)^2 + (1 + \gamma)(R_r^2 + \gamma)\}]$

and ϵ_A = the surface porosity [52] of the spherical packing, $R_r = r_B/r_A$, $R_\rho = \rho_B/\rho_A$, $R_m = m_{B0}/m_{A0}$, and $\gamma = R_r^3 R_\rho / R_m$.

This work followed on from an earlier paper by Tanaka and Ouchikama [52] where it was shown that a completely mixed packing system could be fully described by N, the number of spheres, f(x), the size distrubution frequency, and ϵ_A, the surface porosity. The surface porosity is the void area fraction on a spherical surface of diameter $x + x'$, where x' is the average diameter of particles, defined as :-

$$x' = \int_0^\infty x f(x)\, dx \qquad 10.1$$

A simple packing model was used and the coordination number C(x) was expressed as :-

$$C(x) = 16(1 - \epsilon_A)\left(\frac{x + x'}{2x'}\right)^2 \qquad 10.2$$

Using an equal number of "points-of-coordination" for each sphere, with the coordination number characteristic of the size of the sphere, the total number of points of coordination C_T is given by :-

$$C_T = \int_0^\infty C(x) N f(x) dx0 \qquad 10.3$$

The term "points-of-coordination" refers to a point at which two adjacent spheres have a possiblity of making contact. The number of contact points was shown to be :-

$$n(D,d)\delta D\delta d = \frac{C(D)C(d)}{C_T} N^2 f(D) f(d)\, \delta D\delta d \qquad 10.4$$

where D and d are the diameters of the particles.

When the surface pososity can be assumed to be constant, equations **10.1** to **10.4** can be rewritten as :-

$$\frac{C(x)}{C(x')} = \left(\frac{x + x'}{2x'}\right)^2$$

$$C_T = 16(1 - \epsilon_A) N \left(\frac{3 + [(x^2)'/(x')^2]}{4}\right)$$

$$n(D,d)\,\delta D\delta d = 16(1 - \epsilon_A)\left(\frac{D + x'}{2x'}\right)^2 \frac{\left(\frac{d + x'}{2x'}\right)^2}{\frac{3 + (x^2)'/(x')^2}{4}} N f(D) f(d)\, \delta D\delta d$$

$$\textit{where} \quad C(x) = 16(1 - \epsilon_A)$$

$$(x^2)' = \int_0^\infty x^2 f(x) dx$$

Using the values of various packing characteristics it was then possible to evaluate the number of contacts between spheres of arbitrarily specified sizes. When the surface porosity was regarded as constant, irrespective of the sizes of the spheres, it can be related to the volume porosity ϵ of the packing of uniformed sized spheres. In the case of uniform sized spheres, every sphere makes $16(1 - \epsilon_A)$ direct contacts with neighbors, of size **x**. The volume porosity, ϵ, could then be approximated by the fractional free volume within the spherical space of diameter **2x** :-

$$\epsilon = [\pi(2x)^3/6 - \{\pi x^3/6 + 16(1 - \epsilon_A)(13/16)\ X\ (\pi x^3/12)\}]/\pi(2x)^3/6$$

$$or \qquad \epsilon_A = (16\epsilon - 1)/13$$

A contact point is defined [53,54] as a small connection pipe with finite area and thickness. Examples of one of the many classes of practically important binary mixtures of solid particles are the solid fuel / solid oxidant mixtures extensively used in pyrotechnic applications. The initial interactions of such mixtures are generally assumed to be exothermic solid-solid reactions of the type:

$$aA(s) + bB(s) \rightarrow products$$

although the temperature rises rapidly and melting, vaporisation, decompositions of oxidants, and solid-gas reactions may participate.

Experimentally determined burning rates have been reported for numerous binary fuel/oxidant combinations. Table 10.1 gives a list of a selection of pyrotechnic systems for which a considerable amount of experimental information is available and summarizes the main characteristics of these systems. More details of the fuel and oxidant samples used are given in Table 10.2.

In this section, the assumption of uniform spherical particles of both fuel and oxidant is used to calculate the numbers of contact points between fuel and oxidant particles, $\mathbf{N_R}$, **in each case based on 1.00 g of the specified composition**, for the systems listed in Table 1, and the results of comparison of the values of $\mathbf{N_R}$ obtained and the experimental burning rates, **v**, are given for each individual system, below. (The

TABLE 10.1
Main characteristics of the binary pyrotechnic systems.

SYSTEM	Range of compositions (mass % fuel)	Burning rates (mm s^{-1})	Composition at v_{max} (% fuel)	Reference
$Sb/KMnO_4$	30 - 70	2 - 28	60	15,25,26,55
Fe/BaO_2	15 - 50	6 - 42	30	66
Fe/SrO_2	20 - 55	4 - 9	25,45	66
Mn/BaO_2	15- 65	1.7 - 11.7	20	62 - 65
Mn/SrO_2	20 - 80	4.5 - 12.3	75	62 - 65
Mo/BaO_2	20 - 70	2.7 - 10.1	45	62 - 65
Mo/SrO_2	40 - 45	2.2 - 2.3	40	62 - 65
Si/SnO_2	20 - 55	5 - 17	40	57,58,60,61
Si/Fe_2O_3	20 - 40	2.3 - 4.5	40	57,58,60,61
Si/KNO_3	30 - 85	2 - 35	85	57,59 - 61
Si/Sb_2O_3	20 - 50	1.6 - 8.7	40	57,59 - 61
$W/K_2Cr_2O_7$	30 - 85	1.0 - 25	70	10,19,20,24
Si/Pb_3O_4	5 - 50	40 - 257	15	56

value of the surface porosity, ϵ_A, used was 0.35 [51] and was assumed constant for all compositions of all the systems examined.)

10.2 The antimony/potassium permanganate system.

The $Sb/KMnO_4$ system has been widely used in commercial delays and has been extensively studied [15,25,26,55]. Results for three samples with different average fuel particle-sizes were available. Table **10.3** lists the calculated contact points and experimental burning rates for these three samples.

For a sample of fixed r_{Sb} (e.g., sample (1) in Table **10.3**), the variations of N_R and of v with composition are shown (suitably scaled) in Figure **10.1**. The similarity

TABLE 10.2
Characteristics of the fuels and the oxidants.

Fuels	Melting points °C		ρ / g cm^{-3}	r / μm
Sb	631	(1)*	6.68	13
		(2)		14
		(3)		9
		(4)		3.0
		(5)		2.0
Fe	1535		7.86	2.6
Mo	2610	(1)	10.2	32.0
		(2)		17.2
		(3)		6.9
Mn	1244	(1)	7.2	56.4
		(2)		8.4
Si	1410	(1) & (C)	2.33	2.5
		(2) & (B)		2.0
		(3)		1.7
		(4)		1.3
		(5) & (A)		1.0
W	3410		19.35	0.40
Oxidants	**Decomposition Temperature °C**		**ρ / g cm^{-3}**	**r / μm**
$KMnO_4$	290 exo, 520 endo		2.70	13.0
BaO_2	500 endo		4.96	5.1
SrO_2	390 endo, 525 endo		4.56	1.75
Fe_2O_3	melts 1565		5.24	0.30
SnO_2	melts 1630		6.95	0.45
Sb_2O_3	melts 656, sublimes		5.5	1.2
KNO_3	melts 334, d 400 exo		2.11	6.7
$K_2Cr_2O_7$	melts 398, d 500		2.68	3.0
Pb_3O_4	d 500		9.1	2.5

* **Numbers in brackets refer to the particle sizes in the last column.**

TABLE 10.3
Calculated contact points* (N_R) and experimental burning rates (v) for the Sb/$KMnO_4$ system [15,25,26,55]

$KMnO_4$ r = 13 μm

	Sb sample (1) r = 13 μm		Sb sample (2) r = 9 μm		Sb sample (4) r = 3 μm	
$r_{fuel}/r_{oxidant}$	1.0		0.69		0.23	
%Sb	v (mm s^{-1})	N_R (x 10^7)	v (mm s^{-1})	N_R (x 10^7)	v (mm s^{-1})	N_R (x 10^7)
10	-	1.6	-	3.4	-	50
20	-	3.1	-	6.4	-	86
30	2.0	4.3	2.5	8.8	6.5	105
35	2.5		4.3		8.4	
40	5.5	5.3	7.0	10.6	12.5	111
50	10.0	6.0	11.5	11.6	19.0	106
60	11.0	6.3	11.0	11.8	20.5	94
70	9.5	6.1	11.0	10.9	22.5	77
80	-	5.2	-	8.8	-	54
90	-	3.3	-	5.3	-	29

* based on 1.00 g of the specified composition.

of the two curves and the close coincidence of their maxima suggest a dependence of v upon the value of N_R. Burning fails at a higher value of N_R on the fuel-rich side of the curve.

Both N_R and v increase with decreasing r_{Sb} as shown in Figure 10.2. The maximum value of N_R shifts to lower %Sb as r_{Sb} decreases (see Table 10.3), but v_{max} remains at high proportions of Sb, suggesting incomplete reaction.

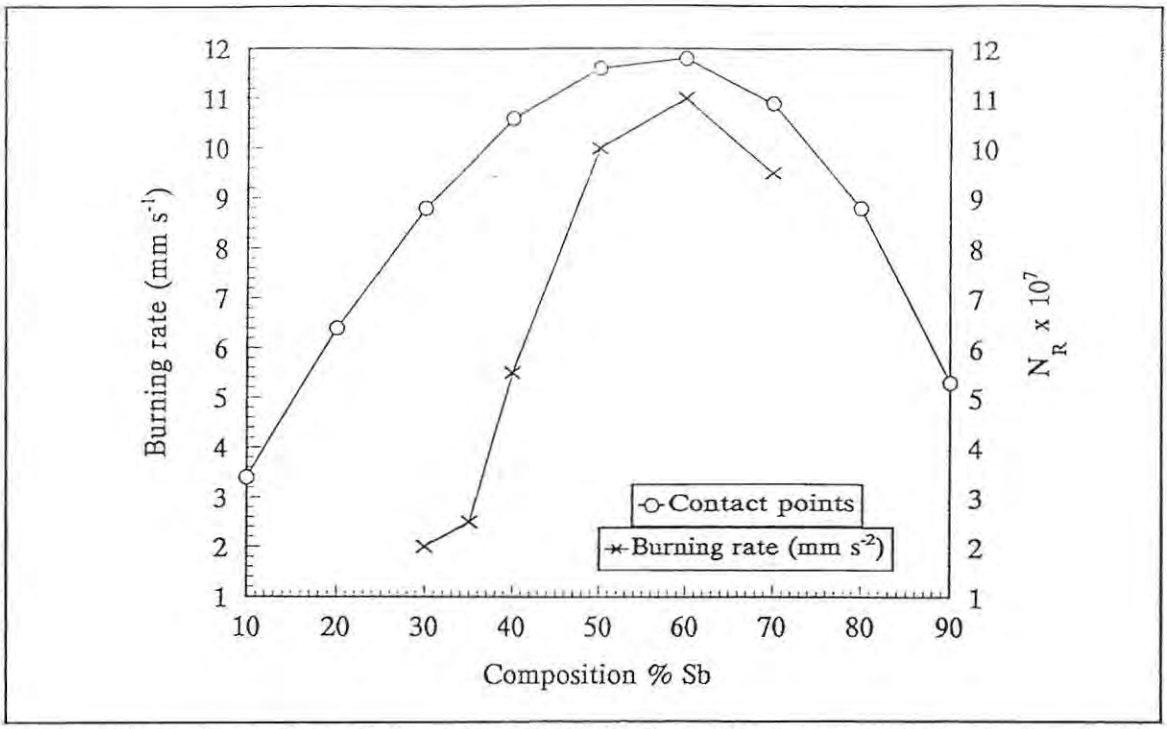

Figure 10.1: Variation of the calculated number of contact points, N_R (r=9μm), and the experimental burning rate, v, with composition of the 40% Sb/$KMnO_4$ system.

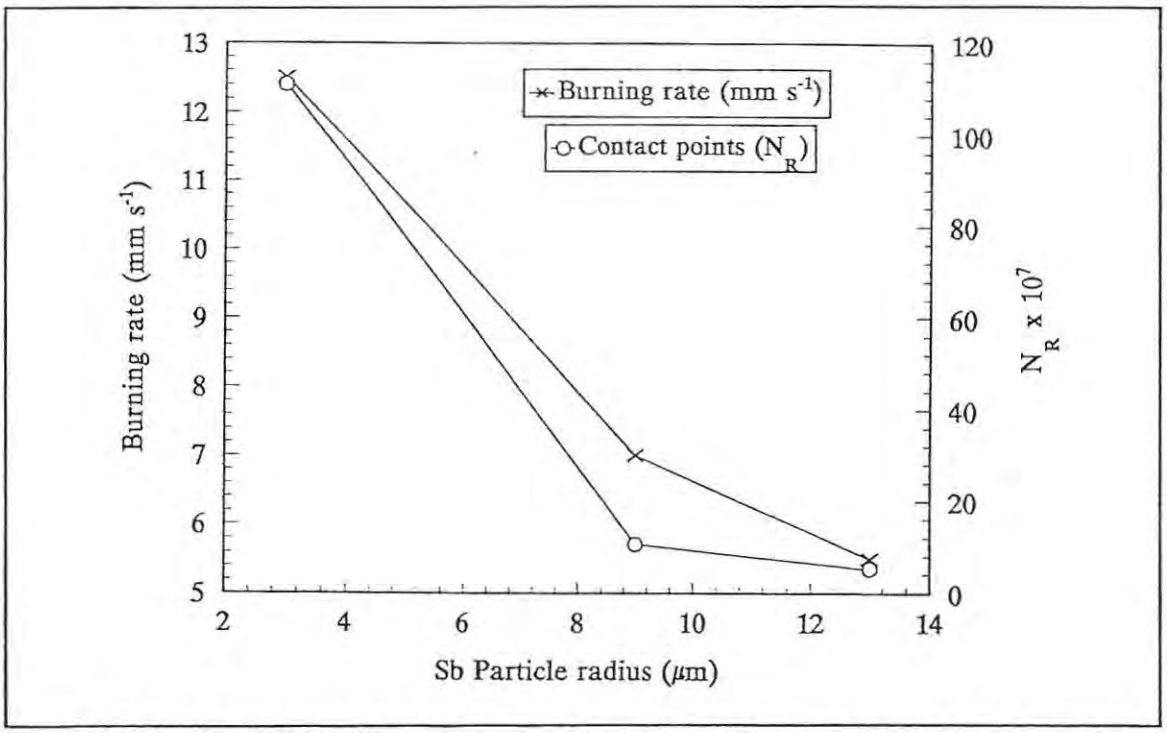

Figure 10.2: Variation of the calculated number of contact points, N_R, and the experimental burning rate, v, with fuel particle-size of the 40% Sb/$KMnO_4$ system,.

10.3 The tungsten/potassium dichromate system.

Another extensively studied system is $W/K_2Cr_2O_7$, which has been very carefully characterized by Boddington, Laye and co-workers at Leeds University [10,19,20,24]. Values of N_R calculated for one of their systems are compared in Table **10.4** with reported burning rates.

The variations of N_R and of v with composition are shown (suitably scaled) in Figure **10.3**. N_R values are at a maximum at 40% W, but v_{max} occurs at about 70% W. The values calculated for N_R are approximately 100 times those calculated for the **Sb(4)/$KMnO_4$** system above, although v_{max} values for the two systems are similar (25 and 21 mm s^{-1}, respectively).

TABLE 10.4

Calculated contact points* (N_R) and experimental burning rates (v) for the $W/K_2Cr_2O_7$ system [10,19,20,24].

W (0.40 μm) $K_2Cr_2O_7$ (3.0 μm) $r_{fuel}:r_{oxidant}$ 1:7.5		
%W	v (mm s^{-1})	N_R (x 10^9)
10	-	74
20	-	141
30	1.43	184
40	8.0	202
50	14.4	201
60	19.7	183
70	25.2	152
80	18.8	110
85	15.0	
90	-	59

* based on 1.00 g of the specified composition.

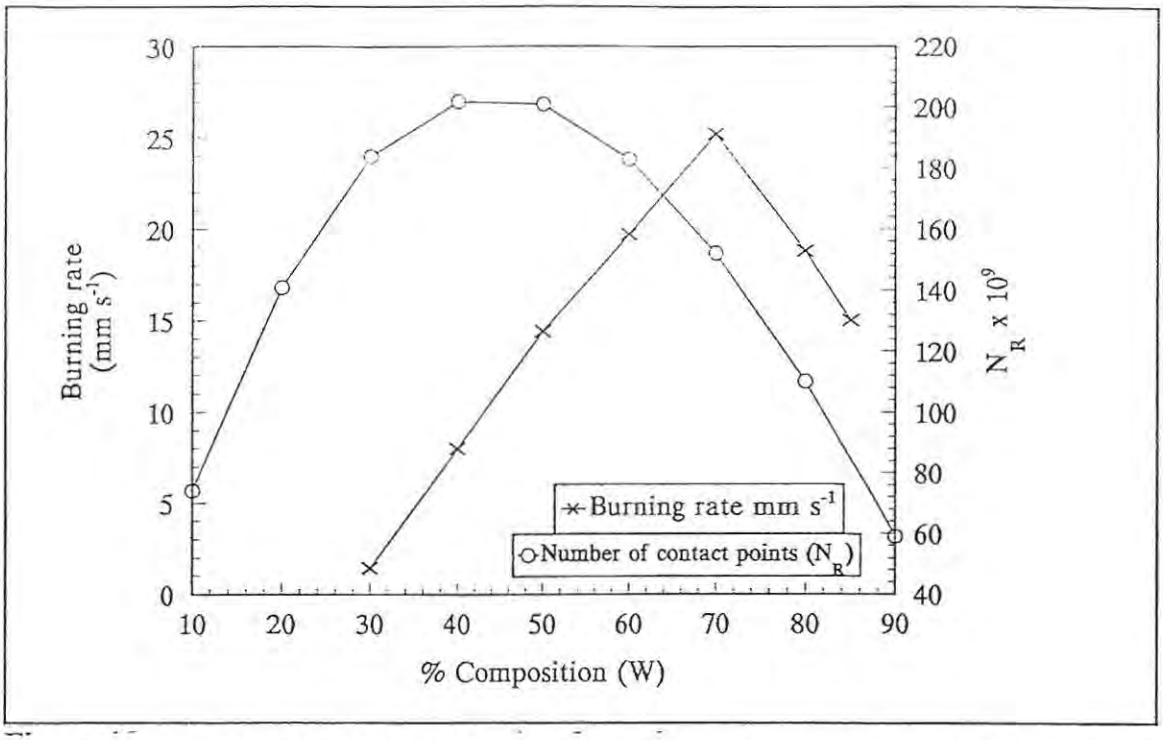

Figure 10.3 Variation of the calculated number of contact points, N_R, and the experimental burning rate, v, with composition of the (0.4 μm) $W/K_2Cr_2O_7$ system.

10.4 Silicon/lead oxide systems.

Silicon/lead oxide systems are of considerable commercial importance for use as short-period delays, i.e. their burning rates are relatively fast, and they have been extensively studied. Data published by Al-Kasraji and Rees [56] have been used to calculate values of N_R for the Si/Pb_3O_4 system. These values are compared with the reported burning rates in Table 10.5.

The variations of N_R and of v with composition are shown (suitably scaled) in Figure **10.4 (a)-(c)**. N_R values for the smallest Si particles (A) are at a maximum at very low % Si, increasing to about 10% Si for the larger particles (B and C), but v_{max} occurs at higher proportions of Si (about 15% (A) to 30% (B and C). Values of v_{max} and of N_R are plotted against particle size in Figure **10.5**.

TABLE 10.5
Calculated contact points* (N_R) and experimental burning rates (v) for the Si/Pb_3O_4 system [56,68].

Pb_3O_4 r = 2.5 μm

	Si sample (A) r = 1.0 μm		Si sample (B) r = 2.0 μm		Si sample (C) r = 2.5 μm	
$r_{fuel}:r_{oxidant}$	1:2.5		1:1.3		1:1	
% Si	v (mm s^{-1})	N_R (x 10^9)	v (mm s^{-1})	N_R (x 10^9)	v (mm s^{-1})	N_R (x 10^9)
5	108.9	18.3	46.1	4.3	42.4	2.8
10	222.2	26.6	94.4	7.0	64.6	4.8
15	257.4	30.2	100.6	8.7	71.5	6.1
20	249.9	31.7	108.7	9.8	79.9	6.9
25	138.8	31.8	134.3	10.3	98.7	7.4
30	139.0	31.1	163.0	10.5	114.8	7.7
35	127.1	29.9	116.6	10.4	86.6	7.7
40	114.7	28.4	89.4	10.2	72.3	7.6
45	94.4	26.6	69.2	9.7	53.2	7.3
50	59.3	24.6	38.8	9.2		7.0
55		22.5		8.5		6.5
60		20.2		7.8		6.0
65		17.9		7.0		5.4
70		15.5		6.1		4.7
75		13.0		5.2		4.0
80		10.5		4.2		3.3
85		7.9		3.2		2.5
90		5.3		2.2		1.7
95		2.7		1.1		0.9

* based on 1.00 g of the specified composition.

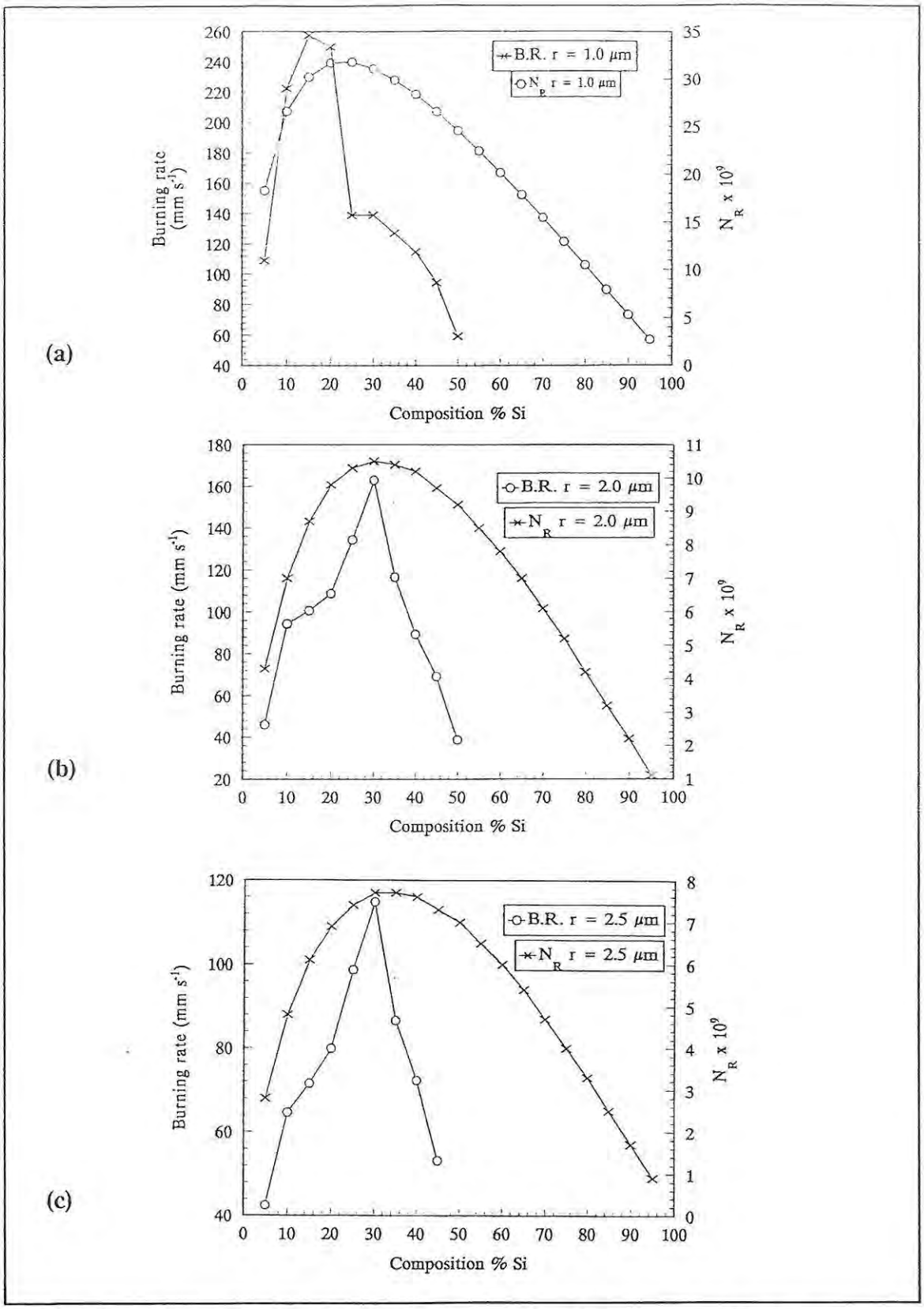

10.4 **Variation of the calculated number of contact points, N_R, and the experimental burning rate, v, with composition of the Si/Pb_3O_4 system: (a) Si radius 1.0 μm, (b) Si radius 2.0 μm and (c) Si radius.**

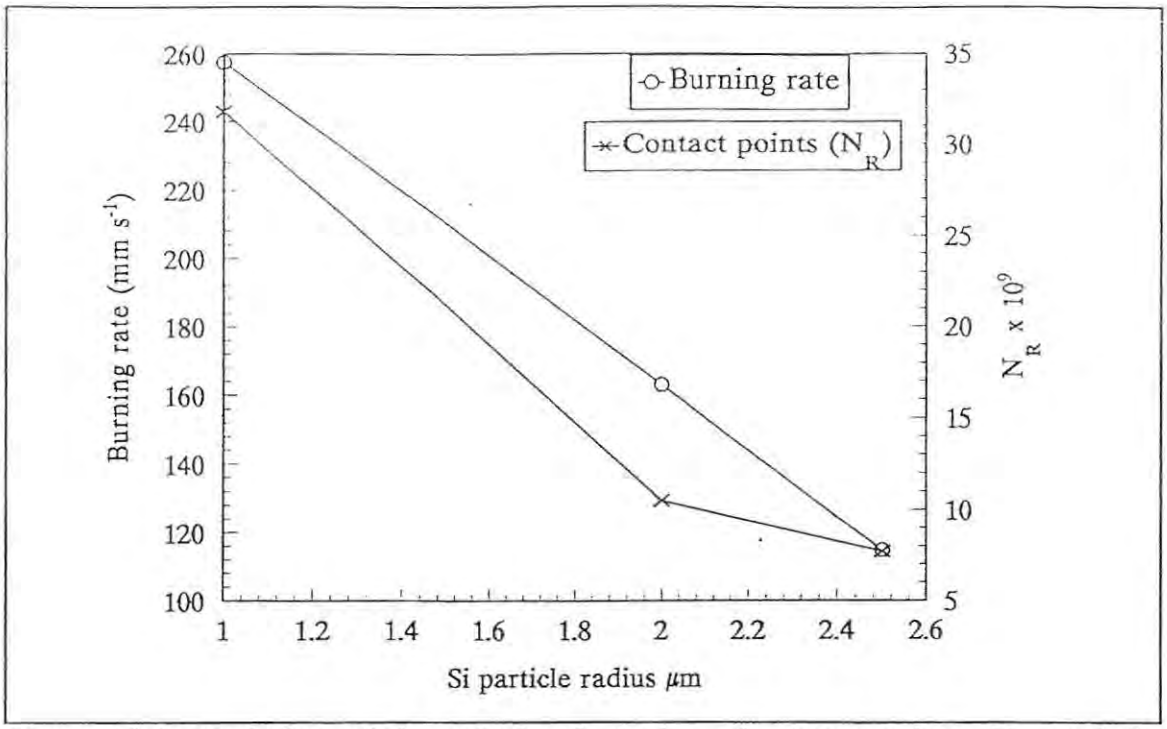

Figure 10.5: Variation of the calculated number of contact points, N_R, and the experimental burning rate, v, with fuel particle-size of the 15% Si/Pb_3O_4 system.

10.5 Other silicon oxidant systems.

A detailed study has been reported [57-61] of silicon as the fuel in binary combination with a variety of oxidants other than the lead oxides (see above). Values of N_R calculated for each of the systems are compared in Table **10.6** with the reported burning rates, and illustrated in Figure **10.6 (a)-(d)**.

TABLE 10.6

Calculated contact points* (N_R) and experimental burning rates (v) for Si/oxidant systems. [57-61]

Si sample (3)			r_f = 1.7 μm					
	Si/SnO_2		Si/Fe_2O_3		Si/Sb_2O_3		Si/KNO_3	
r_f/r_o =	3.8		5.7		1.4		0.25	
% Si	v (mm s^{-1})	N_R ($x10^{10}$)	v (mm s^{-1})	N_R (x 10^{10})	v (mm s^{-1})	N_R (x 10^{10})	v (mm s^{-1})	N_R (x 10^{10})
10		11.6		23.5		2.68		0.704
15		16.9		34.7		3.69		0.907
20	5.25	21.7	2.33	45.5	1.56	4.50		1.03
25	7.54	26.0	3.67	55.8	3.25	5.13		1.10
30	11.6	29.8	3.82	65.5	6.30	5.58	1.65	1.13
35	14.8	33.0	3.60	74.7	8.71	5.89		
40	17.1	35.6	4.54	83.1	8.52	6.05	2.78	1.10
45	15.7	37.6		90.5	8.73	6.08		
50	12.8	38.8		96.9	7.25	5.98	4.96	0.995
55	9.11	39.2		102		5.78		
60		38.7		105		5.46	8.43	0.844
65		37.3		107		5.06		
70		35.0		106		4.56	10.7	0.661
75		31.5		102		3.98	17.1	0.560
80		27.0		93.7		3.32	20.6	0.455
85		21.4		80.1		2.58	34.5	0.346
90		14.8		59.8		1.78		0.234

* based on 1.00 g of the specified composition.

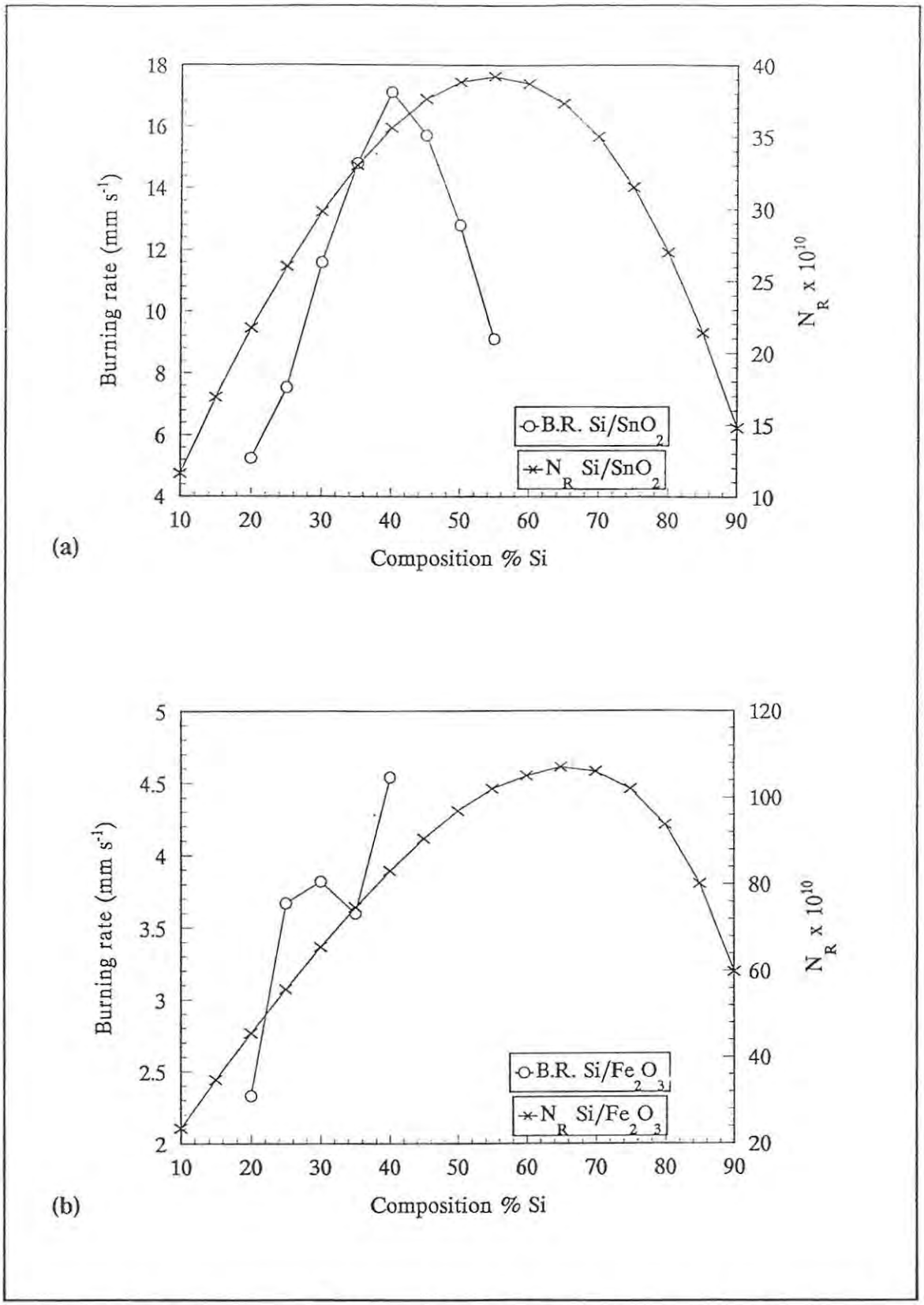

10.6 Variation of the calculated number of contact points, N_R, and the experimental burning rate, v, with composition of the : (a) Si/SnO_2 system; (b) Si/Fe_2O_3 system.

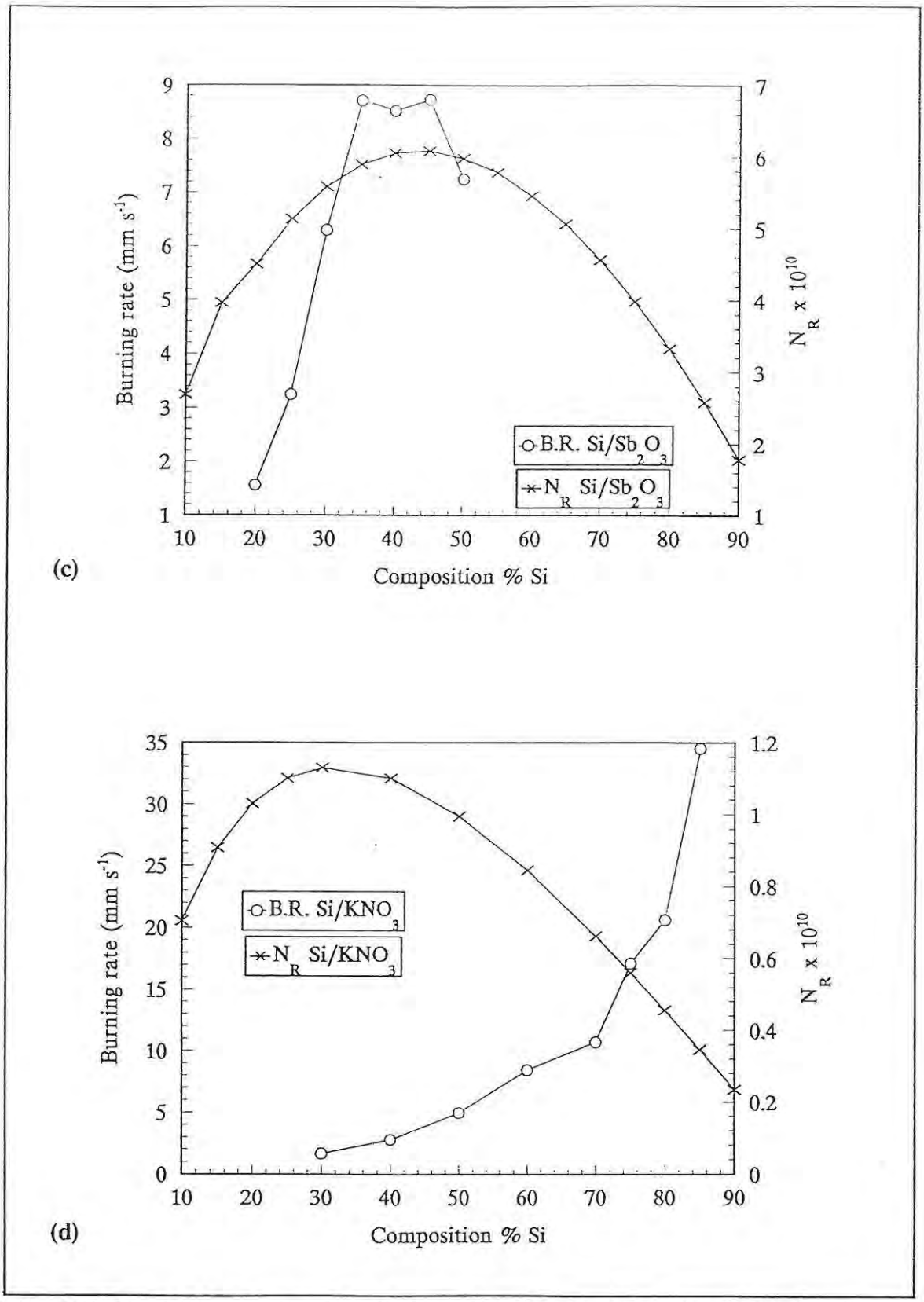

10.6 Variation of the calculated number of contact points, N_R, and the experimental burning rate, v, with composition of the : (c) Si/Sb_2O_3 system; (d) Si/KNO_3 system.

TABLE 10.7
Calculated contact points* (N_R) and experimental burning rates (v) for metal/peroxide systems [62-66].

	Mn r_f = 8.4 μm				Mo r_f = 17.2 μm				Fe r_f = 2.6 μm			
	Mn/BaO_2		Mn/SrO_2		Mo/BaO_2		Mo/SrO_2		Fe/BaO_2		Fe/SrO_2	
r_f/r_o	1.6		4.8		3.4		9.8		0.51		1.5	
% fuel	v mm/s	N_R x10^7	v mm/s	N_R x10^7	v mm/s	N_R x10^7	v mm/s	N_R x10^7	v mm/s	N_R x10^8	v mm/s	N_R x10^8
10		2.18		48.5		2.26		14.0		9.1		26.6
15	6.4	3.21		72.3		3.37		21.0	8.7	12.8		39.0
20	11.7	3.61	4.5	95.8	2.8	4.45		27.9	12.9	16.0	3.6	50.7
25	9.7	3.82	5.1	119	4.1	5.52		34.8	17.1	18.6	6.9	61.6
30	9.5	3.89	6.6	142	4.5	6.56		41.7	35.7	20.6	7.4	71.7
35	7.2	3.87	4.8	164	4.9	7.56		48.5	25.5	22.2	5.9	80.7
40	6.7	3.76	7.5	185	4.7	8.53	2.3	55.3	11.6	23.1	8.3	88.7
45	6.6	3.60	7.1	206	10.1	9.45	2.2	62.0	6.2	23.6	6.5	95.4
50	9.2	3.39	6.8	225	6.0	10.3		68.6	6.7	23.6	6.5	101
55	7.8	3.15	8.3	244	6.2	11.1		75.2		23.1	6.2	104
60	3.3	2.87	10.1	260	6.8	11.8		81.5		22.1		106
65	1.8	2.57	9.5	274	5.5	12.3		87.7		20.7		106
70		2.24	12.0	285	4.8	12.7		93.5		18.8		103
75		1.90	12.3	291		12.9		98.8		16.6		96.9
80		1.54	7.2	289		12.6		103		14.0		87.5
85		1.17		276		11.8		106		11.0		74.1
90		0.79		240		10.0		105		7.7		55.7

* based on 1.00 g of the specified composition.

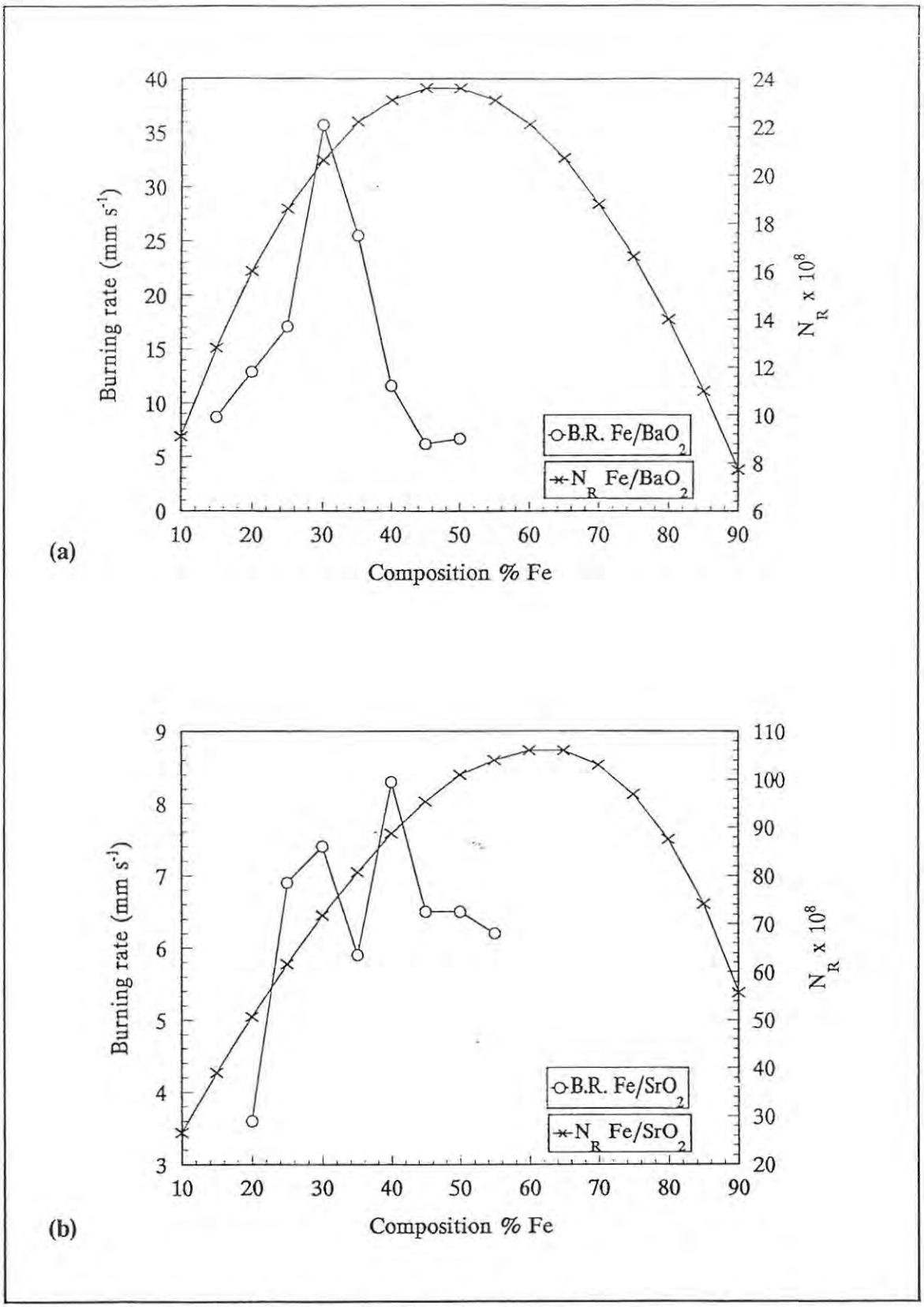

10.7 Variation of the calculated number of contact points, N_R, and the experimental burning rate, v, with composition of the : (a) Fe/BaO_2 system; (b) Fe/SrO_2 system.

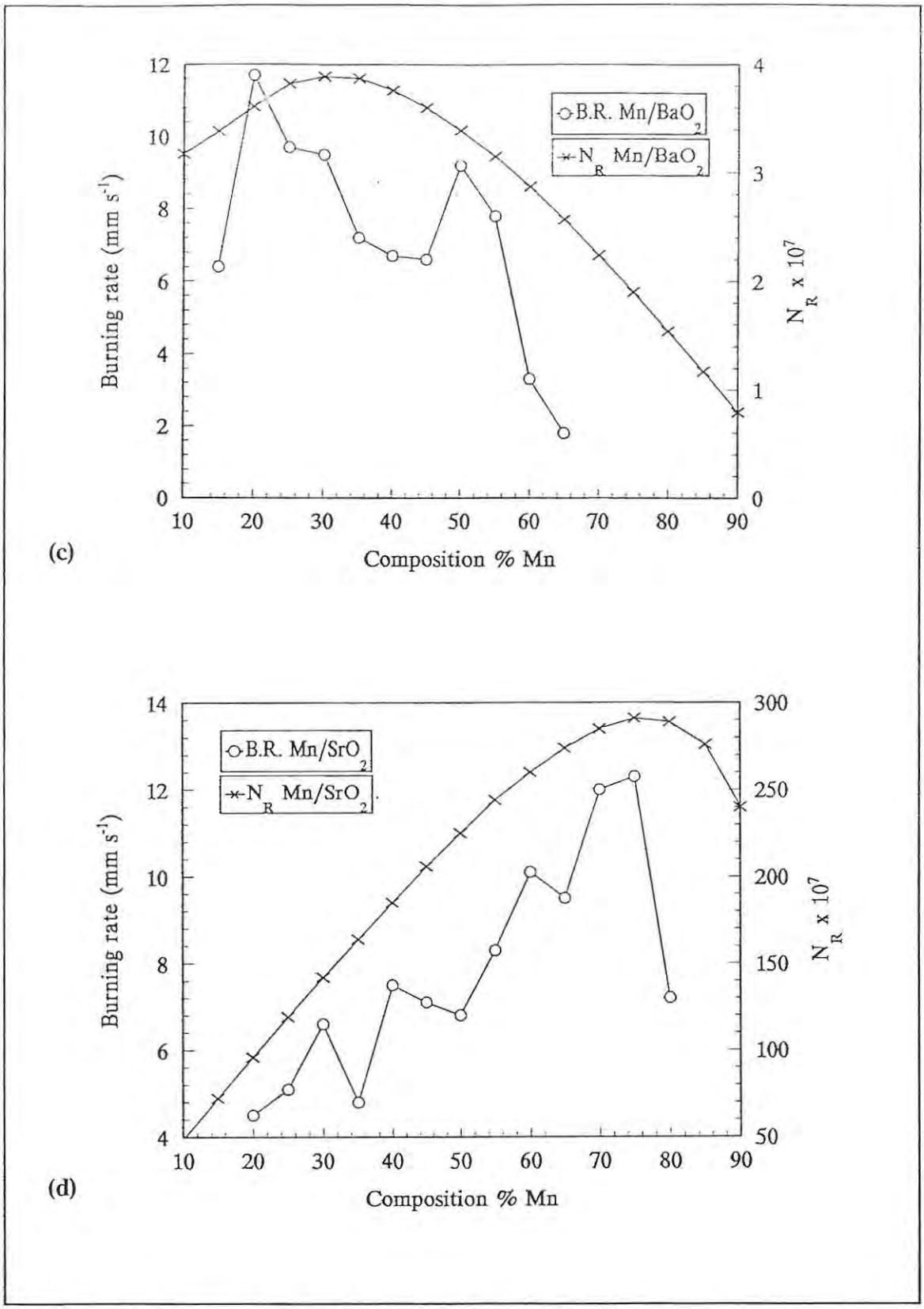

10.7 Variation of the calculated number of contact points, N_R, and the experimental burning rate, v, with composition of the : (c) Mn/BaO_2 system; (d) Mn/SrO_2 system.

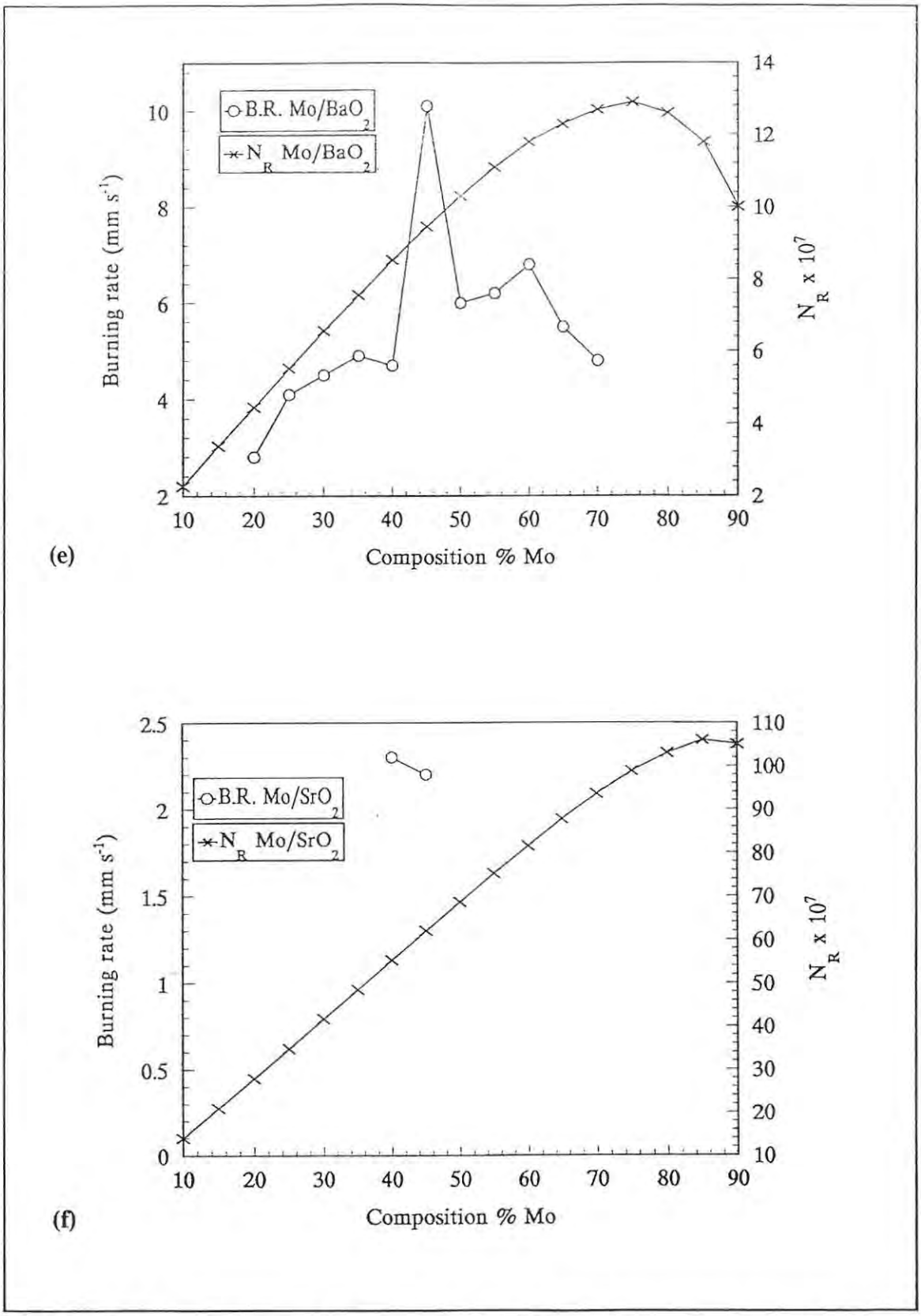

10.7 Variation of the calculated number of contact points, N_R, and the experimental burning rate, v, with composition of the : (e) Mo/BaO_2 system; (f) Mo/SrO_2 system.

10.6 Metal/alkaline-earth metal peroxide systems.

The contact points and burning rates of systems with either barium or strontium peroxide as the oxidant and manganese, molybdenum [62-65], or iron [66] as the fuel are listed in Table **10.7**, and illustrated in Figure **10.7 (a)-(f)**.

10.7 Conclusions.

Dodds [67] has discussed porosity and contact points in multicomponent random sphere packings. The major assumption made is that each sphere touches its neighbour. This allows the simplification that, by joining the centres of the spheres through their contact points, the packing space is divided up into tetrahedral subunits. The geometries of these tetrahedra are completely described by the radii of the four spheres from which they are formed. For an idealised binary packing of two different size spheres, A and B, there are five different tetrahedral subunits: AAAA, AAAB, AABB, ABBB and BBBB. The model is limited to size ratios of less than 1:6.46, and the packing can be described in terms of the relative numbers of the different tetrahedra present.

The real pyrotechnic systems, described above, are very different from this idealised situation. Average radii for fuel and oxidant particles have been used in the calculations without allowance for the range of particle- sizes of each. Particles have also been assumed to be approximately spherical, which is not very realistic for most of the oxidants considered.

It is thus of interest that, for many of the pyrotechnic systems, the trends in experimental burning rates, v, qualitatively parallel the trends in number of contact points (per 1.00 g of composition). However, as shown in Table **10.8** and Figure **10.8** (where the highest values of both variables have been omitted to avoid compression of the data in the neighbourhood of the origin), there is no direct relationship between burning rate and number of contact points over all the systems considered. Such a direct relationship would not be expected since chemical and/or diffusion factors specific to each system must control reaction through the contact point. Another, relatively minor, factor is the assumption of fixed surface porosity, ϵ.

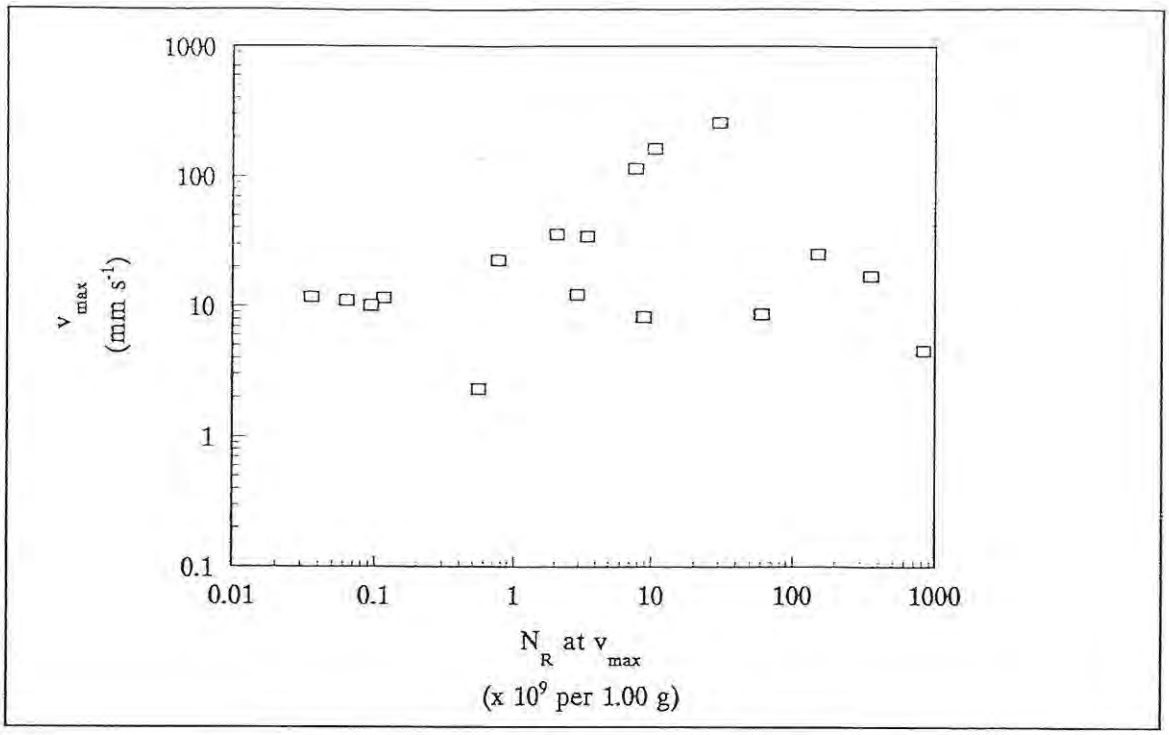

10.8 Plot of the calculated MAXIMUM number of contact points, N_R, against the experimental MAXIMUM burning rate, v_{max}, for the pyrotechnic systems considered (Note log. scale axes).

Several features arise on surveying the systems listed in Table **10.2**. Most of the oxidants, except Fe_2O_3, Sb_2O_3 and SnO_2 decompose with some release of $O_2(g)$ at temperatures (Table **10.1**) often well below the recorded values of T_{max}. Sb_2O_3 melts and vaporises, KNO_3 melts and decomposes, and $K_2Cr_2O_7$ melts. The melting points of the fuels (Table **10.1**) are high (excluding Sb). Substitution of SrO_2 for the apparently chemically similar oxidant, BaO_2, does not affect the burning rate of Mn/peroxide compositions (Table **10.2**) as much as it affects the Mo/peroxide compositions. Thus variation of the *constituents* of the binary mixtures listed can result in burning rates of from 2 to 115 mm s^{-1}. This range is also the maximum variation observed with change of *composition* (20 to 70% fuel) of the fixed binary combination ($Fe/KMnO_4$). The $Sb/KMnO_4$ and Si/KNO_3 systems also show above average ranges of burning rates with varying composition.

Variation of the *particle-size* of the fuel in the $Sb/KMnO_4$ system from a radius of 14 to 2.0 μm changed the burning rate (Table **10.5**) from 2 to 8 mm s^{-1} compared to the range of 2 to 28 mm s^{-1} with change in composition (Table **10.2**). Decreasing the

TABLE 10.8
Comparison of calculated maximum contact points* (N_R) and maximum experimental burning rates (v_{max}).

SYSTEM	v_{max} (mm s^{-1})	N_R at v_{max} (x 10^9 per 1.00 g)
$Sb(1)/KMnO_4$	11.0	0.063
$Sb(3)/KMnO_4$	11.5	0.116
$Sb(4)/KMnO_4$	22.5	0.77
Fe/BaO_2	35.7	2.06
Fe/BaO_2	8.3	8.87
Mn/BaO_2	11.7	0.036
Mn/SrO_2	12.3	2.91
Mo/BaO_2	10.1	0.0945
Mo/SrO_2	2.3	0.553
$Si(3)/SnO_2$	17.1	356
$Si(3)/Fe_2O_3$	4.54	831
$Si(3)/KNO_3$	34.5	3.46
$Si(3)/Sb_2O_3$	8.73	60.8
$W/K_2Cr_2O_7$	25.2	152
$Si(A)/Pb_3O_4$	257	30.2
$Si(B)/Pb_3O_4$	163	10.5
$Si(C)/Pb_3O_4$	115	7.7

particle-radius of Mo from 17.2 to 6.9 μm produced faster burning Mo/peroxide mixtures (Table **10.5**) than were possible by varying the composition of the mixtures with the larger Mo particles (Table **10.2**).

In spite of the severe approximations made, there is a qualitative connection between the calculated numbers of contact points, N_R, and the measured burning rates, v, of those pyrotechnic compositions which are presumed to burn mainly via solid-solid actions.

11. A MONTE CARLO MODEL OF THE COMBUSTION OF PYROTECHNIC SYSTEMS.

11.1 Introduction.

Binary pyrotechnic systems, fuel A/oxidant B, generally burn over a range of compositions. This range and the measured linear rates of burning, v, depend upon a variety of factors including the chemical nature of A and B, and the absolute and relative particle sizes and distributions of A and B.

As an initial (although very idealised) model, a binary pyrotechnic system with uniform particle-size and shape (sphere, cube) for both fuel and oxidant is considered. The densities are further assumed to be in such a ratio that one particle of fuel A would react stoichiometrically with one particle of oxidant B. Packing of the fuel/oxidant mixture is then assumed to be a totally random arrangement (without any influence of the different densities).

The model of the mixture is then of random distribution of A and B on a two-dimensional rectangular matrix in proportions related to the composition to represent a packed column of pyrotechnic mixture. Even at this simplified level, the resulting distributions of A and B over the column show that there are significant clusters of fuel and oxidant particles (see Figure 11.1).

When the arrangement of A and B is suitable for reaction, A-B or B-A, the cell in the column is given a probability of 1 and when reaction cannot occur, i.e. A-A or B-B, a probability of 0. When reaction has occurred, the cell is marked with a 2. Ignition of the mixture is represented by assuming that the first row of the matrix reacts completely and simultaneously irrespective of the neighbouring distribution.

i.e.	1st row	111111111111.....1
	2nd row	0110011100.....

Program **IV** was developed to establish what ratios of reactable (cell with 1's) to non-reactable (cells filled with 0's) would be required to allow for complete burning of the column. The approach involved looking at each cell, row by row down the column, and if it was in contact with a cell which had reacted (been set to 2) and it could react itself

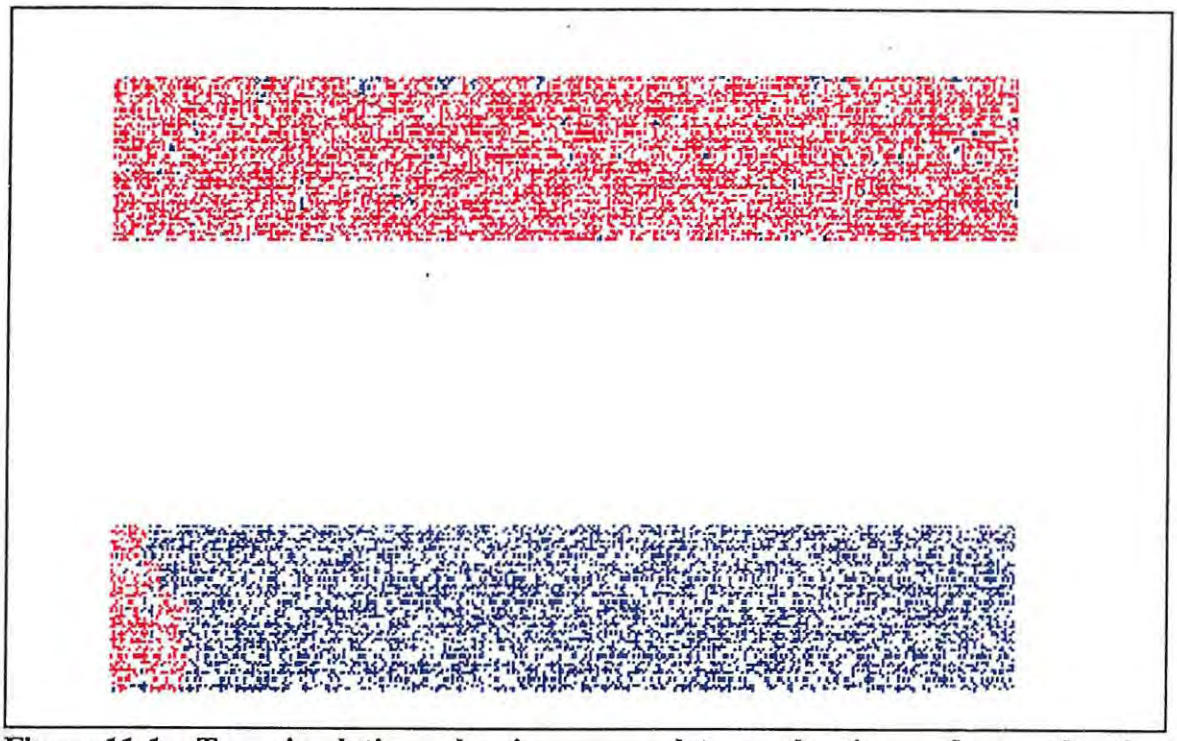

Figure 11.1: Two simulations showing a complete combustion and a combustion failure, showing clusters of reactable cells.

(had a value of 1) then reaction took place. In this way paths could be found through the column, and the results displayed graphically to show the distribution of reacted and unreacted cells throughout the column.

The problem then is to look for the connected paths through the matrix and to estimate the variations in burning rates caused by meanderings of the path through the composition. The path may proceed either :

(i)	straight forward	} progress
(ii)	diagonally forward (two choices)	
(iii)	horizontally (two choices)	pause for 1 unit
(iv)	diagonally backwards	-slow by 2 units
(v)	straight back	- slow by 3 units.

Considering a section of the matrix, the **current** position of the reaction is marked as cell **C**. One of the eight neighbouring positions will be the **input** position **I**.

I	1	2
7	C	3
6	5	4

For progress of the reaction, the remaining 7 positions have to be scanned.

	column	row
Current address of C	i	j
Current address if I	$i + a$	$j + b$

where $a \neq b$, $a \neq -b$ and $a = -1, 0$ or 1.

The I-C link has to be **orientated** relative to the overall forward direction, so that the rate of reaction can be monitored. Orientation is based on the values of a and b above.

(i)	straight forward	$a = -1, b = 0$
(ii)	diagonally forward	$a = -1, b = \pm 1$
(iii)	horizontally	$a = 0, b = \pm 1$
(iv)	diagonally back	$a = 1, b = \pm 1$
(v)	straight back	$a = 1, b = 0.$

11.2 **Results.**

Using the above approach, a set of simulations was carried out varying the ratios of reactable (1) and non-reactable (0) cells.

The minimum number of time steps required for the burning path to reach the end of the column is 500 (the number of cells down the length of the column). This figure was obtained when simulations were done with a column containing only reactable cells. As the proportion of non-reactable cells increased, the number of time steps required for the most direct path also increased. Different paths have different numbers of time steps and the variations in total time are inversely related to variations to be expected in the linear burning rate of a fixed composition. These variations are a consequence of random

Table 11.1
Effect of changing ratio of reactable to non-reactable cells on average number of time steps required to burn through column.

Reactable to non-reactable ratio	Average number of time steps ± std. dev.
1 : 0	500 ± 5
1 : 0.5	578 ± 7
1 : 1	647 ± 20
1 : 1.5	971 ± 40

packing. For a 1 : 1 ratio of reactable and non-reactable cells, the minimum number of time steps was 647 ± 20. This value increased dramatically with values of non-reactable cells higher than 1. Ratios of 1 : 1.2 (reactable to non-reactable) and greater (higher non-reactable value) lead to combustion failure.

This model has a similar, though less quantitative, basis to the contact-point model (Section 10), but serves to illustrate the unavoidable uncertainties in burning rates arising from randomness of the fuel/oxidant packing.

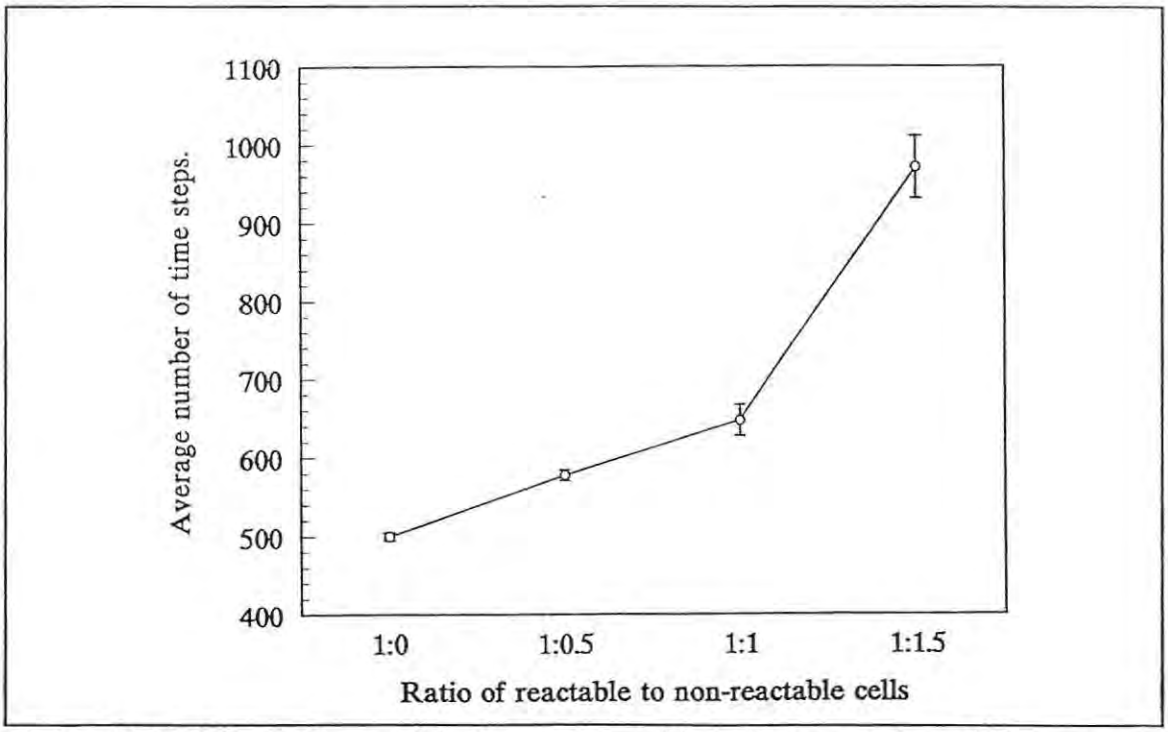

Figure 11.2: Effect of reactable to non-reactable ratio on number of time steps.

12 GENERAL DISCUSSION AND CONCLUSIONS.

12.1 Introduction.

The main aim of this research was to use computer modelling to complement the experimental techniques which have been used to investigate the combustion of pyrotechnic compositions. Thermal analysis of fuels, oxidants and their combinations under controlled heating conditions and analysis of temperature-time profiles from combustion experiments have been used extensively to study the behaviour of numerous pyrotechnic compositions. To investigate fully all the possible combinations of fuels and oxidants would be impossible. Use of a well-defined, reliable computer model can, firstly, cut down the number of experiments required to investigate a specific system fully, and secondly, be used to decide which new systems should be investigated. This study reports some of the models which could be used for predicting the combustion behaviour of pyrotechnic systems.

As in all modelling studies, a balance has to be kept between the complexity of the model (which should be related to the reliability of its predictions) and the practical usefulness of such a model (i.e. time constraints and number of input parameters).

12.2 **Comparison of one-dimensional finite-difference methods and two-dimensional finite-element methods.**

The two approaches (finite-difference and finite-element) attempt to solve the problem of modelling the combustion of a pyrotechnic composition in different ways. The one-dimensional finite-difference method uses a very simple model of the column, with the temperature being calculated at each node at each time step, using an explicit method. No account is taken of heat loss through the sides of the column, and heat loss at the ends of the column is controlled by the use of a single constant, the Biot number. The method depends very heavily on the availability of good kinetic data for the system being investigated. Programming for a model of this type is relatively simple. A small

BASIC program running on a personal computer and use of a spreadsheet for data manipulation and graphing are all that is required. Results from this simple model are promising.

The two-dimensional finite-element method uses a more complex model, which allows for lateral heat loss and different methods of heat loss across boundaries, and permits definition of different materials, e.g. the column and the surrounding casing, within the problem. Extension to two dimensions obviously gives better representation of the shape being investigated than is possible using the one-dimensional finite-difference method. The two-dimensional finite-difference program TOPAZ is designed to solve a variety of different problems, including heat transfer analysis, electrostatics and magnetostatics problems. This makes the program much larger and more complex than the finite-difference program. TOPAZ also requires the use of a pre-processor, MAZE, to define the finite-element mesh, and a post-processor, ORION, to manipulate and graph the output from TOPAZ. The program solves for the change in temperature of an element over time using an implicit method and this is much more demanding on computer resources than the explicit method used with the finite-difference model. Computations based on one set of input parameters tend to take, on average, 10 to 20 minutes, compared with the two minutes for the one-dimensional model. Results from simulations using this method are good, but, as discussed for the one-dimensional model, there is a heavy reliance on the availability of good kinetic data. Additional information can be obtained from the two-dimensional model, such as fringe and contour plots showing the shape of the burning front and the temperature gradient throughout the column and the temperature gradients within the casing material.

The one-dimensional finite-difference model is useful for simple, fast assessments of pyrotechnic systems. It works very well for systems where a lot of experimental work has been done and there is a lot of reliable experimental data available. The main use would be to investigate the effect of altering parameters which are not easily altered in experimental work, to see the effect they have, in isolation, on the system. The model can also be used to decrease the number of experiments that have to be done to investigate a pyrotechnic system fully, by showing which conditions are likely to produce the desired results, and which conditions are likely to lead to combustion failure.

The two-dimensional finite-element model requires more time, effort and computer power, but simulations done using the two-dimensional finite-element model are more realistic than the one-dimensional finite-difference model in that they allow for investigation of the effects of the surroundings, e.g. the casing material type and the temperature of the environment, on the combustion of the column.

In both models, the assumption of first-order reaction kinetics, which is often used, does not produce as good a representation of the experimental profiles as can be obtained by substitution with a more acceleratory kinetic model. A rate equation based on autocatalysis (Section 3.3) provides significant improvement and further, but more marginal, improvement can be produced by using other similar kinetic expressions with additional adjustable parameters.

Since the Arrhenius parameters that are used as input for the simulations are extracted from kinetic analysis of experimental temperature profiles and these analyses assume order-of-reaction kinetic behaviour, a change of kinetic model assumed will significantly influence the values of the Arrhenius parameters. Thus, a point for future consideration might be the re-examination of kinetic analyses of experimental profiles in terms of the acceleratory expressions.

12.3 **Particle-packing considerations.**

The packing of fuel and oxidant particles is well known as being an important factor in pyrotechnic combustion, but modelling of packing of particles can be extremely complex. In this study, a very simple model was used, based on the assumption that the fuel and the oxidant particles both have uniform but different radii and that all particles are spherical in shape. This model gives good qualitative comparisons between the experimental burning rate, v, and the calculated number of contact points, $\mathbf{N_R}$, even though the system is not very realistic. The model needs to be developed further to include a range of sizes for the fuel and the oxidant particles, and to take into consideration the irregular shape of such particles. It is hoped that this will provide a more quantitative result in the comparison between v and $\mathbf{N_R}$.

It may be possible to extend the two-dimensional finite-element model to include the effect of particle-packing on the burning rate by establishing a fine grid to represent the pyrotechnic composition and randomly assigning the elements of the grid to properties of two different materials, corresponding to the fuel and oxidant, in proportions relative to the components. A preliminary basis for such a model is discussed in Section 11.

12.4 The Monte Carlo model.

The Monte Carlo model looks at the effect that the random packing of the two particles (fuel and oxidant) has on the burning rate. The increase in the number of time steps taken for the burning front to travel down the full length of the column (corresponding to a reduction in the burning rate) indicated an increase in the meandering of the path, when the proportion of non-reactable cells is increased. As discussed in Section 12.3 this method may be used to extend the two-dimensional finite-element model.

12.5 Future work.

Investigations into the burning of pyrotechnic systems is being limited by the maximum operating temperature of the nobel metal thermocouples available for use in oxidizing conditions. It is possible that this limitation may be imposing its own limitations on the ranges of kinetic parameters found from analysis of experimental temperature profiles. A possible way in which this limitation might be overcome, could be through insertion of a small-diameter high-temperature ceramic probe of well-defined thermal properties into the pyrotechnic composition. The temperature of this probe at a suitable (also well-defined) point could then be measured using a fine thermocouple (see Figure 12.1). Computer modelling could be used to predict the temperature-time profile expected in such a configuration, based on the properties of the composition and of the probe.

As the resolution of infrared pyrometers [69] improves it may be possible to use

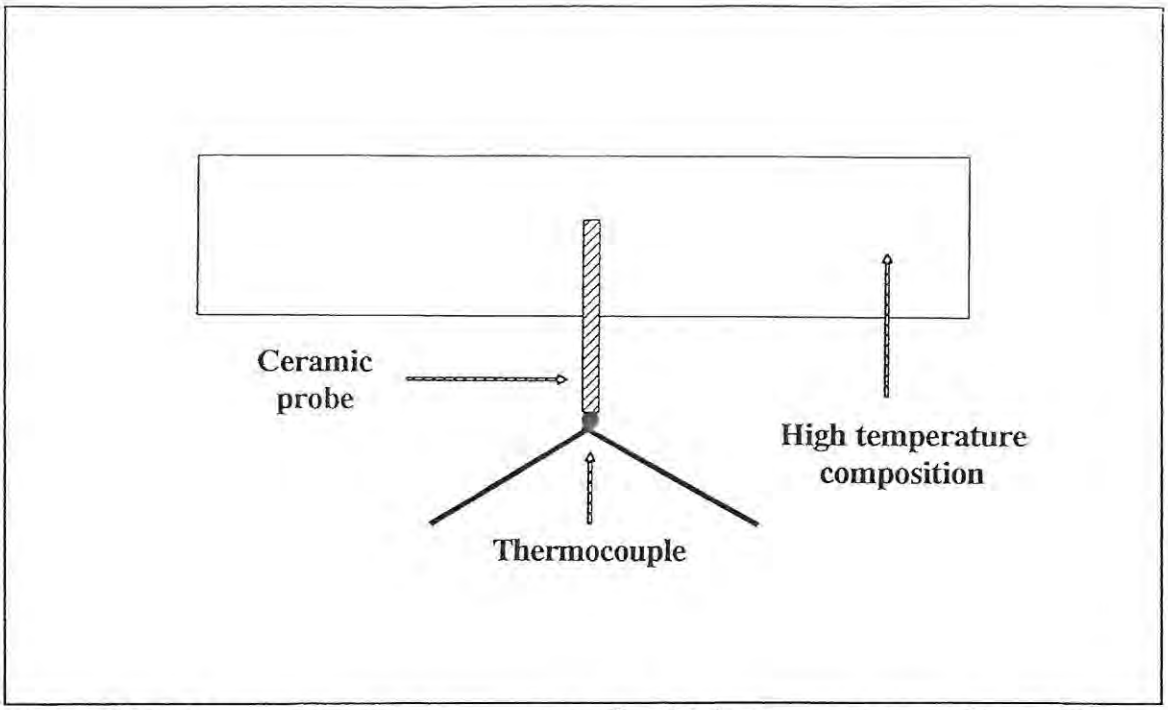

Figure 12.1: Temperature measurement of a high temperature column using a ceramic probe.

models to relate surface or end measurements of temperature to temperatures within the burning pyrotechnic column.

With ever improving computers, the mathematical models will become more complex and more general in nature, being able to solve a series of different problems. Improvements which may become possible include :-

(a) introduction of nonlinear relationships to allow for temperature dependence of properties such as heat capacity, density, thermal conductivity etc, and for changes in these properties during reaction.

(b) Allowance for nonhomogeneous materials within the pyrotechnic column. This would involve defining a column with several material types, fuels, oxidants, additives, etc., in a high-resolution random distribution, taking relative proportions into consideration.

(c) Allowance for direct incorporation of variables such as composition and compaction into the model by building in suitable sub-models of particle packing, rather than having to rely on changing those parameters which would be affected by changing composition and compaction (i.e. density

and thermal conductivity).

(d) A very important area for future improvement might be in the models used for kinetic analyses of experimental temperature profiles, e.g. incorporation of autocatalytic kinetic models as discussed in this thesis.

13 REFERENCES.

1. J. H. McLain, "Pyrotechnics", The Franklin Institute Press, Philadelphia, 1980, p. 2.
2. E. S. Oran and J. P. Boris, "Numerical Simulation of Reactive Flow", Elsevier, New York, 1987, p. 1.
3. K. H. Hueber and E. A. Thornton, "The Finite Element Method for Engineers", Wiley, New York, 1982, p. 596.
4. V. S. Arpaci, "Conduction Heat Transfer", Addison-Wesley, Reading, Mass., 1966.
5. M. E. Brown, D. Dollimore, and A. K. Galwey, "Comprehensive Chemical Kinetics", Vol. 22, Elsevier, Amsterdam, 1980, p. 74.
6. E. G. Prout and F. C. Tompkins, Trans. Faraday Soc., **40** (1944) 488.
7. J. Sestak and G. Berggren, Thermochim. Acta, **3** (1971) 1.
8. P. Gray and M. J. Harper, 4th Int. Symp. on Reactivity of Solids, Elsevier, Amsterdam, 1960, p. 283.
9. M. J. Tribelhorn, PhD Thesis, Rhodes University, 1994, p. 222.
10. T. Boddington, P. G. Laye, J. R. G. Pude, and J. Tipping, Comb. Flame, **47** (1982) 235.
11. A. P. Hardt and P. V. Phung, Comb. Flame, **21** (1973) 77.
12. A. P. Hardt and R. W. Holsinger, Comb. Flame, **21** (1973) 91.
13. F. Booth, Trans. Faraday Soc., **49** (1953) 272.
14. A. H. C. Norgrove, A. F. Jones, and J. A. King-Hele, Comb. Sci. Technol., **76** (1991) 133.
15. M. W. Beck and M. E. Brown, 10th International Pyrotechnic Seminar, Fraunhofer-Institut Fur Treib- und Explosivstoff, 1985, paper 14.
16. D. Loyd, G. Andersson, and H. Nyhlén, Proceedings of Pyroteknikdagen, 1990, p. 13.
17. T. Widlund, Proceedings of Pyroteknikdagen, 1990, p. 31.
18. M. W. Beck and M. E. Brown, J. Chem. Soc. Faraday Trans., **87** (1991) 711.
19. T. Boddington, A. Cottrell, and P. G. Laye, Comb. Flame, **76** (1989) 63.

20. T. Boddington, A. Cottrell, and P. G. Laye, Comb. Flame, **79** (1990) 234.

21. R. A. W. Hill, L. E. Sutton, R. B. Temple, and A. White, Research, **3** (1950) 569.

22. R. A. W. Hill and T. L. Cottrell, 4th Symp. on Combustion, 1953, p. 349.

23. R. Klein, M. Menster, G. von Elbe, and B. Lewis, J. Phys. Chem., **54** (1950) 877.

24. T. Boddington, P. G. Laye, J. Tipping, and D. Whalley, Comb. Flame, **63** (1986) 359.

25. M. W. Beck and M. E. Brown, Comb. Flame, **65** (1986) 263.

26. M. W. Beck and M. E. Brown, Comb. Flame, **66** (1986) 67.

27. J. A. Palasota and S. N. Demming, J. Chem. Ed., **68** (1992) 560.

28. D. R. Croft and D. G. Lilley, "Heat Transfer Calculations Using Finite Difference Equations", Applied Science, London, p. 62, 181 and 224*ff*.

29. S. Kotake and K. Hijikata, "Numerical Simulations of Heat Transfer and Fluid Flow on a Personal Computer", Elsevier, Amsterdam, 1993, p. 23.

30. K. H. Hueber and E. A. Thornton, "The Finite Element Method for Engineers", Wiley, New York, 1982, p. 599.

31. D. R. Croft and D. G. Lilley, "Heat Transfer Calculations Using Finite Difference Equations", Applied Science, London, p. 224.

32. D. R. Croft and D. G. Lilley, "Heat Transfer Calculations Using Finite Difference Equations", Applied Science, London, p. 183.

33. D. R. Croft and D. G. Lilley, "Heat Transfer Calculations Using Finite Difference Equations", Applied Science, London, p. 185.

34. a) J. Crank and Nicholson, Proc. Camb. Phil. Soc., **43** (1947) 50;
b) W. J. Minkowycz, E. M. Sparrow, G. E. Schneider, and R. H. Pletcher, "Handbook of Numerical Heat Transfer", Wiley, New York, 1988, p. 524.

35. W. J. Minkowycz, E. M. Sparrow, G. E. Schneider, and R. H. Pletcher, "Handbook of Numerical Heat Transfer", Wiley, New York, 1988, p. 16.

36. H. S. Carslaw and J. C. Jaeger, "Conduction of Heat in Solids", Clarendon, Oxford, 2nd Edn., 1959, p. 12.

37. G. D. Smith, "Numerical Solutions of Partial Differential Equations: Finite

Difference Methods", Clarendon, Oxford, 3rd Edn., 1985, p. 4.

38. G. D. Smith, "Numerical Solutions of Partial Differential Equations: Finite Difference Methods", Clarendon, Oxford, 3rd Edn., 1985, p. 11.
39. G. D. Smith, "Numerical Solutions of Partial Differential Equations: Finite Difference Methods", Clarendon, Oxford, 3rd Edn., 1985, p. 12.
40. O. C. Zienkiewicz, "The Finite Element Method", McGraw-Hill, London, 3rd Edn., 1977, Appendix 3.
41. E. B. Becker, G. F. Carey, and T. J. Oden, "Finite Elements - An Introduction", Prentice-Hall, New Jersey, 1980, Section 1.3.
42. T. J. R. Hughes, Computer Methods in Applied Mechanics and Engineering, **10** (1977) 135.
43. A. B. Shapiro, TOPAZ, Lawrence Livermore Laboratories, 1986.
44. REFLECTION 4+, ver. 4.0, Walker Richer and Quinn, Inc., 1990.
45. MAZE92, Lawrence Livermore Laboratories, 1986.
46. ORION92, Lawrence Livermore Laboratories, 1986.
47. LOTUS 1-2-3 Release 2.3 for DOS, Lotus Development Corporation, 1991.
48. GRAFTOOL Release 3.3, 3-D Vision Corporation, 1990.
49. A. B. Warren, AECI Report RN.0939/A, 1989.
50. M. W. Beck, AECI Report NR.565/B, 1989.
51. Y-J. Hao and T. Tanaka, Can. J. Chem. Eng., **66** (1988) 761.
52. N. Ouchiyama and T. Tanaka, Ind. Eng. Chem. Fundam., **19** (1980) 338.
53. A. Shimizu and J. Saitou, Solid State Ionics, **38** (1990) 261.
54. Y-J. Hao and T. Tanaka, Can. J. Chem. Eng., **68** (1990) 81.
55. M. W. Beck and M. E. Brown, Thermochim. Acta, **65** (1983) 197.
56. J. A. C. Goodfield and G. J. Rees, Fuel, **60** (1981) 151.
57. R. A. Rugunanan and M. E. Brown, J. Thermal Anal., **37** (1991) 1193.
58. R. A. Rugunanan and M. E. Brown, Comb. Sci. Technol., **95** (1994) 61.
59. R. A. Rugunanan and M. E. Brown, Comb. Sci. Technol., **95** (1994) 85.
60. R. A. Rugunanan and M. E. Brown, Comb. Sci. Technol., **95** (1994) 101.
61. R. A. Rugunanan and M. E. Brown, Comb. Sci. Technol., **95** (1994) 117.
62. M. E. Brown and R. L. Drennan, Proceedings of the 14th International

Pyrotechnic Seminar, Jersey, (1989), 423.

63. R. L. Drennan and M. E. Brown, Thermochim. Acta, **208** (1992) 201.
64. R. L. Drennan and M. E. Brown, Thermochim. Acta, **208** (1992) 223.
65. R. L. Drennan and M. E. Brown, Thermochim. Acta, **208** (1992) 247.
66. M. E. Brown, M. J. Tribelhorn, and M. G. Blenkinsop, Proceedings of the 10th International Congress on Thermal Analysis, Hatfield, U.K., August 1992, J. Thermal Anal., **40** (1993) 1123.
67. J. A. Dodds, J. Colloid Interface Sci., **77** (1980) 317.
68. S. S. Al-Kazraji and G. J. Rees, Fuel, **58**, (1979) 139.
69. R. A. Rugunanan and M. E. Brown, J. Thermal Anal., **37** (1991) 2125.

14. APPENDICES.

14.1 Program I.

```
'PROGRAM I
'ONE-DIMENSONAL FINITE-DIFFERENCE SIMULATIONS
'Q-BASIC program ONEDIM.BAS for simulation of combustion in a one-dimensional
'column of pyrotechnic composition, using 1st Order Kinetics.
'Written by S.J. Taylor
'25/8/94
'
'Uses EXPLICIT method, keeping the left hand side temperature high for 50 time cycles
'
'
'Sub-routine definitions
'
DECLARE SUB kinetic ()
DECLARE SUB reaction ()
'
'Open file for output
'
INPUT "Enter output file name :- "; n$
OPEN n$ FOR OUTPUT AS #1
'
'Define shared variables
'
DIM SHARED alp(50) AS DOUBLE        'Alpha values of each element
DIM SHARED t(50, 1)  AS DOUBLE      'element temperature
DIM SHARED tinit(50) AS DOUBLE      'initial element temperature
DIM SHARED tamb, el, fo, noint      'ambient temp, element length,
                                    'fourier number, number of
                                    'elements in column

DIM SHARED a, e!, tign, q, dens, b, spht, cond, tad
                                    'pre-expo, activation energy, ingition temp,
                                    heat 'gen, density, e!/R, heat cap., thermal
                                    cond., 'q/(spht+tamb)

DIM SHARED time, n, xint, delx, DALP!, dtime, dtr
                                    'time cycle, number elements, number
                                    intervals, 'el/xint, change in alpha, time
                                    interval, '(q/spht)*DALP!
```

```
'
'Initialize variables
'
tamb = 20: REM deg C
el = 0.02: REM m
fo = 0.2 : REM Dimensionless Fourier number
biot = 0.001 : REM Dimensionless BIOT number
noint = 40
n = noint + 1
'
'Initialize kinetic variables, call sub-routine kinetic
kinetic
'
'Read initial temperatures into material
'
FOR i = 1 TO n
READ tinit(i)
NEXT i
DATA 1000,20,20,20,20,20,20,20,20,20
DATA 20,20,20,20,20,20,20,20,20,20,20
DATA 20,20,20,20,20,20,20,20,20,20,20
DATA 20,20,20,20,20,20,20,20,20
'
time = 0
xint = noint
delx = el / xint
dtime = fo * dens * spht * delx ^ 2 / cond
'
'Temperature due to conduction
'
j = 1
repeat:
'
'LH end
IF j <= 50 THEN
        t(1,1) = tinit(1)
ELSE
        t(1,1) = tinit(1) + fo * (tinit(2) - tinit(1)) - biot * (tinit(1) - tamb)
END IF
'
'RH end
t(n,1) = tinit(n) + fo * (tinit(n - 1) - tinit(n)) - biot * (tinit(n) - tamb)
'
'Formular for interior points
FOR i = 2 TO noint
        t(i,1) = tinit(i) + fo * (tinit(i - 1) - 2 * tinit(i) + tinit(i + 1))
```

```
NEXT i
FOR i = 1 TO n
        tinit(i) = t(i,1)
NEXT i
'
'Calculate heat generated by reaction
reaction
'Print temperature and alpha values of nodes 8 and 13
PRINT #1, j * dtime, tinit(8), tinit(13), alp(8), alp(13)
'
'Test for end of calculation
IF j < 2500 THEN j = j + 1: GOTO repeat
END

'Sub-routines
'
'Sub-routine kinetic. Sets kinetic and thermodynamic information
SUB kinetic
        a = 100:            REM s-1
        e! = 350000:        REM J mol-1
        tign = 560:         REM deg C
        q = 820:            REM J g-1
        dens = 2500:        REM kg m-3
        spht = 0.6:         REM J K-1 g-1
        cond = 0.3:         REM J s-1 m-1 K-1
        tad = q / spht + tamb
        b = e! / 8.314
END SUB

'Sub-routine reaction. Calculates heat generation due to reaction.
SUB reaction
        FOR i = 1 TO n
                IF tinit(i) < tign THEN GOTO endit
                rtemp = tinit(i) + 273
                k = a * EXP(-b / rtemp)
                DALP! = k * (1 - alp(i)) * dtime
                alp(i) = alp(i) + DALP!
                IF alp(i) > 1 THEN alp(i) = 1
                dtr = (q / spht) * DALP!
                tinit(i) = tinit(i) + dtr
        NEXT i
        endit:
END SUB
```

14.2 Program II.

```
'PROGRAM II
'ONE-DIMENSONAL FINITE-DIFFERENCE SIMULATIONS
'Q-BASIC program ONEDIM.BAS for simulation of combustion in a one-dimensional
'column of pyrotechnic composition, using Prout-Tompkins Kinetics.
'Written by S.J. Taylor
'15/9/94
'
'Uses EXPLICIT method, keeping the left hand side temperature high for 100 time cycles
'
'
'Sub-routine definitions
'
DECLARE SUB kinetic ()
DECLARE SUB reaction ()
'
'Open file for output
'
INPUT "Enter output file name :- "; n$
OPEN n$ FOR OUTPUT AS #1
'
'Define shared variables
'
DIM SHARED alp(50) AS DOUBLE        'Alpha values of each element
DIM SHARED t(50, 1)  AS DOUBLE      'element temperature
DIM SHARED tinit(50) AS DOUBLE      'initial element temperature
DIM SHARED tamb, el, fo, noint      'ambient temp, element length,
                                    'fourier number, number of
                                    'elements in column

DIM SHARED a, e!, tign, q, dens, b, spht, cond, tad
                                    'pre-expo, activation energy, ingition temp,
                                    heat 'gen, density, e!/R, heat cap., thermal
                                    cond., 'q/(spht+tamb)

DIM SHARED time, n, xint, delx, DALP!, dtime, dtr
                                    'time cycle, number elements, number
                                    intervals, 'el/xint, change in alpha, time
                                    interval, '(q/spht)*DALP!

'
'Initialize variables
'
tamb = 20: REM deg C
el = 0.02: REM m
```

```
fo = 0.4 : REM Dimensionless Fourier number
biot = 0.001 : REM Dimensionless BIOT number
noint = 40
n = noint + 1
'
'Initialize kinetic variables, call sub-routine kinetic
kinetic
'
'Read initial temperatures into material
'
FOR i = 1 TO n
READ tinit(i)
NEXT i
DATA 1000,20,20,20,20,20,20,20,20,20
DATA 20,20,20,20,20,20,20,20,20,20
DATA 20,20,20,20,20,20,20,20,20,20
DATA 20,20,20,20,20,20,20,20,20
'
time = 0
xint = noint
delx = el / xint
dtime = fo * dens * spht * delx ^ 2 / cond
'
'Temperature due to conduction
'
j = 1
repeat:
'
'LH end
IF j <= 50 THEN
        t(1,1) = tinit(1)
ELSE
        t(1,1) = tinit(1) + fo * (tinit(2) - tinit(1)) - biot * (tinit(1) - tamb)
END IF
'
'RH end
t(n,1) = tinit(n) + fo * (tinit(n - 1) - tinit(n)) - biot * (tinit(n) - tamb)
'
'Formular for interior points
FOR i = 2 TO noint
        t(i,1) = tinit(i) + fo * (tinit(i - 1) - 2 * tinit(i) + tinit(i + 1))
NEXT i
FOR i = 1 TO n
        tinit(i) = t(i,1)
NEXT i
'
```

```
'Calculate heat generated by reaction
reaction
'Print temperature and alpha values of nodes 8 and 13
PRINT #1, j * dtime, tinit(8), tinit(13), alp(8), alp(13)
'
'Test for end of calculation
IF j < 2500 THEN j = j + 1: GOTO repeat
END

'Sub-routines
'Sub-routine kinetic. Sets kinetic and thermodynamic information
SUB kinetic
        a = 500:            REM s-1
        e! = 350000:        REM J mol-1
        tign = 560:         REM deg C
        q = 820:            REM J g-1
        dens = 2500:        REM kg m-3
        spht = 0.6:         REM J K-1 g-1
        cond = 0.3:         REM J s-1 m-1 K-1
        tad = q / spht + tamb
        b = e! / 8.314
'Prout-Tompkins does not work for alpha = 0, set alpha at small initial value
        FOR p = 1 TO n
                alp(p) = 0.01
        NEXT p
END SUB

'Sub-routine reaction. Calculates heat generation due to reaction, using Prout-Tompkins
'kinetics
SUB reaction
        FOR i = 1 TO n
                IF tinit(i) < tign THEN GOTO endit
                rtemp = tinit(i) + 273
                k = a * EXP(-b / rtemp)
                IF alp(i) >= 1 THEN
                        DALP! = 0
                ELSE
                        DALP! = k * (1 - alp(i)) * alp(i) * dtime
                END IF
                alp(i) = alp(i) + DALP!
                IF alp(i) > 1 THEN alp(i) = 1
                dtr = (q / spht) * DALP!
                tinit(i) = tinit(i) + dtr
        NEXT i
        endit:
END SUB
```

14.3 Program III.

```
'PROGRAM III
'ONE-DIMENSONAL FINITE-DIFFERENCE SIMULATIONS
'Q-BASIC program ONEDIM.BAS for simulation of combustion in a one-dimensional
'column of pyrotechnic composition, using Johnson-Mehl-Avrami-Erofeev Kinetics.
'Written by S.J. Taylor
'15/9/94
'
'Uses EXPLICIT method, keeping the left hand side temperature high for 100 time cycles
'
'
'Sub-routine definitions
'
DECLARE SUB kinetic ()
DECLARE SUB reaction ()
'
'Open file for output
'
INPUT "Enter output file name :- "; n$
OPEN n$ FOR OUTPUT AS #1
'
'Define shared variables
'
DIM SHARED alp(50) AS DOUBLE        'Alpha values of each element
DIM SHARED t(50, 1)  AS DOUBLE      'element temperature
DIM SHARED tinit(50) AS DOUBLE      'initial element temperature
DIM SHARED tamb, el, fo, noint      'ambient temp, element length,
                                    'fourier number, number of
                                    'elements in column

DIM SHARED a, e!, tign, q, dens, b, spht, cond, tad
                                    'pre-expo, activation energy, ingition temp,
                                    heat 'gen, density, e!/R, heat cap., thermal
                                    cond., 'q/(spht+tamb)

DIM SHARED time, n, xint, delx, DALP!, dtime, dtr, nl
                                    'time cycle, number elements, number
                                    intervals, 'el/xint, change in alpha, time
                                    interval, '(q/spht)*DALP!, order.

'
'Initialize variables
tamb = 20: REM deg C
el = 0.02: REM m
```

```
fo = 0.4 : REM Dimensionless Fourier number
biot = 0.001 : REM Dimensionless BIOT number
noint = 40
n = noint + 1
'
'Initialize kinetic variables, call sub-routine kinetic
kinetic
'
'Read initial temperatures into material
'
FOR i = 1 TO n
READ tinit(i)
NEXT i
DATA 1000,20,20,20,20,20,20,20,20,20
DATA 20,20,20,20,20,20,20,20,20,20,20
DATA 20,20,20,20,20,20,20,20,20,20,20
DATA 20,20,20,20,20,20,20,20,20
'
time = 0
xint = noint
delx = el / xint
dtime = fo * dens * spht * delx ^ 2 / cond
'
'Temperature due to conduction
'
j = 1
repeat:
'
'LH end
IF j <= 50 THEN
        t(1,1) = tinit(1)
ELSE
        t(1,1) = tinit(1) + fo * (tinit(2) - tinit(1)) - biot * (tinit(1) - tamb)
END IF
'
'RH end
t(n,1) = tinit(n) + fo * (tinit(n - 1) - tinit(n)) - biot * (tinit(n) - tamb)
'
'Formular for interior points
FOR i = 2 TO noint
        t(i,1) = tinit(i) + fo * (tinit(i - 1) - 2 * tinit(i) + tinit(i + 1))
NEXT i
FOR i = 1 TO n
        tinit(i) = t(i,1)
NEXT i
'
```

```
'Calculate heat generated by reaction  reaction
'Print temperature and alpha values of nodes 8 and 13
PRINT #1, j * dtime, tinit(8), tinit(13), alp(8), alp(13)
'
'Test for end of calculation
IF j < 2500 THEN j = j + 1: GOTO repeat
END

'Sub-routines
'Sub-routine kinetic. Sets kinetic and thermodynamic information
SUB kinetic
        a = 500:            REM s-1
        e! = 350000:        REM J mol-1
        tign = 560:         REM deg C
        q = 820:            REM J g-1
        dens = 2500:        REM kg m-3
        spht = 0.6:         REM J K-1 g-1
        cond = 0.3:         REM J s-1 m-1 K-1
        nl = 2
        tad = q / spht + tamb
        b = e! / 8.314
'Avrami model does not work for alpha = 0, set alpha at small initial value
        FOR p = 1 TO n
                alp(p) = 0.01
        NEXT p
END SUB

'Sub-routine reaction. Calculates heat generation due to reaction, using Johnson-Mehl-
'Avrami-Erofeev kinetics
SUB reaction
        FOR i = 1 TO n
                IF tinit(i) < tign THEN GOTO endit
                rtemp = tinit(i) + 273
                k = a * EXP(-b / rtemp)
                IF alp(i) >= 1 THEN
                        DALP! = 0
                ELSE
                        DALP! = nl * k * (1 - alp(i)) * (-LOG(alp(i)))^((nl-1)/nl) * dtime
                END IF
                alp(i) = alp(i) + DALP!
                IF alp(i) > 1 THEN alp(i) = 1
                dtr = (q / spht) * DALP!
                tinit(i) = tinit(i) + dtr
        NEXT i
        endit:
END SUB
```

14.4 Program IV.

```
'Program to trace the possible path of combustion through a column where
'there are two types (reacting {1} and nonreacting {0}) of elements, present
'in a weighted proportion. The first row of the column is set to reacted (2)
'state. If a neighboring element is reactable (1) it is set to reacted (2).
'The process continues down the column. The reaction can go in any direction
'including backward (towards the start) and a path is found through the
'column. If the path goes to the end row then the reaction is said to be
'complete.

'A graphic representation of the column is displayed.

'Program written by Steve Taylor, Chemistry Department, Rhodes University
'27 Jan. 1994.

DEFINT A-Z
DECLARE SUB LOOKUP (x%, y%)
DECLARE SUB INITIALIZEGRID ()
DECLARE SUB LOOKSIDE (z%, y%)
DECLARE SUB LOOKNEXT (x%)
DECLARE SUB PRINTGRID ()
DECLARE SUB SETGRID ()

'Global variables

DIM SHARED weight%
DIM SHARED NumberAcross%
DIM SHARED NumberDown%


NumberAcross% = 50
NumberDown% = 500
DIM SHARED GridArray(1 TO NumberAcross%, 1 TO NumberDown%)
ON KEY(30) GOSUB endall: KEY(30) ON
CLS
cont:
LOCATE 20, 30: PRINT "                              "
COLOR 15
LOCATE 23, 50: INPUT "ENTER WEIGHT :- "; weight#
COLOR 12
LOCATE 25, 50: PRINT "F11 to EXIT"
weight% = INT(weight# * 100)
LOCATE 20, 30: PRINT "CALCULATING Please wait"
SETGRID
INITIALIZEGRID
```

```
FOR p% = 1 TO NumberDown% - 1
LOOKNEXT p%
NEXT p%
PRINTGRID
GOTO cont


endall: KEY(30) OFF: END

'Subroutine to start reaction, sets all elements in first line to reacted
'i.e. state 2
SUB INITIALIZEGRID
      FOR i% = 1 TO NumberAcross%
        RANDOMIZE (VAL(RIGHT$(TIME$, 2)))
        x% = INT(RND * 100)
        IF x% < weight% THEN x% = 2 ELSE x% = 0
        GridArray(i%, 1) = x%
      NEXT i%
END SUB

'Looks at the elements around the element x% and sets them to reacted (2) if
'they are reactable (1).
SUB LOOKNEXT (x%)
   IF x% <= NumberDown% THEN
      IF GridArray(1, x%) = 2 THEN
        IF GridArray(1, x% + 1) = 1 THEN GridArray(1, x% + 1) = 2
        IF GridArray(2, x% + 1) = 1 THEN GridArray(2, x% + 1) = 2
        LOOKSIDE 1, x%
        IF x% > 1 THEN LOOKUP 1, x%
      END IF
      IF GridArray(NumberAcross%, x%) = 2 THEN
         IF GridArray(NumberAcross%, x% + 1) = 1 THEN
GridArray(NumberAcross%, x% + 1) = 2
        IF GridArray(NumberAcross% - 1, x% + 1) = 1 THEN
GridArray(NumberAcross - 1, x% + 1) = 2
        LOOKSIDE NumberAcross, x%
        IF x% > 1 THEN LOOKUP NumberAcross, x%
      END IF
      FOR i% = 2 TO NumberAcross% - 1 STEP 1
           IF GridArray(i%, x%) = 2 THEN
             IF GridArray(i% - 1, x% + 1) = 1 THEN GridArray(i% - 1, x% + 1)
= 2
             IF GridArray(i%, x% + 1) = 1 THEN GridArray(i%, x% + 1) = 2
             IF GridArray(i% + 1, x% + 1) = 1 THEN GridArray(i% + 1, x% +
1) = 2
             LOOKSIDE i%, x%
```

```
            IF x% > 1 THEN LOOKUP i%, x%
          END IF
      NEXT i%
   END IF
END SUB

'Looks at the element each side of element z%. If the element z%-1 is 1 it is
'set to 2 and the element z%-2 is then investigated.
SUB LOOKSIDE (z%, y%)
      IF z% = 1 AND GridArray(1, y%) = 2 AND GridArray(2, y%) = 1 THEN
         GridArray(2, y%) = 2
      ELSE
       IF z% = NumberAcross% AND GridArray(NumberAcross%, y%) = 2 AND
GridArray(NumberAcross% - 1, y%) = 1 THEN
         GridArray(NumberAcross% - 1, y%) = 2
         LOOKNEXT y%
       ELSE
         IF z% <> 1 AND z% <> NumberAcross% AND GridArray(z%, y%) =
2 THEN
            IF GridArray(z% - 1, y%) = 1 THEN
               GridArray(z% - 1, y%) = 2
               LOOKSIDE z% - 1, y%
               LOOKNEXT y%
            END IF
            IF GridArray(z% + 1, y%) = 1 THEN GridArray(z% + 1, y%) = 2
         END IF
       END IF
      END IF
END SUB

SUB LOOKUP (x%, y%)
   IF GridArray(x%, y%) = 2 THEN
      IF x% = 1 THEN
        IF GridArray(x%, y% - 1) = 1 THEN
           GridArray(x%, y% - 1) = 2
           LOOKNEXT y% - 1
        ELSE
           IF GridArray(x% + 1, y% - 1) = 1 THEN
                GridArray(x% + 1, y% - 1) = 2
                LOOKNEXT y% - 1
           END IF
        END IF
      ELSE
        IF x% = NumberAcross% THEN
           IF GridArray(x%, y% - 1) = 1 THEN
                GridArray(x%, y% - 1) = 2
```

```
                LOOKNEXT y% - 1
            ELSE
                IF GridArray(x% - 1, y% - 1) = 1 THEN
                    GridArray(x% - 1, y% - 1) = 2
                    LOOKNEXT y% - 1
                END IF
            END IF
        ELSE
            IF GridArray(x% - 1, y% - 1) = 1 THEN
                GridArray(x% - 1, y% - 1) = 2
                LOOKNEXT y% - 1
            END IF
            IF GridArray(x%, y% - 1) = 1 THEN
                GridArray(x%, y% - 1) = 2
                LOOKNEXT y% - 1
            END IF
            IF GridArray(x% + 1, y% - 1) = 1 THEN
                GridArray(x% + 1, y% - 1) = 2
                LOOKNEXT y% - 1
            END IF
        END IF
    END IF
  END IF
END SUB

'Prints out the grid and gives a few statistics of the simulation
SUB PRINTGRID
    a% = 0
    B% = 0
    c% = 0
    SCREEN 12
    LOCATE 20, 30: PRINT "Drawing                                    "
    COLOR 15
    LINE (40, 70)-(540, 170), , B
    Across1% = 40
    Across2% = Across1% + (500 / NumberDown%)
    Down1% = 70
    Down2% = Down1% + (100 / NumberAcross%)
'    PRINT "Weight = ", weight% / 10 ;"          "
    FOR i% = 1 TO NumberDown% STEP 1
        FOR j% = 1 TO NumberAcross% STEP 1
          d% = GridArray(j%, i%)
          IF d% = 1 THEN co% = 9 ELSE IF d% = 2 THEN co% = 12 ELSE
co% = 15
          COLOR co%
          LINE (Across1%, Down1%)-(Across2%, Down2%), , BF
```

```
            Down1% = Down1% + (100 / NumberAcross%)
            Down2% = Down2% + (100 / NumberAcross%)
'                LPRINT d%; " ";
            IF d% = 1 THEN
               a% = a% + 1
            ELSE
               IF d% = 2 THEN
                  a% = a% + 1
                  B% = B% + 1
               ELSE
                  c% = c% + 1
               END IF
            END IF
         NEXT j%
      Down1% = 70
      Down2% = Down1% + (100 / NumberAcross%)
      Across1% = Across1% + (500 / NumberDown%)
      Across2% = Across2% + (500 / NumberDown%)
'     LPRINT
     NEXT i%
'    LPRINT
'    LPRINT
     COLOR 14
     LOCATE 15, 30: PRINT "Number of reactable elements = "; a%; "      "
     LOCATE 16, 30: PRINT "Number of reacted elements = "; B%; "        "
     LOCATE 17, 30: PRINT "Number of unreacted elements = "; c%; "      "
     LOCATE 18, 30: PRINT "Weight = "; weight% / 100; "         "
    FOR f% = 1 TO NumberAcross%
        IF GridArray(f%, NumberDown%) = 2 THEN
           COLOR 12
           LOCATE 19, 30: PRINT "Reaction complete        "
           EXIT FOR
        END IF
        IF f% = NumberAcross% THEN
         COLOR 9
         LOCATE 19, 30: PRINT "Reaction incomplete"
        END IF
   NEXT f%
END SUB

'Sets up the grid, filling each element of an array with either a 1
'(reactable) or 0 (nonreactable). The number of each type is dependent on a
'weighted value. This is compared to a generated random number and depending
'on if it is above or below the weight number the element is set to 0 or 1.
SUB SETGRID
'     RANDOMIZE (VAL(RIGHT$(TIME$, 2)))
```

```
        FOR i% = 1 TO NumberAcross% STEP 1
            FOR j% = 1 TO NumberDown% STEP 1
                RANDOMIZE (VAL(RIGHT$(TIME$, 2)))
                x% = INT(RND * 100)
                IF x% < weight% THEN x% = 1 ELSE x% = 0
                GridArray(i%, j%) = x%
            NEXT j%
        NEXT i%
END SUB
```